# Chemogenetic approaches for interrogation and influence of biological systems

Submitted in partial fulfillment of the requirements for the degree of

Doctor of Philosophy in

Department of Chemistry

Dmytro Kolodieznyi

Carnegie Mellon University

Pittsburgh, PA

August 2020

ACKNOWLEDGEMENTS

My PhD journey was a five-year journey full of events and discoveries. I am grateful for everyone who has supported and helped me to grow as a scientist and a person along the way. I would like to thank my advisors Dr. Bruce Armitage and Dr. Marcel Bruchez for all the help and guidance they have provided me along the way. You worked great as co-advisors for me, and I always had someone to talk to about science or life and had suggestions about my experiments and life choices.

I would like to especially thank Dr. Brigitte Schmidt and Dr. Nicholas Schulz for having my home and family away from home. It is hard to describe how much I appreciate all the dinners that we have had on the back porch and all the gardening I have learned.

I would like to thank my committee members Dr. Alan Waggoner, Dr. Subha Das and Dr. Stefan Bernhard for guidance and discussions we had about life and research.

I would like to thank my undergraduate advisor and friend Dr. Denis Svechkarev who set me on the path of science filled with mysteries, discoveries, and new adventures. Because of your support and opportunities you created, I was able to get into a PhD program in the United States and finish it.

I would like to thank all members of MBIC and Armitage labs who helped and supported me during my journey: Dr. Cheryl Telmer, Dr. Matha Naganbabu, Dr. Mae Carpenter, Dr. Chris Pratt, Dr. Dan Ackerman, Dr. Taylor Canady, Dr. Lydia Perkins, Iris Yang, Dr. Jianjun He, Dr. Huaxia Shi, Ping Ping Liang, Dr. Xiaohong Tang, Dr. April Belyoung, Bruce Feldman, and Christina Cabana. My time at CMU would have been less fun without you.

I would like to thank senior scientists and supporting members of MBIC and CMU for all the help I had when I was stuck with experiments or instrumentation. Dr. Yehuda Creeger, Dr.

Haibing Ten, Dr. Greg Fisher, Dr. Byron Ballou, Dr. Roberto Gil, Dr. Logan Plath. Your expertise and advices helped me immensely when I encountered some mysterious problems.

I would also like to thank my CMU cohort (Daniel Siroky, Dr. Dinithi Perera, Lydia Jahl, Meredith Schvervish, Paul Kornbluh, and Dr. Tastuya Higaki) for activities and discussions we had about life outside of our lab space. I would like to thank my friends who always gladly listened to my complaints and supported me on my journey.

I would like to thank members of MellonFIT (Dr. Jon Wilcox, Dr. Nick Audette, Sara Wainer, Dr. Kate Lagree, Sarah Lass, Dr. April Berlyoung, and Megan Treichel) and Matt Baker who introduced me to a variety of activities and especially to rock climbing that helped me immensely to maintain my sanity during my time in the grad school.

I would like to thank our collaborators (Dr. Simon Watkins, Dr. Bennet Van Houten, Dr. Edward Burton, Dr, Patricia Opresko, Dr. Elise Fouquerel, Travis Wheeler, Dr. Jonathan Jarvik) for our great work together and amazing science we have done together.

Last but not least, I would like to thank my friends and family who were patient with me and supported me on my bad days. With you my life was brighter, and I don't think I would be where I am without you.

ABSTRACT

In current biology, there is a noticeable trend in developing new tools and methods for targeting proteins of interest as well as various cell compartments for interrogating their position and function. Fluorogen activating proteins (FAPs) offer an approach for specific protein targeting with a high activation ratio which allows their vast applications. Their inherent modularity allows researchers to modify only fluorogen to alter the properties or function of the resulting fluorogen-FAP complex. This work focuses on a rational design and validation of several new fluorogens for already existing FAP systems.

We developed a novel fluorogenic dye, an azetidine modified variant of malachite green esters previously used in our lab, that preferentially labels FAPs located in acidic compartments of the cell due to a shifted carbinol-chromophore equilibrium. This fluorogen-FAP pair shows high colocalization with LysoTracker without noticeable background from protein located in neutral cellular locations. This fluorogen provides a novel chemoselective labeling platform for studies of protein trafficking in acidic compartments of the cell which might be applicable for lysosomal storage disorders.

Another fluorogenic dye that we developed is an iodinated analog of the synthetic GFP chromophore that preserves tight binding to a previously published de novo designed protein mFAP2b. In addition to having high activation upon binding to the protein, this fluorogen also demonstrates singlet oxygen production capabilities. Addition of this new fluorogen-fluorophore pair to our toolbox of cellular probes would allow researchers to induce targeted ROS-mediated damage in live cells in two separate genetically targeted locations.

In order to make population-scale experiments that include photoablation and targeted protein damage possible, we have worked on the development and validation of several different

versions of LED-based illumination setups (Lightbox 1.1, Lightbox 2.0, LightCoffin). With these setups researchers can select what wavelength they want to use for their illumination experiment, if they want to have a flat illumination field or a spread of different light doses received by samples and perform the experiments in a reproducible fashion.

TABLE OF CONTENTS

LIST OF TABLES

LIST OF FIGURES

# 1 RATIONAL DESIGN OF FLUOROGENS TO ALTER PROPERTIES OF THE FLUOROGEN/MACROMOLECULE COMPLEX

Targeting is a widely known problem for fluorescent imaging, therapy, and sensing. The core idea is to exhibit signal or effect only in the areas where it is needed. A large variety of fluorescence probes was developed for targeting a specific location in cell[1,2], sensing of a specific molecule[3] or ion[4], or performing a specific function like photoablation[5,6]. There are several approaches for targeting in a cell, the most commons ones include targeting a specific environment (hydrophobic membranes, acidic lysosomes, etc.), recognition of the labeling target by an antibody/aptamer, genetic targeting of the protein with an encoded tag or usage of the aptamers.

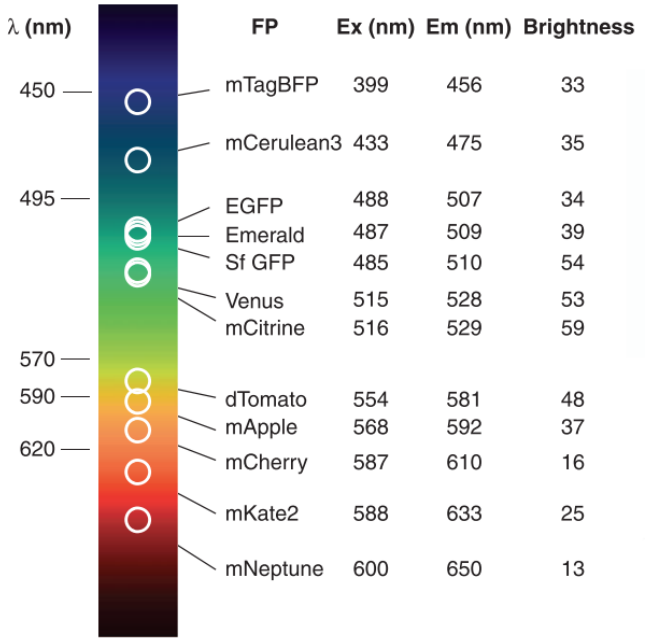


Figure 1.1 Pallette of available fluorescent proteins. Modified from Figure 1 of Crivat et al, 2012[7]

Genetic targeting allows for high specificity for protein targets and is widely used in research. Advance in fluorescent proteins allow them to be placed in any part of the spectra (Figure 1.1). This targeting makes it possible to observe any protein in cells relatively easily, however, fluorescent proteins are always on and can be turned off only by destroying protein or fluorophore directly.

An approach where the advantage of fluorescent targeting is preserved but the signal can be added externally is in the form of a fluorescence probe. Fluorescent tags can be attached to a protein of interest (POI) using different genetic tags (Figure 1.2).

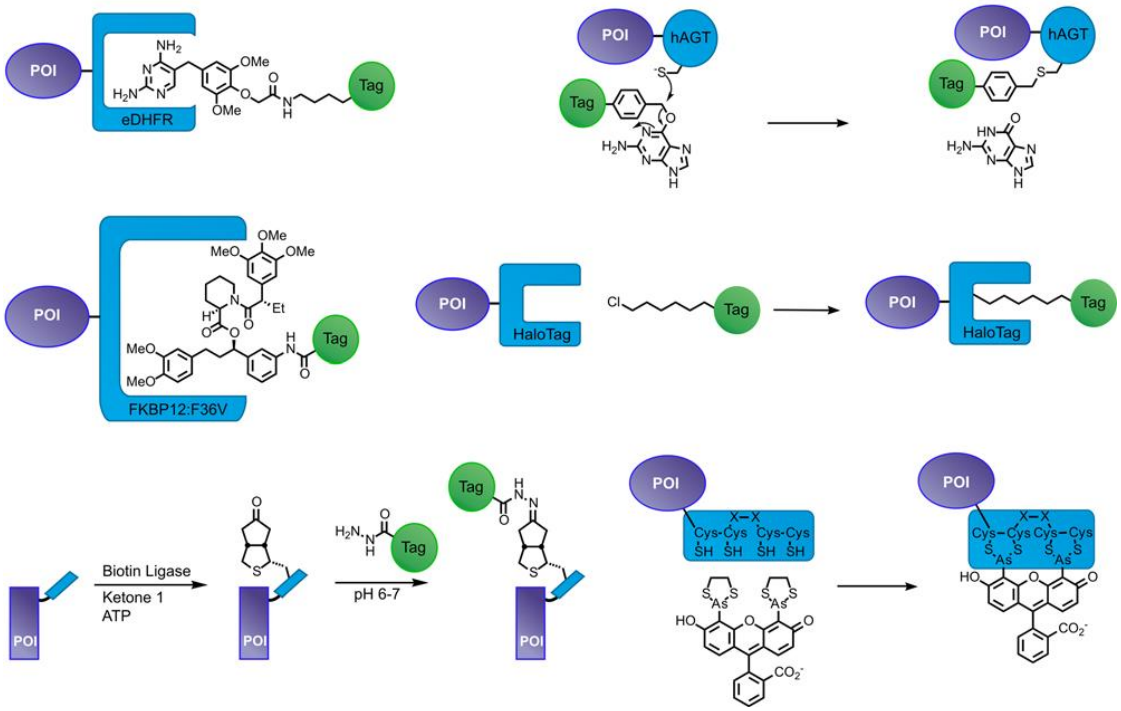


Figure 1.2 Chemical fluorescent labels can be attached to a protein of interest (POI) using different tagging approaches. Modified from Figure 1 of Wombacher et al, 2011[8]

Most of these probes can be split into two components – a targeting moiety that will interact with a protein tag and a payload part that can be a fluorescent protein or be a drug[9] thus decreasing the time required to adopt new probes (Figure 1.3).

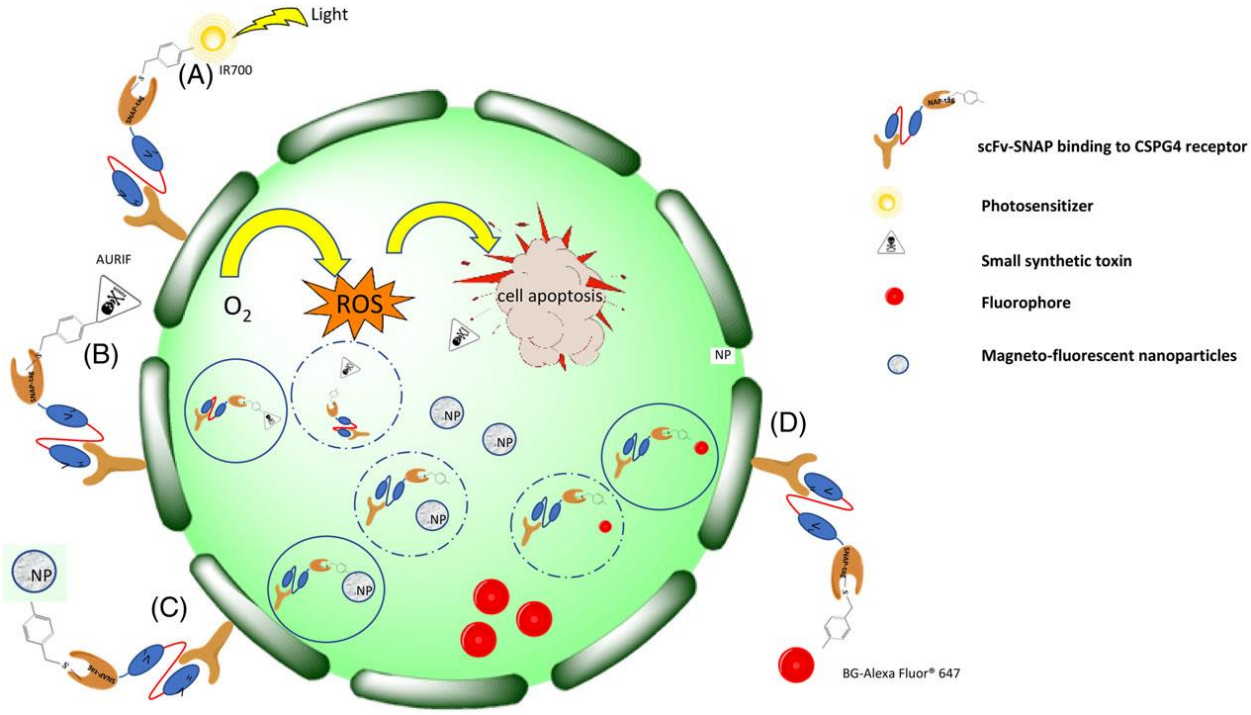


Figure 1.3 Same genetic tag (SNAP-Tag in this case) can be used with a number of different probes or drugs. Modified from Figure 4 of Padayachee et al, 2019[10]

Fluorogenic probes perform in a similar fashion as previously discussed labels by using a genetic component for targeting and a separate synthetic molecule to generate fluorescent signal when the complex is formed (Figure 1.4) thus increasing the contrast for fluorescent imaging. There is a number of fluorogenic labels available to cover even wider range than fluorescent proteins (Figure 1.5). Absence of the fluorescent signal from the unbound dye makes no-wash labeling strategies possible[11] which simplifies experiments and reduces possible errors.

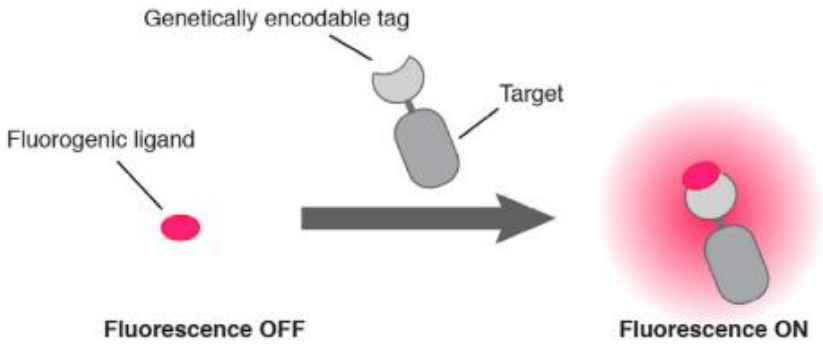


Figure 1.4 Fluorogenic labeling requires binding of the fluorogen to a tag in order to produce signal. Modified from Figure 1 of of Jullien et al, 2015[12]

Exploiting the concept of the complex where one component is responsible for targeting (protein) and another one for function (synthetic molecule) allows for rational design of the system with target properties in mind.

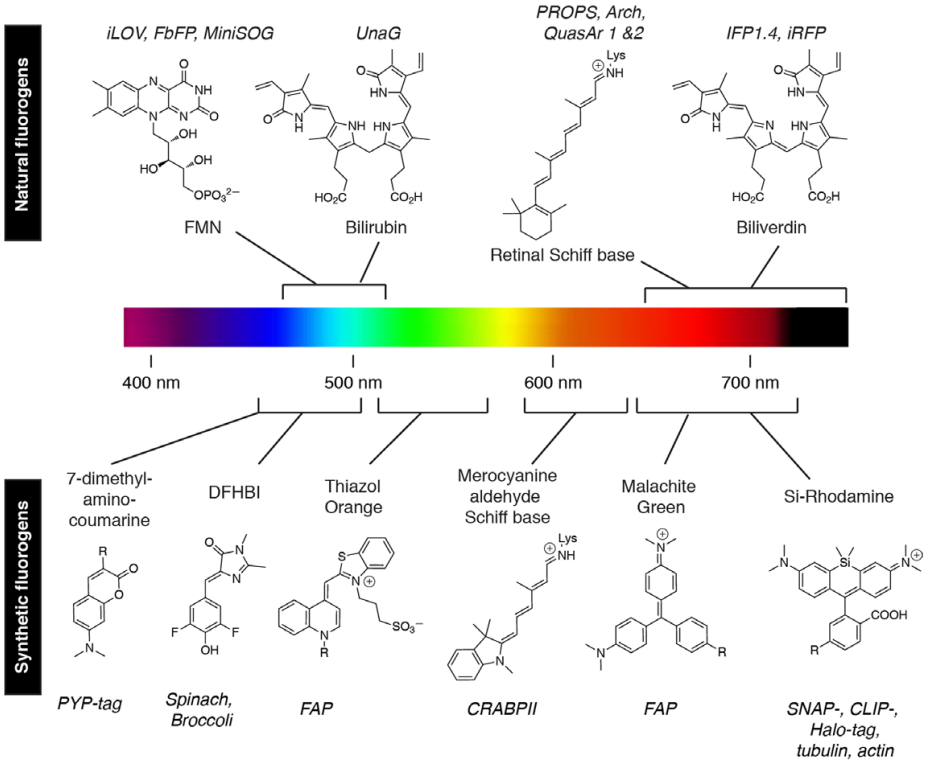


Figure 1.5 Fluorogens of different origin cover a wide spectral range. Modified from Figure 2 of Jullien et al, 2015[12]

Our lab has developed a system where Malachite Green (MG) binds to scFv derived protein with an impressive activation. Initially, a number of different constructs containing heavy chains, light chains or heavy chains connected to light chains of human single-chain antibody were screened for their capability of activation of MG-2p[13]. Our lab has also selected proteins to bind to TO1-2p while Alan Waggoner and Bruce Armitage labs selected proteins for cyanine dye derivatives (OTB and DIR)[14].

Later, we discovered that MG derivatives get activated by dimerized proteins that our lab has selected in 2008 work. MG binds between two L5 chains leaving the chain at the bottom part of the molecule exposed and flexible[15]. Binding of the Since the linker part of the molecule is exposed and is not a major component for the binding, lots of different modifications can be incorporated to give MG different properties (Figure 1.6).

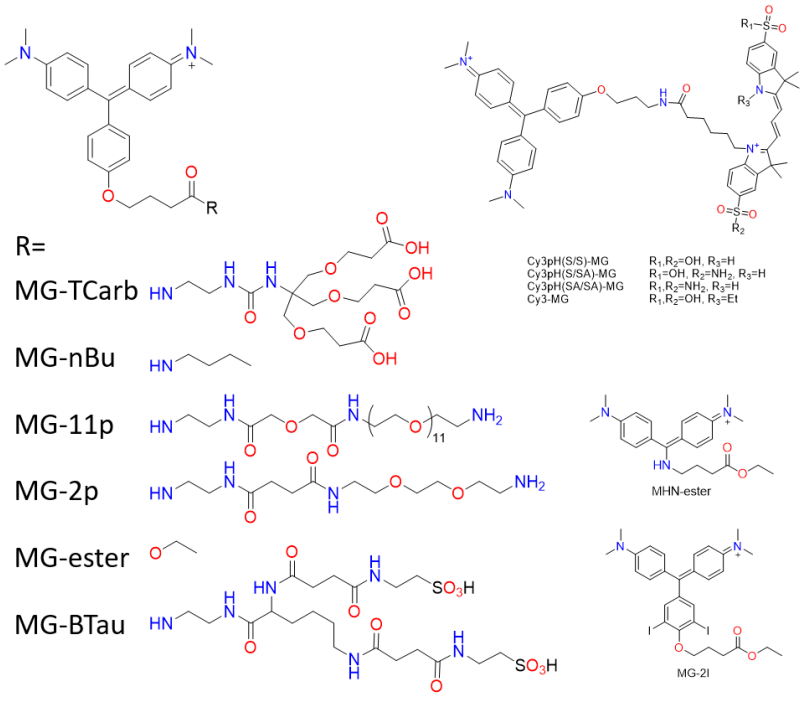


Figure 1.6 Structures of some of the MG derivatives made in our lab

We have further validated this fluorogen activating protein (FAP) system for targeting proteins in different cellular compartments (peroxisomes, mitochondria, cytosol, nucleus, and endoplasmic reticulum) by complexing with MG derivatives[16]. Upon binding, the dye displays activation (ratio of the fluorescence intensity of the dye-protein complex to fluorescence intensity of the dye alone) on the order of tens of thousands.

Table 1.1 FAP-binding probes and their applications

| Dye | Application | Ref |
|---|---|---|
| MG-ester | Cell-permeable dye | [13] |
| MG-nBu | Cell permeable dye with higher quantum yield than MG-ester | [18] |
| MG-2p | Cell-impermeable dye initially used for selection if the protein binding partner | [13] |
| MG-11p | Version of MG-11p with higher water solubility due to a longer PEG fragment in a linker | [13] |
| MG-BTau | Cell-impermeable dye with 2 negative charges on the linker | [18] |
| MG-TCarb | Cell-impermeable dye with 3 negative charges on the linker | [19] |
| Cy3pH(*)-MG | pH-responsive dyes with MG acceptor and acid-activated Cy3 donor with different $pK_a$ | [20] |
| TCM-dyedron | FRET-based system with MG acceptor and 4 Cy3 donors | [21] |
| HCM-dyedron | FRET-based system with MG acceptor and 6 Cy3 donors | [22] |
| MHN-ester | Blue-shifted analog operating in a different spectral channel | [18] |
| MG-2I | Photosensitizer with red-shifted absorption and emission | [23] |
| Blur1/2 | Cell permeable dyes with FRET excitation from Coumarin | [22] |

FAP system was developed in a truly great tool – binding of the modular exogeneous dye with high affinity, activation ratio and photostability in a cellular environment. Different MG derivatives can be used for different purposes ranging from simple protein labeling to protein trafficking, pH sensing and even generation of ROS at specific region of interest (Table 1.1).

These modifications can be separated in two groups – modifications of the linker and modifications of the chromophore. Modifications of the chromophore (MHN-ester, MG-2I) result in change of spectral properties or a function of the probe. Modifications of the linker can either affect only permeability (e.g. MG-nBu is cell permeable while MG-BTau is cell-excluded) or add additional functionality (e.g. attachment of additional fluorophores) while preserving spectral and fluorogenic binding properties.

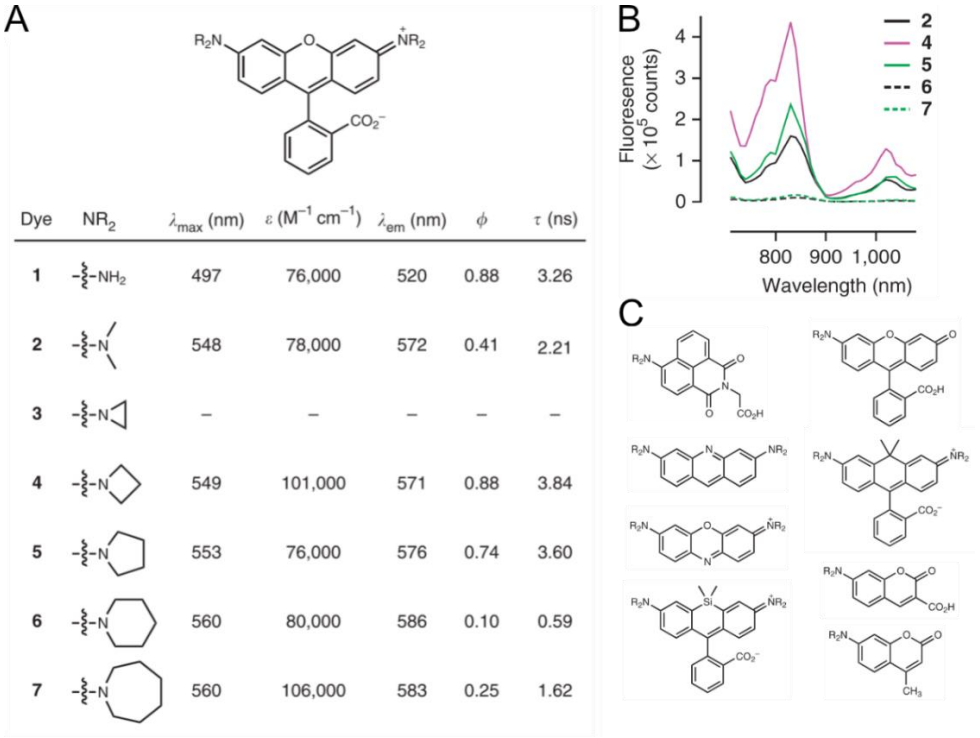


| Dye | $NR_2$ | $\lambda_{max}$ (nm) | $\varepsilon$ ($M^{-1}$ $cm^{-1}$) | $\lambda_{em}$ (nm) | $\phi$ | $\tau$ (ns) |
|---|---|---|---|---|---|---|
| 1 | $-NH_2$ | 497 | 76,000 | 520 | 0.88 | 3.26 |
| 2 | N | 548 | 78,000 | 572 | 0.41 | 2.21 |
| 3 | N | – | – | – | – | – |
| 4 | N | 549 | 101,000 | 571 | 0.88 | 3.84 |
| 5 | N | 553 | 76,000 | 576 | 0.74 | 3.60 |
| 6 | N | 560 | 80,000 | 586 | 0.10 | 0.59 |
| 7 | N | 560 | 106,000 | 583 | 0.25 | 1.62 |

Figure 1.7 Systematic study of substituents showed that change of dimethylamino group to azetidine (A) improves fluorescence (B) of a number of different dye families (C). Adopted from Grimm et al, 2015[24]

Luke Lavis (HHMI) with coworkers have made several systematic studies in modification of chromophore for Halotag-centered system. Their first study[24] was centered around improvement of the fluorescence quantum yield of different families of fluorophores. This study started as a theoretical calculation of stability of molecules in twisted internal charge transfer state and later their theoretical findings were confirmed experimentally. They have demonstrated that the brightness of 8 different fluorescent dye scaffolds can be improved by the same substitution (Figure 1.7).

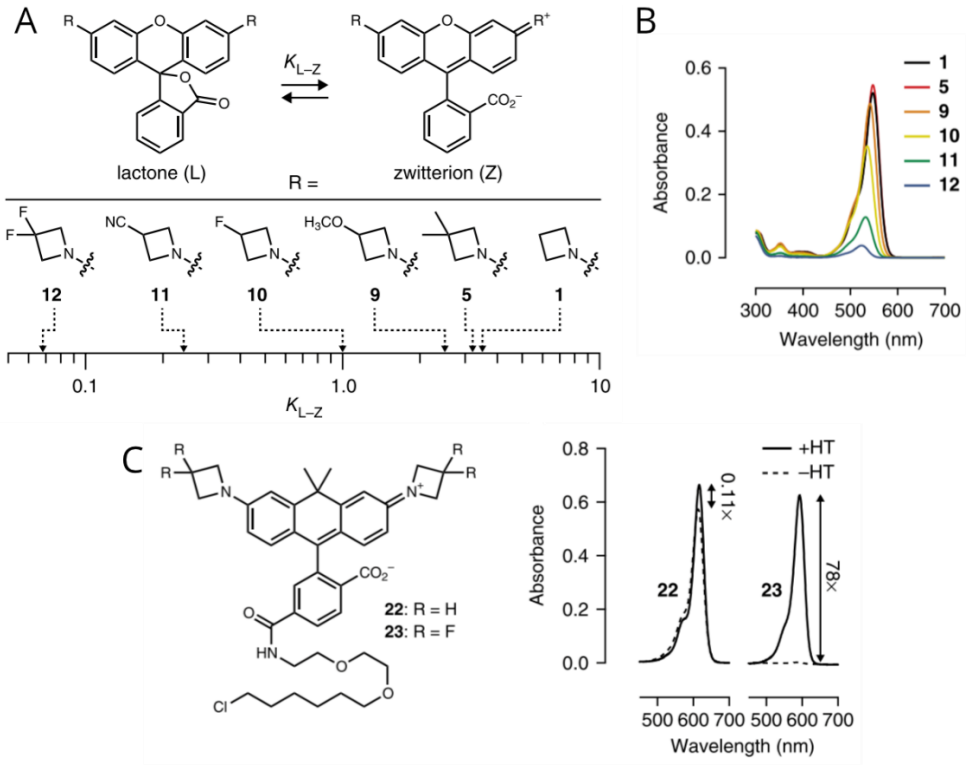


Figure 1.8 Changes in the azetidine cycle of fluorescein-derived fluorophores (A) affect the fraction of the dyes that is colored in solution (B) and result in improvement of fluorogenic behaviour upon binding to Halotag (HT) (C). Modified from Grimm et al, 2017[25]

Their later study[25] demonstrated that by testing more modifications of the same position in rhodamine molecule they can modulate L-Z equilibrium where fluorescein goes from colorless

lactone to a colored zwitterion. This change in $K_{L\text{-}Z}$ allowed them to convert fluorescein from a fluorophore that is always turned on to a fluorophore that becomes colored and fluorescent only upon binding to a Halotag (Figure 1.8).

Other modifications of the core fluorophore can be utilized to alter the spectral properties[26] or increase photostability of the complex. B. Armitage (Carnegie Mellon University) have modified dimethylindoline red[27] and thiazole orange[28] with a cyano group (following the example of K. Hahn's lab[29]) in order to increase their photostability (Figure 1.9).

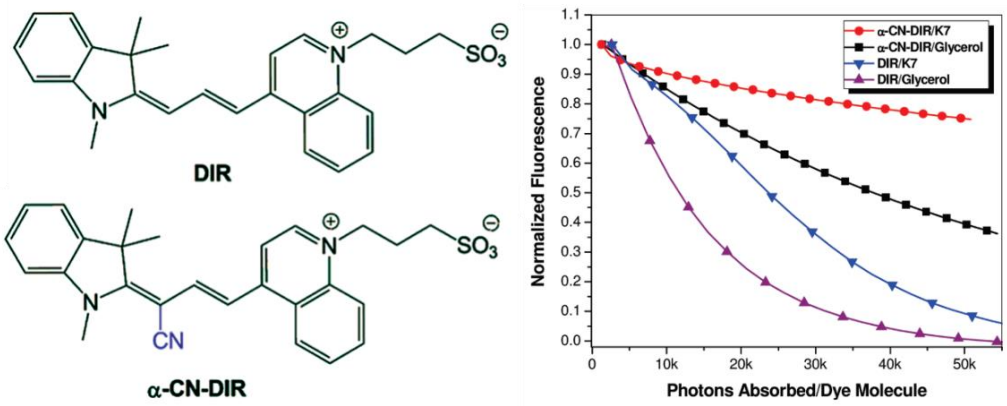


Figure 1.9 Substitution of hydrogen to cyano group in dimethylindoline red results in superior photostability. Modified from Shank et al, 2009[27]

Modifications to the fluorophore can also be used to add a sensing functionality to the existing system. One of the ways how this can be done is addition of the protective groups that can be cleaved be the enzymes[30] or react with molecules present in the cellular environment[31].

Fluorophores can also be modified to convert them into photosensitizers by addition of heavy atoms. It has been demonstrated a while back that addition of atoms like iodine and bromine to the conjugated system can result in the increase of the singlet oxygen production rate[32–34]. We have demonstrated that addition of the iodine to the MG-ester molecule converts

MG-ester/FAP system into photosensitizer[23]. Not only iodine but also sulfur can be used as a general modification that can induce singlet oxygen production in a fluorophore[35].

Fluorogenic systems that include macromolecular tagging and a fluorophore that binds to them allow for rational design of parts of the fluorogen to add additional functionality, targeting of the probe towards a specific cellular location or change in photophysical properties. In the following chapters we will employ several of these methods for improving spectral properties of the existing fluorophore (Chapter 2) and to convert a known fluorogen to a photosensitizer (Chapter 3).

## 1.1 References


(1) Demchenko, A. P.; Mély, Y.; Duportail, G.; Klymchenko, A. S. Monitoring Biophysical Properties of Lipid Membranes by Environment-Sensitive Fluorescent Probes. *Biophys. J.* **2009**, *96* (9), 3461–3470. https://doi.org/10.1016/j.bpj.2009.02.012.

(2) Xu, W.; Zeng, Z.; Jiang, J. H.; Chang, Y. T.; Yuan, L. Discerning the Chemistry in Individual Organelles with Small-Molecule Fluorescent Probes. *Angew. Chemie - Int. Ed.* **2016**, 13658–13699. https://doi.org/10.1002/anie.201510721.

(3) Giepmans, B. N. G. The Fluorescent Toolbox for Assessing Protein Location and Function. *Science (80-. ).* **2006**, *312* (5771), 217–224. https://doi.org/10.1126/science.1124618.

(4) Hyman, L. M.; Franz, K. J. Probing Oxidative Stress: Small Molecule Fluorescent Sensors of Metal Ions, Reactive Oxygen Species, and Thiols. *Coord. Chem. Rev.* **2012**, *256* (19–20), 2333–2356. https://doi.org/10.1016/j.ccr.2012.03.009.

(5) Ormond, A. B.; Freeman, H. S. Dye Sensitizers for Photodynamic Therapy. *Materials (Basel).* **2013**, *6* (3), 817–840. https://doi.org/10.3390/ma6030817.

(6) Allison, R. R.; Downie, G. H.; Cuenca, R.; Hu, X. H.; Childs, C. J. H.; Sibata, C. H. Photosensitizers in Clinical PDT. *Photodiagnosis Photodyn. Ther.* **2004**, *1* (1), 27–42. https://doi.org/10.1016/S1572-1000(04)00007-9.

(7) Crivat, G.; Taraska, J. W. Imaging Proteins inside Cells with Fluorescent Tags. *Trends Biotechnol.* **2012**, *30* (1), 8–16. https://doi.org/10.1016/j.tibtech.2011.08.002.

(8) Wombacher, R.; Cornish, V. W. Chemical Tags: Applications in Live Cell Fluorescence Imaging. *J. Biophotonics* **2011**, *4* (6), 391–402. https://doi.org/10.1002/jbio.201100018.

(9) Thiel, Z.; Nguyen, J.; Rivera-Fuentes, P. Genetically Encoded Activators of Small

Molecules for Imaging and Drug Delivery. *Angew. Chemie - Int. Ed.* **2020**, 7669–7677. https://doi.org/10.1002/anie.201915521.

(10) Padayachee, E. R.; Adeola, H. A.; Van Wyk, J. C.; Nsole Biteghe, F. A.; Chetty, S.; Khumalo, N. P.; Barth, S. Applications of SNAP-Tag Technology in Skin Cancer Therapy. *Heal. Sci. Reports* **2019**, *2* (2), 1–12. https://doi.org/10.1002/hsr2.103.

(11) Leng, S.; Qiao, Q. L.; Gao, Y.; Miao, L.; Deng, W. G.; Xu, Z. C. SNAP-Tag Fluorogenic Probes for Wash Free Protein Labeling. *Chinese Chem. Lett.* **2017**, *28* (10), 1911–1915. https://doi.org/10.1016/j.cclet.2017.03.034.

(12) Jullien, L.; Gautier, A. Fluorogen-Based Reporters for Fluorescence Imaging: A Review. *Methods Appl. Fluoresc.* **2015**, *3* (4). https://doi.org/10.1088/2050-6120/3/4/042007.

(13) Szent-Gyorgyi, C.; Schmidt, B. A.; Creeger, Y.; Fisher, G. W.; Zakel, K. L.; Adler, S.; Fitzpatrick, J. A. J.; Woolford, C. A.; Yan, Q.; Vasilev, K. V; Berget, P. B.; Bruchez, M. P.; Jarvik, J. W.; Waggoner, A. Fluorogen-Activating Single-Chain Antibodies for Imaging Cell Surface Proteins. *Nat. Biotechnol.* **2008**, *26* (2), 235–240. https://doi.org/10.1038/nbt1368.

(14) Zanotti, K. J.; Silva, G. L.; Creeger, Y.; Robertson, K. L.; Waggoner, A. S.; Berget, P. B.; Armitage, B. A. Blue Fluorescent Dye-Protein Complexes Based on Fluorogenic Cyanine Dyes and Single Chain Antibody Fragments. *Org. Biomol. Chem.* **2011**, *9* (4), 1012–1020. https://doi.org/10.1039/c0ob00444h.

(15) Szent-Gyorgyi, C.; Stanfield, R. L.; Andreko, S.; Dempsey, A.; Ahmed, M.; Capek, S.; Waggoner, A. S.; Wilson, I. A.; Bruchez, M. P. Malachite Green Mediates Homodimerization of Antibody VL Domains to Form a Fluorescent Ternary Complex with Singular Symmetric Interfaces. *J. Mol. Biol.* **2013**, *425* (22), 4595–4613.

https://doi.org/10.1016/j.jmb.2013.08.014.

(16) Telmer, C. A.; Verma, R.; Teng, H.; Andreko, S.; Law, L.; Bruchez, M. P. Rapid, Specific, No-Wash, Far-Red Fluorogen Activation in Subcellular Compartments by Targeted Fluorogen Activating Proteins. *ACS Chem. Biol.* **2015**, *10* (5), 1239–1246. https://doi.org/10.1021/cb500957k.

(17) Perkins, L. A.; Bruchez, M. P. Fluorogen Activating Protein Toolset for Protein Trafficking Measurements. *Traffic* **2020**, *21* (4), 333–348. https://doi.org/10.1111/tra.12722.

(18) Pratt, C. P.; He, J.; Wang, Y.; Barth, A. L.; Bruchez, M. P. Fluorogenic Green-Inside Red-Outside (GIRO) Labeling Approach Reveals Adenylyl Cyclase-Dependent Control of BKα Surface Expression. *Bioconjug. Chem.* **2015**, *26* (9), 1963–1971. https://doi.org/10.1021/acs.bioconjchem.5b00409.

(19) Pratt, C. P.; Kuljis, D. A.; Homanics, G. E.; He, J.; Kolodieznyi, D.; Dudem, S.; Hollywood, M. A.; Barth, A. L.; Bruchez, M. P. Tagging of Endogenous BK Channels with a Fluorogen-Activating Peptide Reveals B4-Mediated Control of Channel Clustering in Cerebellum. *Front. Cell. Neurosci.* **2017**, *11* (October), 1–18. https://doi.org/10.3389/fncel.2017.00337.

(20) Perkins, L. A.; Yan, Q.; Schmidt, B. F.; Kolodieznyi, D.; Saurabh, S.; Larsen, M. B.; Watkins, S. C.; Kremer, L.; Bruchez, M. P. Genetically Targeted Ratiometric and Activated PH Indicator Complexes (TRApHIC) for Receptor Trafficking. *Biochemistry* **2018**, *57* (5), 861–871. https://doi.org/10.1021/acs.biochem.7b01135.

(21) Szent-Gyorgyi, C.; Schmidt, B. F.; Fitzpatrick, J. A. J.; Bruchez, M. P. Fluorogenic Dendrons with Multiple Donor Chromophores as Bright Genetically Targeted and

Activated Probes. *J. Am. Chem. Soc.* **2010**, *132* (32), 11103–11109. https://doi.org/10.1021/ja9099328.

(22) Naganbabu, M.; Perkins, L. A.; Wang, Y.; Kurish, J.; Schmidt, B. F.; Bruchez, M. P. Multiexcitation Fluorogenic Labeling of Surface, Intracellular, and Total Protein Pools in Living Cells. *Bioconjug. Chem.* **2016**, *27* (6), 1525–1531. https://doi.org/10.1021/acs.bioconjchem.6b00169.

(23) He, J.; Wang, Y.; Missinato, M. A.; Onuoha, E.; Perkins, L. A.; Watkins, S. C.; St Croix, C. M.; Tsang, M.; Bruchez, M. P. A Genetically Targetable Near-Infrared Photosensitizer. *Nat. Methods* **2016**, *13* (3), 263–268. https://doi.org/10.1038/nmeth.3735.

(24) Grimm, J. B.; English, B. P.; Chen, J.; Slaughter, J. P.; Zhang, Z.; Revyakin, A.; Patel, R.; Macklin, J. J.; Normanno, D.; Singer, R. H.; Lionnet, T.; Lavis, L. D. A General Method to Improve Fluorophores for Live-Cell and Single-Molecule Microscopy. *Nat. Methods* **2015**, *12* (3), 244–250. https://doi.org/10.1038/nmeth.3256.

(25) Grimm, J. B.; Muthusamy, A. K.; Liang, Y.; Brown, T. A.; Lemon, W. C.; Patel, R.; Lu, R.; Macklin, J. J.; Keller, P. J.; Ji, N.; Lavis, L. D. A General Method to Fine-Tune Fluorophores for Live-Cell and in Vivo Imaging. *Nat. Methods* **2017**, *14* (10), 987–994. https://doi.org/10.1038/nmeth.4403.

(26) Rastede, E. E.; Tanha, M.; Yaron, D.; Watkins, S. C.; Waggoner, A. S.; Armitage, B. a. Spectral Fine Tuning of Cyanine Dyes: Electron Donor-Acceptor Substituted Analogues of Thiazole Orange. *Photochem. Photobiol. Sci.* **2015**, *14* (9), 1703–1712. https://doi.org/10.1039/c5pp00117j.

(27) Shank, N. I.; Zanotti, K. J.; Lanni, F.; Berget, P. B.; Armitage, B. A. Enhanced Photostability of Genetically Encodable Fluoromodules Based on Fluorogenic Cyanine

Dyes and a Promiscuous Protein Partner. *J. Am. Chem. Soc.* **2009**, *131* (36), 12960–12969. https://doi.org/10.1021/ja9016864.

(28) Shank, N. I.; Pham, H. H.; Waggoner, A. S.; Armitage, B. A. Twisted Cyanines: A Non-Planar Fluorogenic Dye with Superior Photostability and Its Use in a Protein-Based Fluoromodule. *J. Am. Chem. Soc.* **2013**, *135* (1), 242–251. https://doi.org/10.1021/ja308629w.

(29) Toutchkine, A.; Nguyen, D.-V. V.; Hahn, K. M. Merocyanine Dyes with Improved Photostability. *Org. Lett.* **2007**, *9* (15), 2775–2777. https://doi.org/10.1021/ol070780h.

(30) Xu, F.; Fan, M.; Kang, S.; Duan, X. A Genetically Encoded Fluorescent Biosensor for Detecting Nitroreductase Activity in Living Cancer Cells. *Anal. Chim. Acta* **2019**, *1088* (xxxx), 131–136. https://doi.org/10.1016/j.aca.2019.08.058.

(31) Srikun, D.; Albers, A. E.; Nam, C. I.; Iavarone, A. T.; Chang, C. J. Organelle-Targetable Fluorescent Probes for Imaging Hydrogen Peroxide in Living Cells via SNAP-Tag Protein Labeling. *J. Am. Chem. Soc.* **2010**, *132* (12), 4455–4465. https://doi.org/10.1021/ja100117u.

(32) Nifiatis, F. Substituent Effects of Porphyrin on Singlet Oxygen Generation Quantum Yields. *Open Spectrosc. J.* **2011**, *5* (1), 1–12. https://doi.org/10.2174/1874383801105010001.

(33) Noh, I.; Lee, D. Y.; Kim, H.; Jeong, C. U.; Lee, Y.; Ahn, J. O.; Hyun, H.; Park, J. H.; Kim, Y. C. Enhanced Photodynamic Cancer Treatment by Mitochondria-Targeting and Brominated Near-Infrared Fluorophores. *Adv. Sci.* **2018**, *5* (3), 1–11. https://doi.org/10.1002/advs.201700481.

(34) Köksoy, B.; Kaya, E. N.; Hacıvelioğlu, F.; Yeşilot, S.; Durmuş, M. Effect of Iodine

Substitution Pattern on the Singlet Oxygen Generation and Solvent Depended Keto-Enol Tautomerization Behavior of BODIPY Photosensitizers. *Dye. Pigment.* **2017**, *140*, 384–391. https://doi.org/10.1016/j.dyepig.2017.01.067.

(35) Tang, J.; Wang, L.; Loredo, A.; Cole, C.; Xiao, H. Single-Atom Replacement as a General Approach towards Visible-Light/near-Infrared Heavy-Atom-Free Photosensitizers for Photodynamic Therapy. *Chem. Sci.* **2020**. https://doi.org/10.1039/d0sc02286a.

# 2 NEW FLUOROGEN ALLOWS LYSOTROPIC CHEMO-GENETIC LABELING OF THE PROTEINS

After the original discovery of GFP[1] it, along with other fluorescent proteins, started to play a critical role in biological studies[2]. Genetically fused fluorescent proteins are incredibly useful in tracking the location and quantity of any given protein and work on simplifying tagging of endogenous proteins[3] makes it relatively simple for researchers to ask more questions about their biological systems.

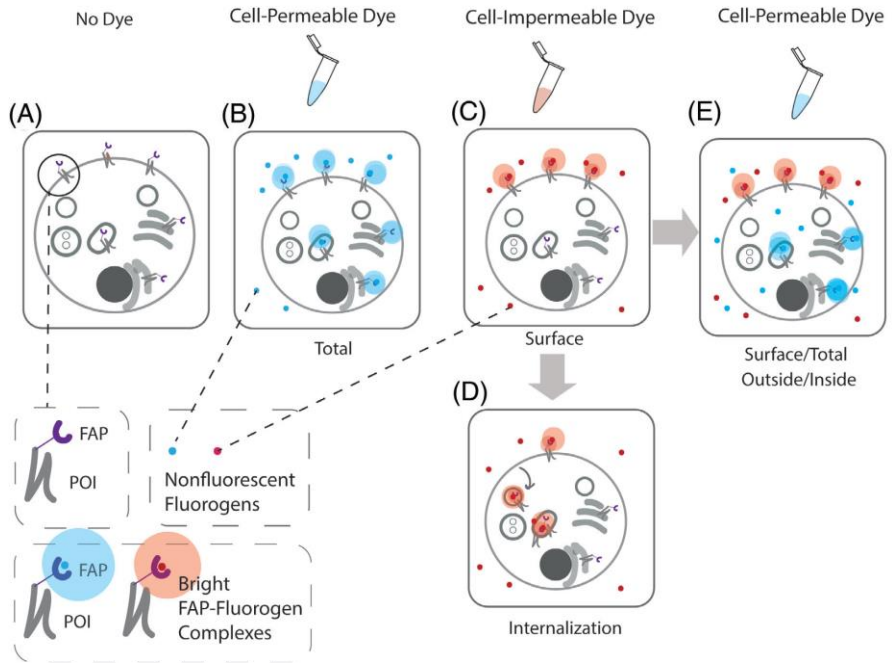


Figure 2.1 FAPs can be used for protein localization and trafficking in a number of ways. Modified from Figure 2 in Perkins et al, 2020[4]

One of the disadvantages of the fluorescent proteins was their always-on nature – if the protein is expressed in the cell it also has a fluorescent signal which limits the number of available fluorescent channels for labeling other targets in the same cell. One of the ways to avoid this limitation is to use Fluorogen Activating Proteins (FAPs)[5,6] that preserve the

possibility of genetically targeting cellular proteins but add the possibility to turn the fluorescence on by adding a fluorogenic small molecule.

The system where the same genetic component can be used with different fluorogens adds flexibility in spectral positioning[5,7], brightness[8] or even function[9–11] of the resulting complex in the same cell. FAPs were used in a number of applications including protein localization and trafficking (Figure 2.1)[4].

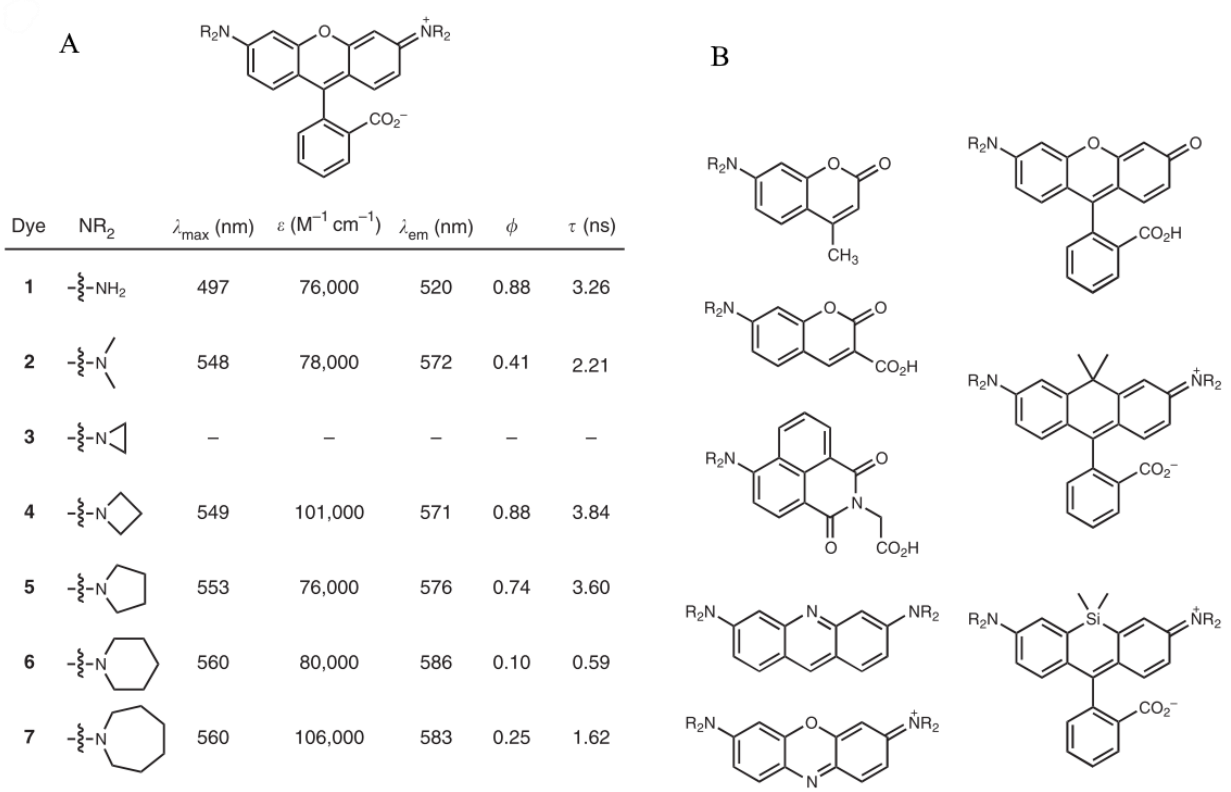


| Dye | $NR_2$ | $\lambda_{max}$ (nm) | $\varepsilon$ ($M^{-1}$ $cm^{-1}$) | $\lambda_{em}$ (nm) | $\phi$ | $\tau$ (ns) |
|---|---|---|---|---|---|---|
| 1 | -NH$_2$ | 497 | 76,000 | 520 | 0.88 | 3.26 |
| 2 | -N(CH$_3$)$_2$ | 548 | 78,000 | 572 | 0.41 | 2.21 |
| 3 | azetidine | – | – | – | – | – |
| 4 | azetidine | 549 | 101,000 | 571 | 0.88 | 3.84 |
| 5 | pyrrolidine | 553 | 76,000 | 576 | 0.74 | 3.60 |
| 6 | piperidine | 560 | 80,000 | 586 | 0.10 | 0.59 |
| 7 | azepane | 560 | 106,000 | 583 | 0.25 | 1.62 |

Figure 2.2 Systematic study of the influence of the alkyl variations of dialkylamino group on spectral properties demonstrates the improvement azetidine substituents bring to fluorescein (A) and other families of dyes (B) that have improved brightness upon change from dimethylamino group to azetidine. Modified from Figure 1 and Table 1 from Grimm et al, 2015[12].

Recently, L. Lavis (HHMI) demonstrated[12] that substitution of dimethylamino group to azetidine group results in the significant brightness increase for a variety of fluorescent tags (Figure 2.2). With this goal in mind we decided to adopt this modification to our system by changing dimethylamino groups on MG-ester to azetidines resulting in Azetidino-MG-ester (AMG-ester) (Figure 2.3).

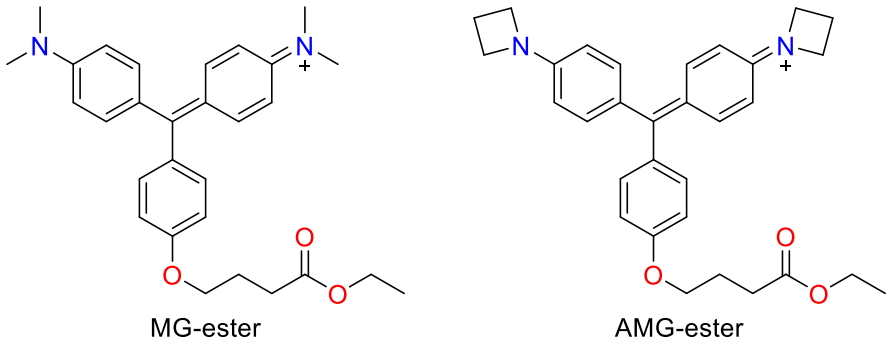


Figure 2.3 Comparison of the chemical structure of MG-ester (left) and AMG-esster (right)

In our group we use several different ways to make derivatives used as fluorogens (Figure 2.4). Majority of the dyes is made by condensing the corresponding aldehyde with N,N-dimethylaniline using one of several available methods in the literature[6,13]. Another way allows to use a different starting material – phenol instead of the aldehyde[14] for the bottom ring in the structure which might be advantageous for some synthetic routes.

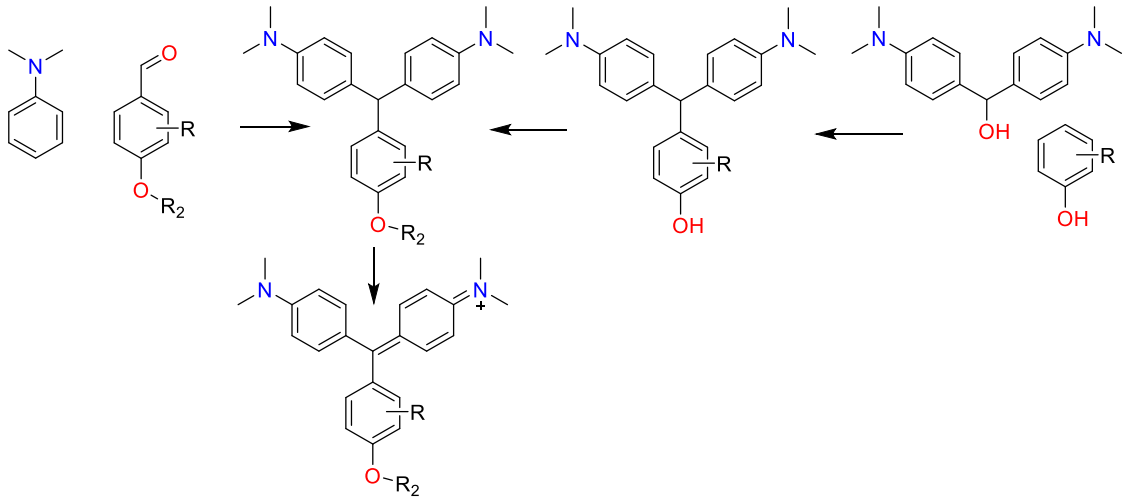


Figure 2.4 Synthetic ways used to make Malachite Green derivatives in our group[14]

For synthesis of AMG-ester we had several options in which direction to move with the synthesis (Figure 2.5). One of the most obvious ways would be to repeat what L. Lavis has done for his recent papers for a similar fluorophore[12]. This method, however, would not allow us to introduce iodine atoms as substituents in the lower ring of the molecule since iodine can leave the molecule in the presence of palladium catalyst.

Another possibility would be to use our traditional way of making MG derivatives with N-phenylazetidine as a starting material. Unfortunately, N-phenylazetidine is not commercially available so to use this synthetic route we would need to make it. Next possible synthetic route has a similar problem – formation of azetidine ring that is highly constrained[15]. Last method would be to create a version of Michler's hydrol with azetidine rings instead of the dimethylamino groups and use it as a starting material.

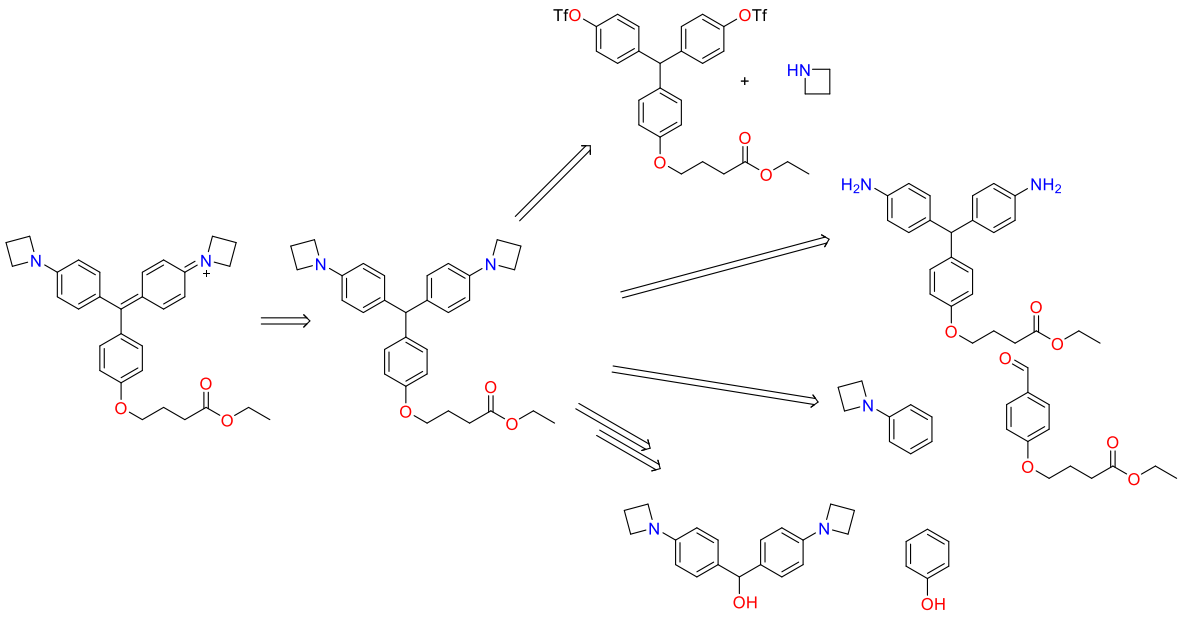


Figure 2.5 Possible synthetic pathways to get AMG-ester

## 2.1 Results and discussion

We initially decided to use the strategy of formation of azetidine rings on the reduced form of Amino Malachite Green derivative (AmMG[H]-ester) that we have synthesized following a known procedure for a similar compound[13]. Having this key intermediate we tested a simple procedure of adding 1,3-dibromopropane to amino compound and heating the mixture[16] that resulted in a small amount of product that we were able to detect using mass spectrometry but nowhere near enough to proceed with our studies with the main byproduct being oligomer of several AmMG[H]-ester molecules linked by the propane bridges.

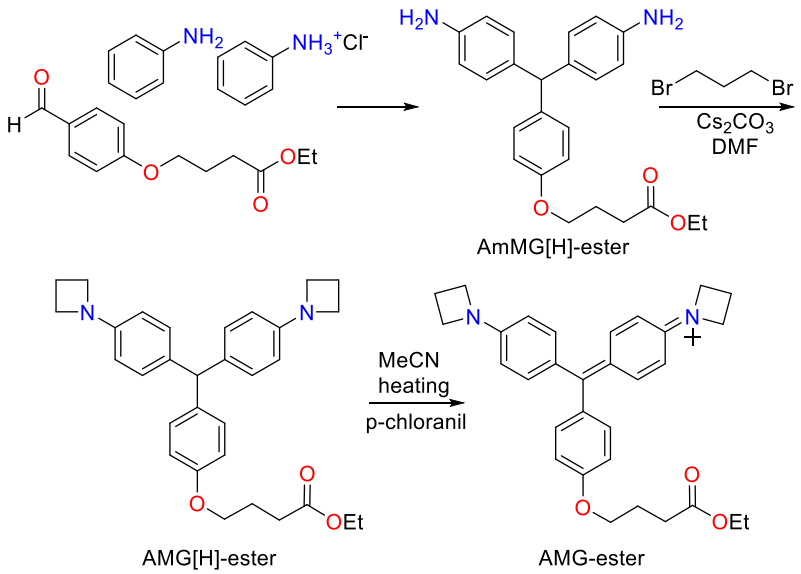


Figure 2.6 Synthetic scheme for the AMG-ester

The original paper[16] used potassium carbonate and DMSO that we substituted for DMF (as it is easier to work with) and cesium carbonate. Unfortunately, only one of the reactions that we tried with these conditions resulted in conversion of a noticeable part of AmMG[H]-ester to AMG[H]-ester (reduced form of AMG-ester). Synthetic scheme for AMG-ester that worked is

presented on Figure 2.6. We will discuss more of our attempts in making this molecule in the end of the chapter.

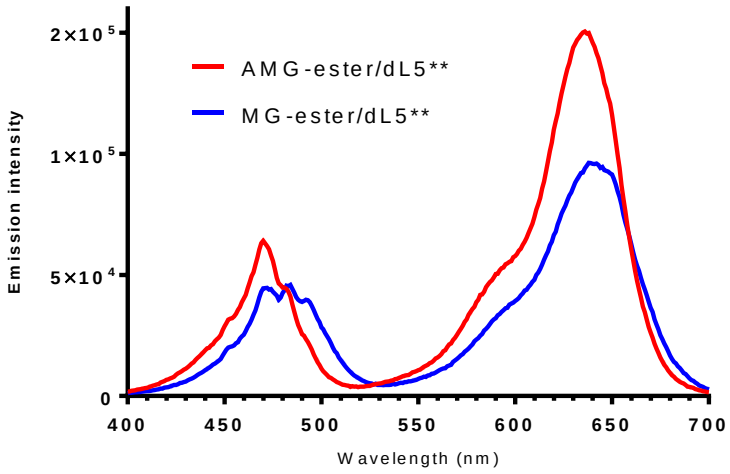


Figure 2.7 Excitation spectra of MG-ester and AMG-ester complexed to dL5**

As we predicted, azetidine ring is not significantly larger than dimethylamino group so AMG-ester was able to bind to the dL5** (two linked light chains of human antibody selected and characterized for activation of MG-ester in our lab earlier[6,17,18]) as evident by the fluorescence activation of the mixture of AMG-ester and dL5**. Upon binding, it has close spectral characteristics to the MG-ester, demonstrating 1 nm bathochromic shift in absorption (Figure 2.7) and 10 nm hypsochromic shift in emission spectra (Figure 2.8).

Unfortunately, due to low amounts of the protein, we were not able to measure $K_d$ in a reliable way, but from the experiment that we have conducted we can tell that AMG-ester has lower affinity towards dL5** than MG-ester (Figure 2.9).

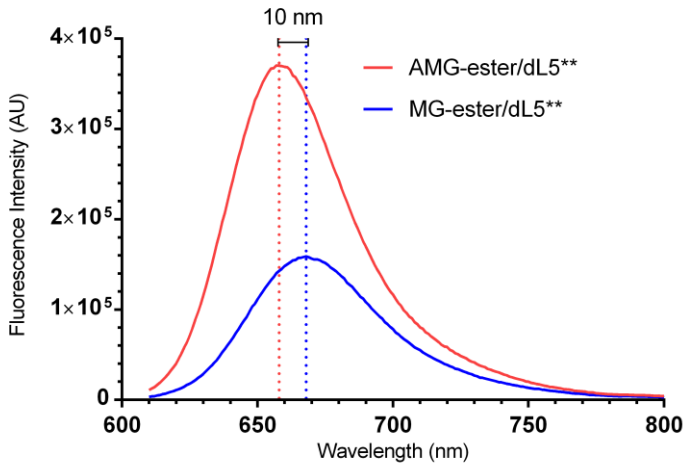


Figure 2.8 Emission of AMG-ester/FAP complex is red-shifted by 10 nm in comparison to MG-ester complex with FAP

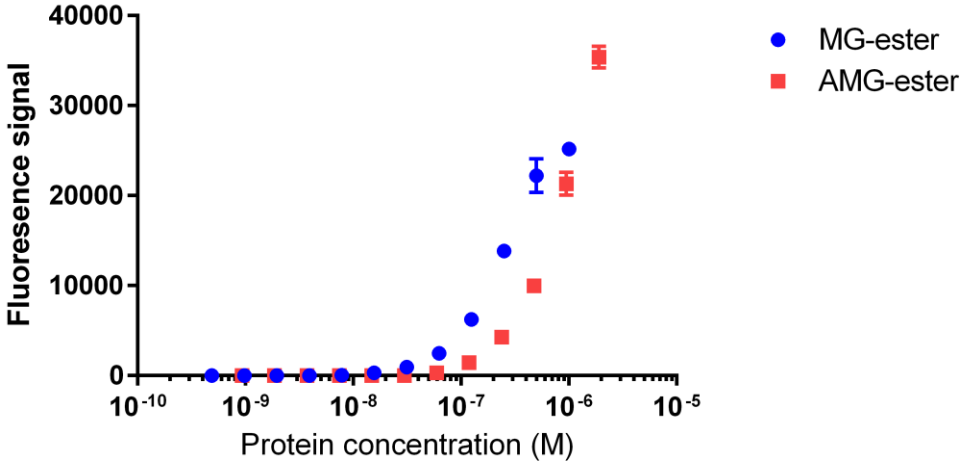


Figure 2.9 AMG-ester binds less tight to dL5** than MG-ester

Based on the measurement of the fluorescence intensity of the AMG-ester and MG-ester complexes with excess of dL5** of equal optical density (Figure 2.8) quantum yield of the new complex is 29%. This corresponds to 2.4-fold improvement of the fluorescence quantum yield. We have also tested the brightness of the complex using fluorescence correlation spectroscopy with photon counting histogram method available in the Zeiss software we obtained the same relative brightness for AMG-ester in comparison to MG-ester (15763 vs 6546 respectively).

Extinction coefficient of AMG-ester/dL5** is also slightly higher than MG-ester/dL5** ($74600 M^{-1}cm^{-1}$ vs $74250 M^{-1}cm^{-1}$) which makes AMG-ester/dL5** complex much brighter than MG-ester (15763 vs 6543; we define brightness as a product of extinction coefficient and quantum yield).

Having promising results in vitro, we moved to test the performance of the new dye with cells. We used FAP-TM HEK293[19] cells (FAP expressed on the surface of the cells) and checked the cell penetration and background signal from AMG-ester in comparison with MG-ester. Using dyes in equal concentration their brightness and background staining is quite similar (Figure 2.10). This is both good and bad news – on one hand, we have preserved cell permeability and low background for the dye with modifications, but we do not see the same increase in brightness as we have seen in vitro.

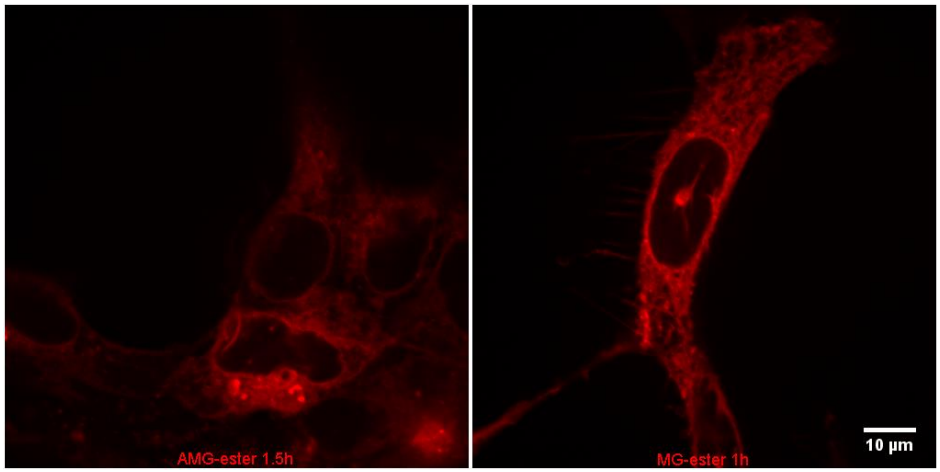


Figure 2.10 Background test for AMG-ester (left) and MG-ester (right) with FAP-TM cells and 1.3µM AMG-ester, LUTs are matched

It is possible that one of the possible reasons for this performance is low Kd that we have observed for AMG-ester to dL5**. In our lab we have previously made a version of dL5** with E52K mutation (here and after named dK) which should result in more space in the binding

pocket where dimethylamino groups are located[20,21]. Since we did not have purified dK on hands, we decided to test AMG-ester on dK-TM cells (Figure 2.11). As expected, MG-ester showed better signal localization on the cell surface where more of the dK is present. Unfortunately, AMG-ester was significantly dimmer with the higher limit for LUT set 8-fold lower than for MG-ester (2034 vs 16074 respectively). From this data we can conclude that binding to dK instead of dL5** would not solve out brightness issue.

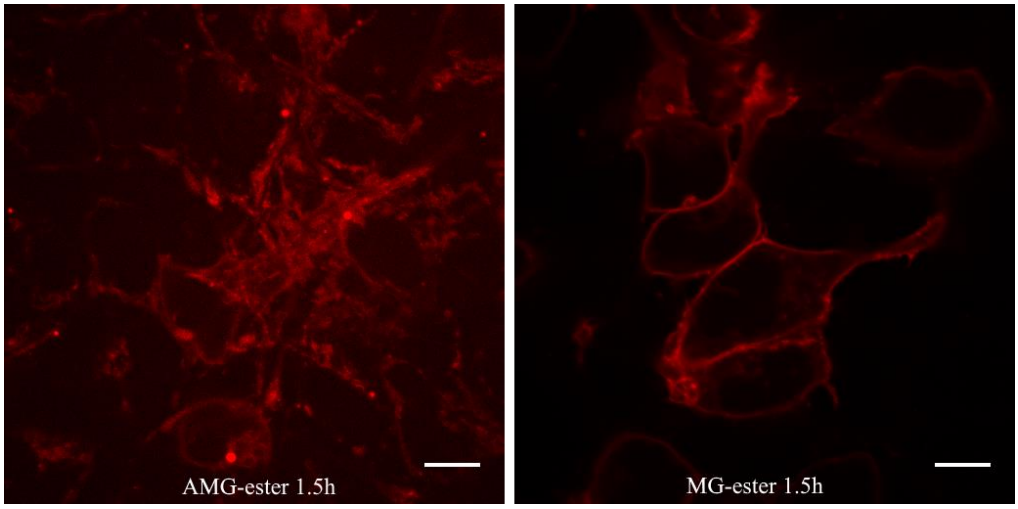


Figure 2.11 Labeling test for AMG-ester and MG-ester with FAP-dK cells, LUTs are not matched, scale bar 10μm

Next thing that we evaluated was the influence of the labeling time on the brightness of the cells with MG-ester and AMG-ester (Figure 2.12) in FAP-TM cells. Despite AMG-ester/dL5** complex being much brighter in solution, AMG-ester even with twice higher concentration (which is way above 200-500nM of MG-ester we would normally use) does not reach the same brightness as MG-ester does over an hour and a half.

To test the influence of concentration on the brightness of the labeled cells we have tested the brightness of FAP-BK cells[22] (big potassium channel that is expressed on the inside and

outside of the cell) with MG-ester and AMG-ester at concentrations between 1.2µM and 37.5nM. AMG-ester is consistently lower in the mean cell fluorescence even though not statistically significantly (mostly due to the wide error bars).

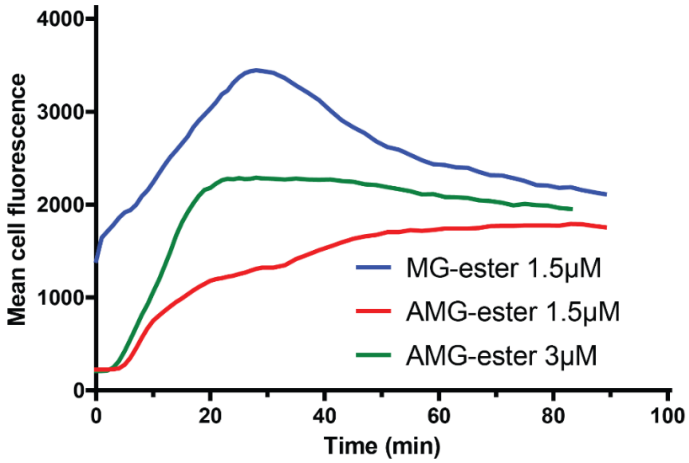


Figure 2.12 AMG-ester does not reach same level of brightness as MG-ester using equal or larger concentration in cellular experiments with FAP-TM cells

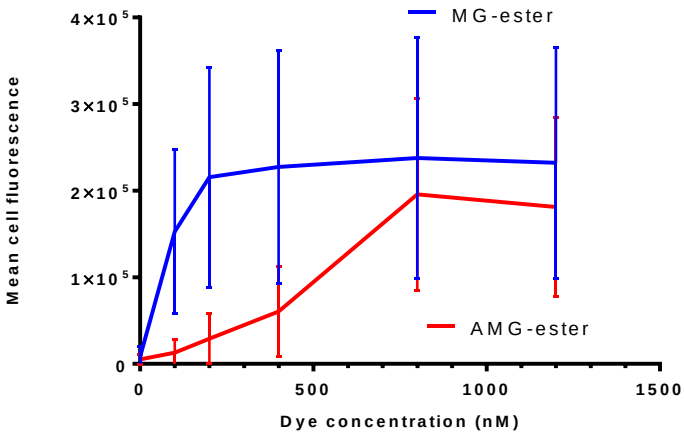


Figure 2.13 AMG-ester barely reaches the same level of signal at high concentrations with FAP-BK cells (measured by FACS)

For all the experiments that we have discussed so far, dyes stocks in PBS were diluted from ethanol stocks and used immediately. When we examined one of the intermediate stocks of the AMG-ester in PBS the next day we noticed that the solution lost all the color. This can be

due to the pH-dependent equilibrium where carbinol form breaks the conjugation in the core of the molecule and results in the loss of color (Figure 2.14).

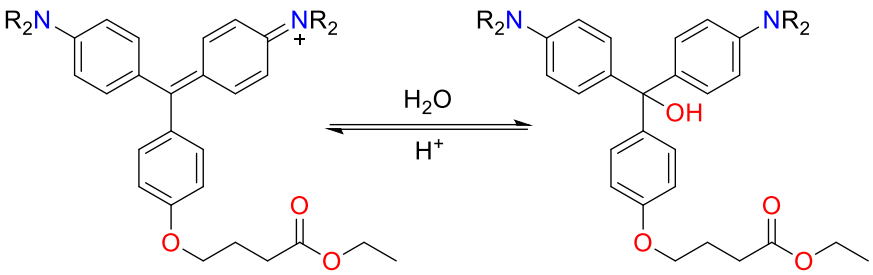


Figure 2.14 MG-ester-based dyes can undergo a pH-dependent decolorization

Once we chose this hypothesis as an explanation for poor performance of AMG-ester in cell-based experiments (where pH of the media is 7.4) we needed to investigate it and potentially find a way to use it to our advantage. AMG-ester has pKa lower than MG-ester almost by 2 (Figure 2.15). This shift from 8.0 for MG-ester to 6.0 for AMG-ester means that at pH 7.4 instead of majority of dye being in a colored form (for MG-ester) only ~15% of the dye is colored (for AMG-ester).

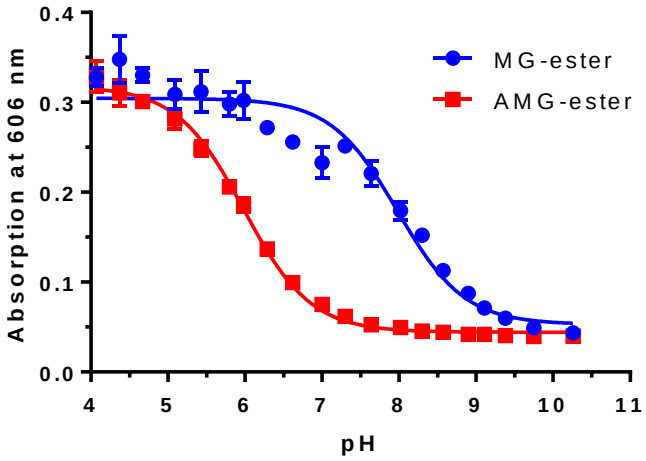


Figure 2.15 Change of dimethylamino groups to azetidine groups in the dye structure results in drop of $pK_a$ by 2

To further explore dye decolorization we have evaluated the time it takes for AMG-ester to decolorize and recolorize (Figure 2.16). From the kinetic data we can tell that recolorization is mostly complete after 1hr of the dye being present at pH 5 while decolorization takes 4 hours to be mostly completed. This difference in kinetics allows us to explore the possibility of using this dye to specifically target the acidic components of the cell – lysosomes.

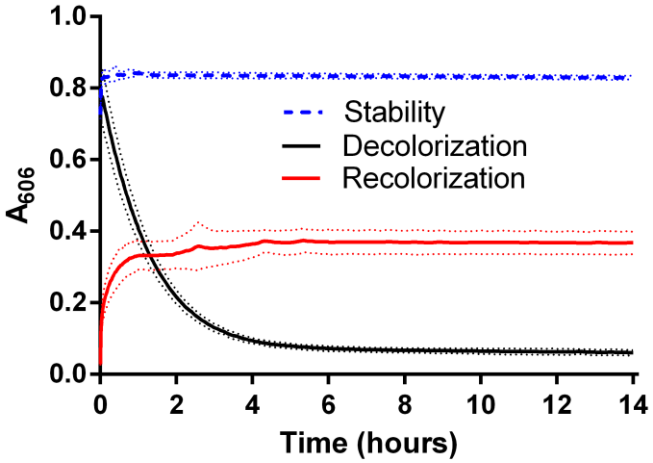


Figure 2.16 AMG-ester changes colorized form within hours with recolorization happening faster than decolorization, dotted lines represent standart deviation

In order to test the possibility of using AMG-ester as a selective lysosome targeting fluorogen we tested colocalization of AMG-ester signal with Lysotracker Green (dye selectively activating in acidic environments) in FAP-LAMP1 HEK293 cells[23] (Lysosomal Associated Membrane Protein). When FAP-LAMP1 cells are labeled with fluorogen like MG-ester, signal is present not only in lysosomes but also in Trans Golgi Network as well as early and late endosomes which would decrease colocalization of the fluorogen signal and Lysotracker.

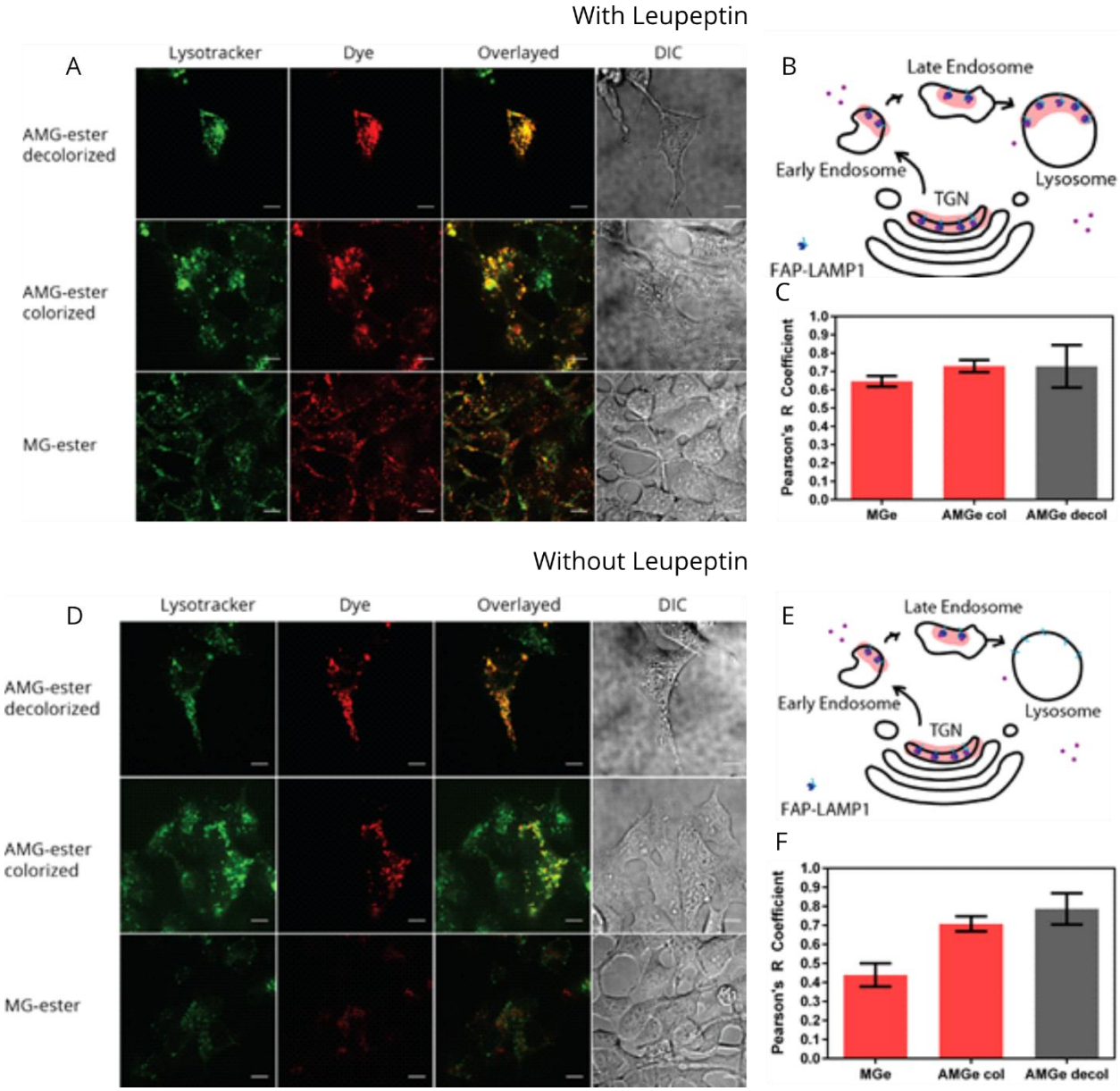


Figure 2.17 With leupeptin (top) more FAP accumulates in lysosome (B[23]) resulting in better FAP signal colocalization with Lysotracker for all fluorogens (A,C) while without leupeptin (bottom) lysosomal FAP is being digested by proteases (E[23]) and AMG-ester shows higher colozalization with Lysotracker (D,F); LUTs are not matched between samples, scale bar is 10µm. FAP-LAMP1 trafficking pathway adopted from Perkins, 2018[23]

This property of AMG-ester to be active only in acidic compartments of the cell potentially allows us to use it for tagging proteins that are located only in lysosomes or late endosomes instead of all locations where proteins are expressed and trafficked (Figure 2.18).

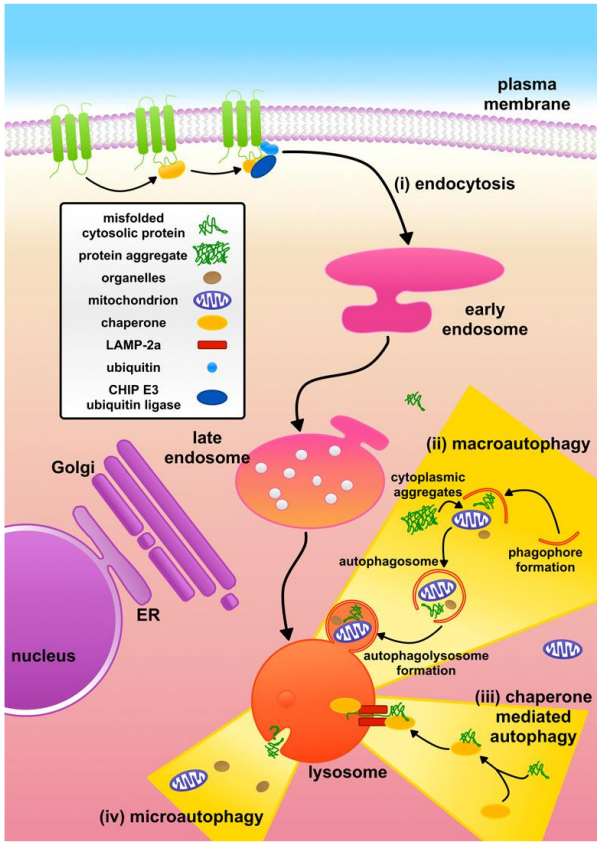


Figure 2.18 Proteins can be present in a number of cellular locations throughout their lifecycle. This example shows pathways how surface proteins, after being delivered from Golgi to the surface, join misfolded proteins and protein aggregates in lysosomes to be digested. Modified from Figure 2 in Jackson et al, 2016[24].

## 2.2 Synthetic challenges

One of the most challenging parts of this project turned out to be the synthetic part as the reactions were not reproducible and low yield. As opposed to five- and six-member cycles, formation of a four-member cycle requires to overcome a noticeable ring strain[25] that is utilized in ring-opening polymerizations[26].

We have successfully made a batch of AMG-ester using alkylation/cyclization of AmMG[H]-ester in DMF with 1,3-dibromopropane and cesium carbonate. We were not successful in reproducing this success even trying different addition rates, temperatures, and reaction times. We decided to try to make 1-phenylazetidine first as the reagents are much simpler to work with and allow us to tune critical parameters for the reaction and use that experience for making AMG[H]-ester.

We started our microwave tests based on the reaction of aniline with dichloropropane in water with potassium carbonate[27]. Using a video feed from the microwave, we quickly discovered that at this temperature (120°C) aniline and dichloropropane dissolve in water. We have also observed that hydrolysis was our major product for this reaction (Figure 2.19).

To decrease the hydrolysis, we decided to test some organic bases that we had in the lab (DIEA and DBU) as well as some different temperatures/length of reaction (Table 2.1). Same as aniline, DIEA upon heating dissolves in water while DBU stays as large droplets which resulted in its poor performance. As we have predicted, DIEA significantly decreased the amount of hydrolyzed product.

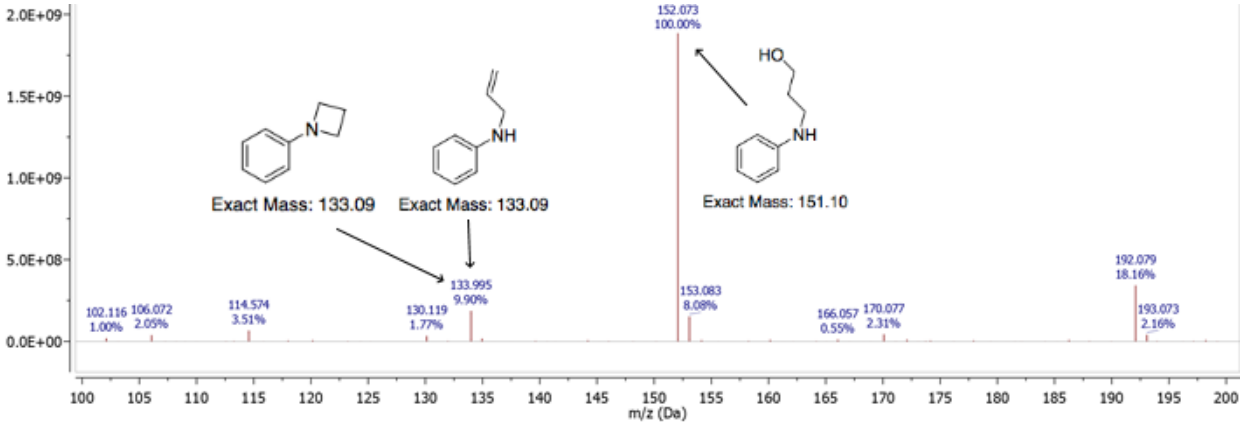


Figure 2.19 ESI-MS of the reaction mixture after the microwave reaction of aniline, dichloropropane with potassium carbonate in water

Table 2.1 Testing of different reaction conditions for 1-phenylazetidine synthesis in microwave, ratio of reagents was always 1:1.1:2.2 (aniline:1,3-dichloropropane:base), reaction ran on 5 mmol scale

| Base | Solvent | Time (min) | Temperature (°C) | Comment |
|---|---|---|---|---|
| DIEA | water | 20 | 120 | Base reaction for test |
| DIEA | water | 20 | 110 | No difference from the base reaction |
| DIEA | water | 20 | 130 | No difference from the base reaction |
| DIEA | water | 30 | 120 | Not full conversion |
| DBU | water | 20 | 120 | Base is not soluble |
| DIEA | EtOH | 12 | 100 | No product |
| DIEA | Acetonitrile | 12 | 100 | No product |
| DIEA | DMF | 10 | 120 | No product |
| DIEA | water | 90 | 130 | Not full conversion |

Different temperature with DIEA did not result in significant alterations of the aniline conversion rate. Tests with different solvents (acetonitrile, ethanol and DMF) contained some amount of mono-alkylated product but no cyclized product so we stayed with water for the rest of the trials. Long reaction in water (90 minutes) did give us a marginally better reaction based on the TLC. The biggest downside of the microwave reaction for us was the scale that it can be performed at – with the largest vial available to us the scale of the reaction was capped at 5-10 mmol which is not a lot considering losses during the purification and potential poor yield of the condensation step for making AMG[H]-ester.

To mitigate the issue of the low reaction scale we have switched to running the reaction in the autoclave (Figure 2.20). For these reactions we were using water, aniline and DIEA in the autoclave and injecting dichloropropane once the autoclave reached internal pressure of 2 atm which corresponds to ~120°C. This experiment allowed us to obtain larger quantities of the 1-phenylazetidine and test different purification methods with the best one being chromatography with basic alumina as a solid phase and hexane->ethyl acetate gradient elution. We obtained in total ~100 mg of the a-phenylazetidine and tried to perform a condensation reaction with the appropriate aldehyde but we saw no signs of the reaction happening, so we abandoned this synthetic route.

After we got confident that there is a way for us to form a four-member cycle on aniline, we moved on to trying to convert AmMG[H]-ester to AMG[H]-ester. Unfortunately, AmMG[H]-ester stayed as an oil and did not disperse in water even after heating which resulted in us not being able to use a well-established procedure for the formation of azetidine rings on aromatic amines.

Figure 2.20 Autoclave used for synthesis of 1-phenylazetidine

We briefly tried to do an alkylation with an asymmetrical alkylating reagent (1-bromo-3-chloropropane) so we can try using mixed ethanol/water system for cyclization[28] but we never achieved a clean alkylation of each of the amine group only once. Alkylation/cyclization reaction in absolute ethanol with calcium hydroxide[29] resulted in products of polymerization rather than target product.

After facing these problems, we decided to try to combine conditions from different publications that we thought were reasonable and perform our version of a reaction. The key to avoid polymerization is to perform a reaction at low concentrations, however, we also need for AmMG[H]-ester to react twice with the alkylating agent (since it has 2 amino groups that should be modified). For solvent we settled on using N-methyl-2-pyrrolidinone (NMP), a well-established polar solvent that should be able to dissolve our starting materials and DIEA as our base. To minimize the risk of hydrolysis we have distilled NMP before the reaction and

performed a reaction under Ar. Since we have dropped the concentration of our starting materials, we had to increase the time for the reaction which ended up being 30 days at 80°C which is higher than some of the reported successful attempts at making 1-phenylazetidine with 1,3-dichloropropane. This reaction had noticeable amount of byproducts and we have lost our product during the purification as we were not able to elute it off the alumina column.

Before we were forced to shut down for the quarantine, we made the intermediate for making AMG[H]-ester from AmMG[H]-ester using cyclic sulfate of 1,3-propanediol[30] (Figure 2.21). Synthesis of the intermediate went exactly as it was described in the paper but because we have two amino groups in our molecule, we have encountered a problem of having mono- and double- alkylation products (Figure 2.22).

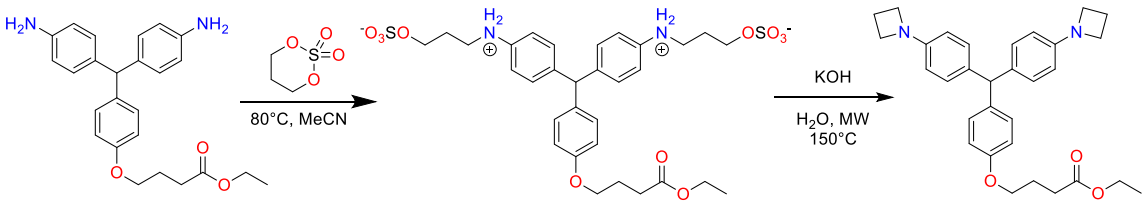


Figure 2.21 Microwave synthetic pathway for making AMG[H]-ester using 1,3-propanediol cyclic sulfate

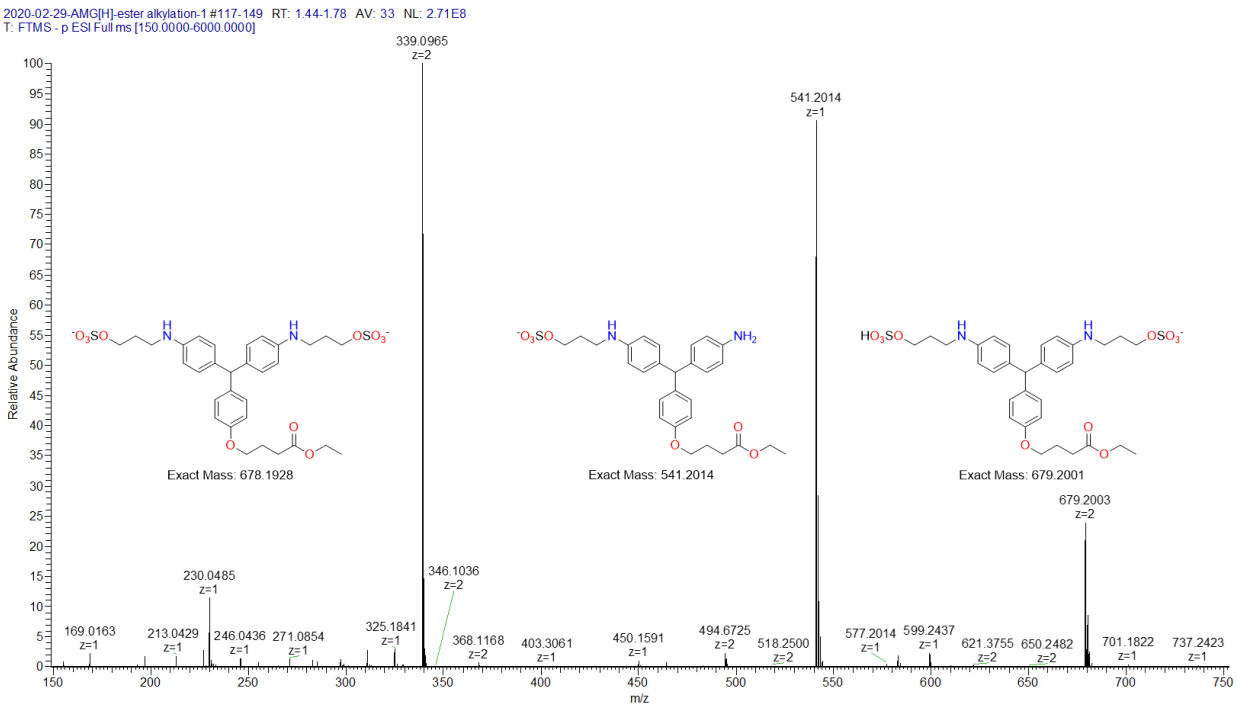


Figure 2.22 ESI-MS in a negative mode of the intermediate for AMG[H]-ester synthesis

## 2.3 Summary and outlook

We set out to make an analog of MG-ester with similar spectral characteristics but higher brightness. Synthesis of the dye was not an easy task and we are still struggling with a reproducible way of making a new dye where dimethylamino groups are substituted by azetidine groups (AMG-ester). We were not able to try the cyclization of the alkylated product in a microwave because of the time constraint, but this method looks promising so far.

AMG-ester has spectral position close to the MG-ester but with 2.4-fold higher brightness (Table 2.2). An unfortunate side effect of this modification was a shift in pKa for decolorization reaction by 2 units which made AMG-ester a poor candidate for general cell imaging.

Table 2.2. Changes in key characteristics of the fluorogen complexes after modification of the fluorophore

| | MG-ester | AMG-ester | Change |
|---|---|---|---|
| $\lambda_{max}$ (nm) PBS | 606 | 607 | + 1 nm |
| ε($M^{-1}cm^{-1}$) | 74 250 | 74 600 | + 0.5% |
| $\lambda_{ex}^{bound}$(nm) | 638 | 636 | - 2 nm |
| $\lambda_{em}^{bound}$(nm) | 668 | 658 | -10 nm |
| Brightness (φ) | 6 543 (0.12) | 15 763 (0.29) | x 2.4 |
| $pK_a$ | 8.0 | 6.0 | - 2 |

The same change, however, made AMG-ester a promising candidate for selective imaging of lysosomal proteins. We tested this hypothesis with the dye that was initially colored as well as with pre-decolorized dye and found that decolorized dye was slightly better than colorized for labeling LAMP-FAP cells (based on colocalization with Lysotracker Green) and significantly better than MG-ester.

This property of AMG-ester to generate signal only from acidic components of the cell adds another layer of selectivity to the signal generation on top of genetic targeting. This means, that we can use FAPs to measure how much of a protein we have in lysosomes (or late endosomes) only. This potential use of AMG-ester might allow to fill the niche of quantification of proteins in acidic compartments of cells since current chemogenetic labels (e.g. SNAP-tag, HaloTag) are not functional in acidic compartments while quantification based on colocalization of the signal with chemical probes such as LysoTracker possess different set of problems – it limits the scope of methods that might be used for the protein quantification and it directly influences the cell biology itself by neutralizing lysosomal pH gradients.

AMG-ester does not have those disadvantages and can be useful for developing assays for disorders that involve deviation from normal lysosomal degradation of a protein. Class of disease that involves defective activity of lysosomal proteins and trafficking of the lysosomal proteins to lysosomes can be one of the reasons of the diminished lysosomal activity[31].

A simple experiment to demonstrate the applicability of AMG-ester/dL5** system for measuring the amount of a protein in a lysosome can be measurement of relative LAMP-1 amount (which is elevated for individuals with lysosomal storage disorder)[32] modulated by propranolol which was showed to affect the size of lysosomes[33,34].

## 2.4 Materials and Methods

### Synthesis of the dye

**Ethyl 4-(4-(bis(4-aminophenyl)methyl)phenoxy)butanoate**(AmMG[H]-ester)[35].

3.2 mL of freshly distilled aniline (35 mmol), 2.36 g of the ethyl 4-(4-formylphenoxy)butanoate (10 mmol) and 0.24 g (10% w/w of the aldehyde) were stirred at 100°C under argon for 22h. After the mixture was cooled down it was fractioned between ethyl acetate and brine and washed three times with brine. Organic layer was dried over $MgSO_4$ and the solvent was removed in vacuo. Final product was purified using column chromatography with gradient elution hexane to hexane:ethyl acetate 8:2. MW $C_{25}H_{28}N_2O_3$ 404.51 g/mol, yield 0.6g (15 %).

$^1$H NMR (300 MHz, Chloroform-*d*) δ 7.02 (d, *J* = 8.8 Hz, 2H), 6.89 (d, *J* = 8.2 Hz, 4H), 6.80 (d, *J* = 8.8 Hz, 2H), 6.62 (d, *J* = 8.7 Hz, 4H), 5.30 (s, 1H), 4.16 (q, *J* = 7.1 Hz, 2H), 3.99 (t, *J* = 6.1 Hz, 2H), 3.56 (s, 5H), 2.52 (t, *J* = 7.3 Hz, 2H), 2.11 (p, *J* = 6.9 Hz, 3H), 1.27 (t, *J* = 7.1 Hz, 3H).

**Ethyl 4-(4-(bis(4-(azetidin-1-yl)phenyl)methyl)phenoxy)butanoate**(AMG[H]-ester).

223 µL (2.2 mmol) of 1,3-dibromopropane in 2 mL of dry DMF were added dropwise to a solution of 0.4 g (1 mmol) of AmMG[H]-ester and 1.99 g (6.1 mmol) of $Cs_2CO_3$ in 20 mL of dry DMF and stirred under argon for 48h at 80°C. DMF was removed in vacuo and the residual was fractioned between ethyl acetate and brine and washed five times with brine. The organic layer was dried over $MgSO_4$ and the solvent was removed in vacuo. The final product was purified using column chromatography with gradient elution hexane to hexane:ethyl acetate 8:2. MW $C_{31}H_{36}N_2O_3$ 484.64 g/mol, yield 50 mg (10 %).

$^1$H NMR (300 MHz, Chloroform-*d*) δ 7.02 (d, *J* = 8.2 Hz, 2H), 6.94 (d, *J* = 8.1 Hz, 4H), 6.79 (d, *J* = 8.4 Hz, 2H), 5.32 (s, 1H), 4.16 (q, *J* = 7.2 Hz, 2H), 3.99 (t, *J* = 6.1 Hz, 2H), 3.86 (t, *J*

= 6.9 Hz, 8H), 2.52 (t, *J* = 7.3 Hz, 2H), 2.35 (p, *J* = 6.9 Hz, 4H), 2.11 (p, *J* = 6.8 Hz, 2H), 1.28 (t, *J* = 7.2 Hz, 4H).

**1-(4-((4-(azetidin-1-yl)phenyl)(4-(4-ethoxy-4-oxobutoxy)phenyl)methylene)cyclohexa-2,5-dien-1-ylidene)azetidin-1-ium**(AMG-ester). Oxidation of the product was performed by boiling in acetonitrile with an excess of the p-chloranil. After 6h of boiling mixture was cooled down, filtered and solid was washed with acetonitrile. The solvent was removed under reduced pressure and the product was purified using chloroform to chloroform:ethanol 8.5:1.5 gradient. MW Chemical Formula: $C_{31}H_{35}N_2O_3^+$ 483.63 g/mol.

**NMR**

$^1$H NMR spectra were recorded using Bruker Avance™ 300 instrument and analyzed using Mestre Nova 11.0.2-18153 software. Chloroform-d used for spectra was purchased from Cambridge Isotope Laboratories.

**Imaging**

Imaging of the cells was carried on Andor Revolution XD Spinning Disk with a 60x objective. Cells were placed in the imaging media (HBSS buffer) and incubated in this buffer for 30 minutes to exclude the possibility of the media change influence the imaging results. After the addition of the dye, solution cells were incubated in 37°C incubator. If imaging experiment was longer than 30 minutes stage incubator was used to control temperature, $CO_2$ content, and humidity. For each sample, at least three fields of view were collected. Fields of view were manually separated into regions of interest corresponding to different cells and the statistical analysis was performed using GraphPad Prism 6.01 software.

**Flow cytometry**

All flow cytometry experiments were performed with FAP-BK cells or WT HEK 293 cells as a control. Cells were incubated with an appropriate concentration of the dye (or ethanol) in cell culturing media overnight. Next day media was removed, and cells were detached from the surface by incubation with 5mmol EDTA (containing a dye of the same concentration) for 5 minutes and transferred to a 96 round-bottom plate. Flow cytometry was performed on the Accuri flow cytometer and obtained data was analyzed using FlowJo 10.0.8r1 software.

**Kinetic studies**

Fluorescence activation kinetics was measured using Tecan M1000. Prior to the experiment injector was washed with DI water and 70% Ethanol several times. Before the actual experiment 2mL of the dye solution were dispensed into empty wells of 96-well plate. 50 µL of decolorized dye stock (made by overnight incubation at room temperature in PBS) were injected to 200 µL of protein solution. The final concentration of the dye and protein are 200 nM. First, 20 minutes fluorescence data was measured as fast as instrument permitted, the following hour – every 10 seconds.

For activation kinetics in cells (figure 6) after time-lapses have been acquired each field of view was divided in regions of interest which contained individual cells if cells were spread enough. Average of mean fluorescence of each cell were used to plot final data. In the case of MG-ester kinetics 9 cells were used, AMG-ester 1.5 µM – 14 cells, 3 µM – 7 cells.

**Fluorescence Correlation Spectroscopy**

Samples of dye and protein (1 µM each) with 0.1% BSA were incubated overnight at 4°C. Before the imaging, samples were centrifuged for 40 minutes and only top part was used (to avoid any aggregates that might have formed) and diluted to a final concentration of 20 nM. FCS

measurements were performed according to the instrument recommendations (were dialed by Haibing Teng). Binning time for PCH was set to 20 μs.

**Dye labeling test with FAP-TM cells**

FAP-TM cells were incubated in a media (HBSS or pH 5 high Potassium Nigericin clamping media) for specified period of time (25 minutes for pH 5 and 40 minutes for pH 7.4) with 400 nM of colorized (diluted in pH 5 buffer and incubated overnight) or decolorized (diluted in pH 7.4 PBS and incubated overnight) dye. After the appropriate incubation time, several fields of view for each plate were acquired with laser power set to 20%.

**LAMP-FAP experiment**

FAP-LAMP1 cells were incubated with 100 μM chloroquine for 24h, with 21 μM Leupeptin for 4h, 400 nM AMG-ester was added 40 minutes before imaging (in the case of colorized dye it was added from pH 5 stock, in case of decolorized dye media with the dye was incubated overnight at 4°C), 45 nM Lysotracker Green was added 5 minutes prior to imaging.

**Colorization and decolorization tests**

To 248 μL of buffer (pH 5.0 for photostability test and recolorization test and pH 7.4 for decolorization test, ionic strength of buffers was matched) 2 μL of EtOH stock of dye were added (2.43 mM stock for photostability and decolorization tests, twice diluted stock with 10% KOH was used as decolorized stock). Resulting solutions were mixed and absorption at 606 nm was monitored over the course of 14 h.

## 2.5 References


(1) Shimomura, O.; Johnson, F. H.; Saiga, Y. Extraction, Purification and Properties of Aequorin, a Bioluminescent Protein from the Luminous Hydromedusan,Aequorea. *J. Cell. Comp. Physiol.* **1962**, *59* (3), 223–239. https://doi.org/10.1002/jcp.1030590302.

(2) Specht, E. A.; Braselmann, E.; Palmer, A. E. A Critical and Comparative Review of Fluorescent Tools for Live-Cell Imaging. *Annu. Rev. Physiol.* **2017**, *79* (1), 93–117. https://doi.org/10.1146/annurev-physiol-022516-034055.

(3) Leonetti, M. D.; Sekine, S.; Kamiyama, D.; Weissman, J. S.; Huang, B. A Scalable Strategy for High-Throughput GFP Tagging of Endogenous Human Proteins. *Proc. Natl. Acad. Sci. U. S. A.* **2016**, *113* (25), E3501–E3508. https://doi.org/10.1073/pnas.1606731113.

(4) Perkins, L. A.; Bruchez, M. P. Fluorogen Activating Protein Toolset for Protein Trafficking Measurements. *Traffic* **2020**, *21* (4), 333–348. https://doi.org/10.1111/tra.12722.

(5) Özhalici-Ünal, H.; Pow, C. L.; Marks, S. A.; Jesper, L. D.; Silva, G. L.; Shank, N. I.; Jones, E. W.; Burnette, J. M.; Berget, P. B.; Armitage, B. A. A Rainbow of Fluoromodules: A Promiscuous ScFv Protein Binds to and Activates a Diverse Set of Fluorogenic Cyanine Dyes. *J. Am. Chem. Soc.* **2008**, *130* (38), 12620–12621. https://doi.org/10.1021/ja805042p.

(6) Szent-Gyorgyi, C.; Schmidt, B. A.; Creeger, Y.; Fisher, G. W.; Zakel, K. L.; Adler, S.; Fitzpatrick, J. A. J.; Woolford, C. A.; Yan, Q.; Vasilev, K. V; Berget, P. B.; Bruchez, M. P.; Jarvik, J. W.; Waggoner, A. Fluorogen-Activating Single-Chain Antibodies for Imaging Cell Surface Proteins. *Nat. Biotechnol.* **2008**, *26* (2), 235–240.

https://doi.org/10.1038/nbt1368.

(7) Pratt, C. P.; He, J.; Wang, Y.; Barth, A. L.; Bruchez, M. P. Fluorogenic Green-Inside Red-Outside (GIRO) Labeling Approach Reveals Adenylyl Cyclase-Dependent Control of BKα Surface Expression. *Bioconjug. Chem.* **2015**, *26* (9), 1963–1971. https://doi.org/10.1021/acs.bioconjchem.5b00409.

(8) Zhang, Q.; Wang, Q.; Sun, Y.; Zuo, L.; Fetz, V.; Hu, H. Y. Superior Fluorogen-Activating Protein Probes Based on 3-Indole-Malachite Green. *Org. Lett.* **2017**, *19* (17), 4496–4499. https://doi.org/10.1021/acs.orglett.7b02055.

(9) Naganbabu, M.; Perkins, L. A.; Wang, Y.; Kurish, J.; Schmidt, B. F.; Bruchez, M. P. Multiexcitation Fluorogenic Labeling of Surface, Intracellular, and Total Protein Pools in Living Cells. *Bioconjug. Chem.* **2016**, *27* (6), 1525–1531. https://doi.org/10.1021/acs.bioconjchem.6b00169.

(10) Perkins, L. A.; Yan, Q.; Schmidt, B. F.; Kolodieznyi, D.; Saurabh, S.; Larsen, M. B.; Watkins, S. C.; Kremer, L.; Bruchez, M. P. Genetically Targeted Ratiometric and Activated PH Indicator Complexes (TRApHIC) for Receptor Trafficking. *Biochemistry* **2018**, *57* (5), 861–871. https://doi.org/10.1021/acs.biochem.7b01135.

(11) He, J.; Wang, Y.; Missinato, M. A.; Onuoha, E.; Perkins, L. A.; Watkins, S. C.; St Croix, C. M.; Tsang, M.; Bruchez, M. P. A Genetically Targetable Near-Infrared Photosensitizer. *Nat. Methods* **2016**, *13* (3), 263–268. https://doi.org/10.1038/nmeth.3735.

(12) Grimm, J. B.; English, B. P.; Chen, J.; Slaughter, J. P.; Zhang, Z.; Revyakin, A.; Patel, R.; Macklin, J. J.; Normanno, D.; Singer, R. H.; Lionnet, T.; Lavis, L. D. A General Method to Improve Fluorophores for Live-Cell and Single-Molecule Microscopy. *Nat. Methods* **2015**, *12* (3), 244–250. https://doi.org/10.1038/nmeth.3256.

(13) Hou, J.-T.; Gao, J.-W.; Zhang, Z.-H. An Efficient and Convenient Protocol for the Synthesis of Diaminotriarylmethanes. *Monatshefte für Chemie - Chem. Mon.* **2011**, *142* (5), 495–499. https://doi.org/10.1007/s00706-011-0461-2.

(14) He, J. Utilizing Malachite Green Derivatives to Diversify Fluorogen- Activating Proteins ( FAPs )' Applications, Carnegie Mellon University, 2016. https://doi.org/10.1184/R1/10059941.v1.

(15) Cerichelli, G.; Luchetti, L. Ring-Opening Reactions. Stability and Reactivity of Aziridinum and Azetidinium Ions in Solution. *J. Chem. Soc. Chem. Commun.* **1985**, No. 6, 339. https://doi.org/10.1039/c39850000339.

(16) Ismailov, V. M.; Mamedov, I. A.; Yusubov, N. N. Aniline Alkylation with Di- and Tribromopropane. *Russ. J. Org. Chem.* **2009**, *45* (8), 1250–1251. https://doi.org/10.1134/S1070428009080247.

(17) Wang, Y.; Telmer, C. A.; Schmidt, B. F.; Franke, J. D.; Ort, S.; Arndt-Jovin, D. J.; Bruchez, M. P. Fluorogen Activating Protein–Affibody Probes: Modular, No-Wash Measurement of Epidermal Growth Factor Receptors. *Bioconjug. Chem.* **2015**, *26* (1), 137–144. https://doi.org/10.1021/bc500525b.

(18) Szent-Gyorgyi, C.; Stanfield, R. L.; Andreko, S.; Dempsey, A.; Ahmed, M.; Capek, S.; Waggoner, A. S.; Wilson, I. A.; Bruchez, M. P. Malachite Green Mediates Homodimerization of Antibody VL Domains to Form a Fluorescent Ternary Complex with Singular Symmetric Interfaces. *J. Mol. Biol.* **2013**, *425* (22), 4595–4613. https://doi.org/10.1016/j.jmb.2013.08.014.

(19) Telmer, C. A.; Verma, R.; Teng, H.; Andreko, S.; Law, L.; Bruchez, M. P. Rapid, Specific, No-Wash, Far-Red Fluorogen Activation in Subcellular Compartments by

Targeted Fluorogen Activating Proteins. *ACS Chem. Biol.* **2015**, *10* (5), 1239–1246. https://doi.org/10.1021/cb500957k.

(20) Wang, Y. Labeling and Photo-Manipulation of Endogenous Protein, Carnegie Mellon University, 2015.

(21) Carpenter, M. Tie-Dyes for Detection of Protein Interactions. A Tool Towards Fluorescence Based Detection of Synapses, 2019. https://doi.org/10.1184/R1/10008563.v1.

(22) Pratt, C. P.; Kuljis, D. A.; Homanics, G. E.; He, J.; Kolodieznyi, D.; Dudem, S.; Hollywood, M. A.; Barth, A. L.; Bruchez, M. P. Tagging of Endogenous BK Channels with a Fluorogen-Activating Peptide Reveals B4-Mediated Control of Channel Clustering in Cerebellum. *Front. Cell. Neurosci.* **2017**, *11* (October), 1–18. https://doi.org/10.3389/fncel.2017.00337.

(23) Perkins, L. Built for the Dye-Way: Fluorogenic Tools for Protein Traffic, Carnegie Mellon University, 2018. https://doi.org/10.1184/R1/6715046.v1.

(24) Jackson, M. P.; Hewitt, E. W. Cellular Proteostasis: Degradation of Misfolded Proteins by Lysosomes. *Essays Biochem.* **2016**, *60* (2), 173–180. https://doi.org/10.1042/EBC20160005.

(25) Fletcher, R. A.; Pilcher, G. Measurements of Heats of Combustion by Flame Calorimetry. Part 6. - Formaldehyde Glyoxal. *Trans. Faraday Soc.* **1970**, *66*, 794–799. https://doi.org/10.1039/TF9706600794.

(26) Goethals, E. J.; Schacht, E. H.; Bogaert, Y. E.; Ali, S. I.; Tezuka, Y. The Polymerization of Azetidines and Azetidine Derivatives. *Polym. J.* **1980**, *12* (9), 571–581. https://doi.org/10.1295/polymj.12.571.

(27) Ju, Y.; Varma, R. S. Aqueous N-Heterocyclization of Primary Amines and Hydrazines with Dihalides: Microwave-Assisted Syntheses of N -Azacycloalkanes, Isoindole, Pyrazole, Pyrazolidine, and Phthalazine Derivatives. *J. Org. Chem.* **2006**, *71* (1), 135–141. https://doi.org/10.1021/jo051878h.

(28) Bird, R.; Knipe, A. C.; Stirling, C. J. M.; Sciences, M.; Wales, N. Intramolecular Reactions. Part X. Transition States in the Cyclisation of N-ω-Halogeno-Alkylamines and Sulphonamides. *J. Chem. Soc. Perkin Trans. 2* **1973**, No. 9, 1215–1220. https://doi.org/10.1039/P29730001215.

(29) Barak, S. The Condensation of 2-Aminofluorene with α, ω-Dibromoalkanes. *Isr. J. Chem.* **1968**, *6* (4), 471–476. https://doi.org/10.1002/ijch.196800060.

(30) Burkett, B. A.; Ting, S. Z.; Gan, G. C. S.; Chai, C. L. L. Microwave-Assisted Synthesis of Azetidines in Aqueous Media. *Tetrahedron Lett.* **2009**, *50* (47), 6590–6592. https://doi.org/10.1016/j.tetlet.2009.09.063.

(31) Futerman, A. H.; van Meer, G. The Cell Biology of Lysosomal Storage Disorders. *Nat. Rev. Mol. Cell Biol.* **2004**, *5* (7), 554–565. https://doi.org/10.1038/nrm1423.

(32) Meikle, P. J.; Yan, M.; Ravenscroft, E. M.; Isaac, E. L.; Hopwood, J. J.; Brooks, D. a. Altered Trafficking and Turnover of LAMP-1 in Pompe Disease-Affected Cells. *Mol. Genet. Metab.* **1999**, *66*, 179–188. https://doi.org/10.1006/mgme.1998.2800.

(33) Logan, R.; Kong, A. C.; Krise, J. P. Time-Dependent Effects of Hydrophobic Amine-Containing Drugs on Lysosome Structure and Biogenesis in Cultured Human Fibroblasts. *J. Pharm. Sci.* **2014**, *103* (10), 3287–3296. https://doi.org/10.1002/jps.24087.

(34) Logan, R.; Kong, A.; Krise, J. P. Evaluating the Roles of Autophagy and Lysosomal Trafficking Defects in Intracellular Distribution-Based Drug-Drug Interactions Involving

Lysosomes. *J. Pharm. Sci.* **2013**, *102* (11), 4173–4180. https://doi.org/10.1002/jps.23706.

(35) Guzmán-Lucero, D.; Guzmán, J.; Likhatchev, D.; Martínez-Palou, R. Microwave-Assisted Synthesis of 4,4′-Diaminotriphenylmethanes. *Tetrahedron Lett.* **2005**, *46* (7), 1119–1122. https://doi.org/10.1016/j.tetlet.2004.12.091.

# 3 DIHBI (NEW FAP-TAP SYSTEM BASED ON THE MIMIC OF THE GFP FLUOROPHORE)

Reactive Oxygen Species (ROS) are presented natively in the biological systems. These species are short-lived and highly reactive. Examples of these ROS are Singlet Oxygen ($^1O_2$), superoxide anion ($O_2^-$), hydroxy peroxide ($H_2O_2$), hydroxy radical ($HO\cdot$). Endogenous ROS generation was initially attributed to be a byproduct of the mitochondrial respiratory chain[1] but more sources of native and environmental ROS have been unveiled[2] (Figure 3.1).

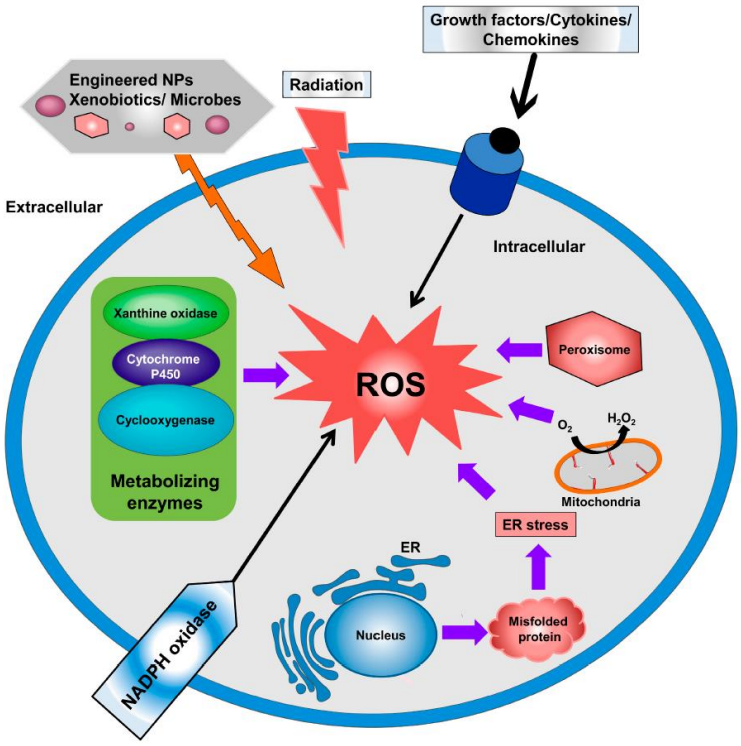


Figure 3.1 ROS can be generated by a number of different pathways. Modified from Figure 1 in Dayem et al, 2017[3]

ROS has been shown to be involved in a wide range of activities including inflammatory and metabolic signaling,[4] receptor-like kinase signaling in plants[5] as well as signaling within and

between cells depending on the organism[6]. It is hard to overstate the importance of the roles ROS fulfill for a normal cell and organism function.

Being highly reactive, ROS can react with varied cellular components and is implicated in a number of cell death pathways (Figure 3.2). This property of modifying cellular components as well as triggering cell death makes ROS producing molecules potential therapeutic agents.

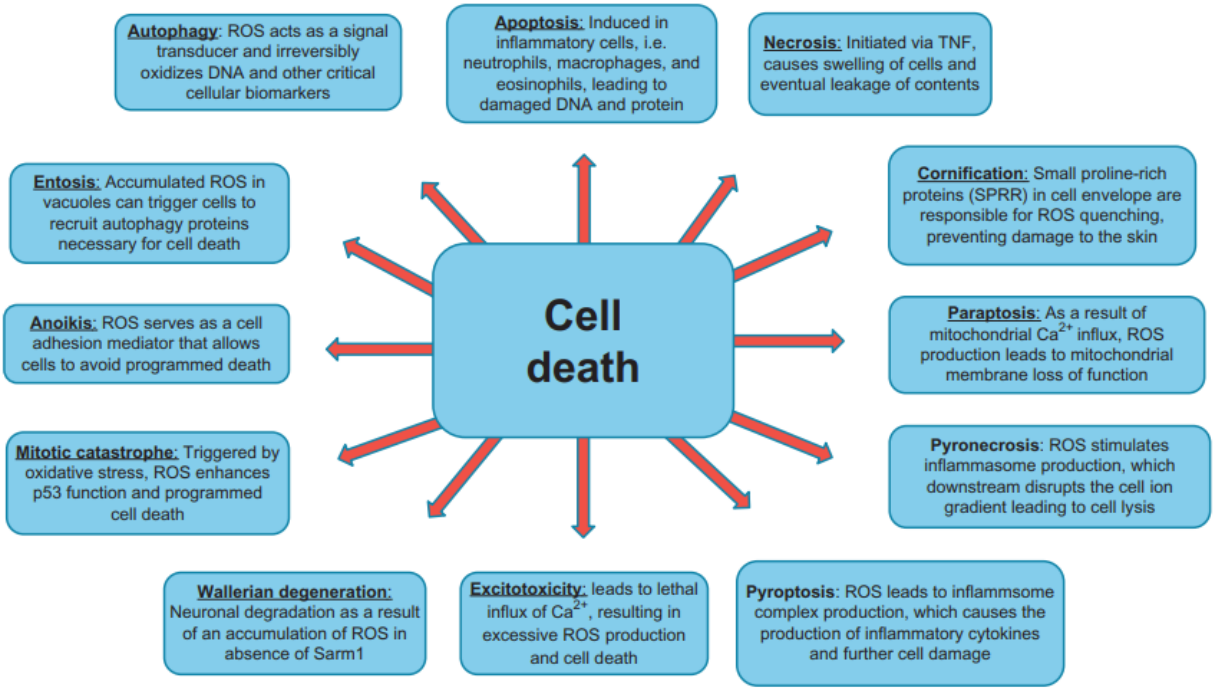


Figure 3.2 Cell death pathways that involve ROS. Modified from figure 4.2 in Ghosh et al, 2017[7]

Agents that can generate ROS from light are called photosensitizers. This large group of agents includes proteins[8], dyes[9], nanoparticles[10] and others. Most widespread systems for ROS production can be divided into two categories: molecules that contain either large conjugated systems such as porphyrins, fullerenes, and phthalocyanines[11] or the presence of heavy atoms such as iodine, bromine or sulfur[12,13].

While dye-based photosensitizers have great flexibility in spectral properties and can be modified if necessary, targeting of specific location in the cell with a particular photosensitizer molecule has proven to be challenging. Chemical targeting is not easy – it is possible to target cell components that have distinct environments like different pH for lysosomes and late endosome or hydrophobic environment of the membranes. This level of control does not allow for genetic targeting of specific proteins or discrimination between many similar organelles in the cell.

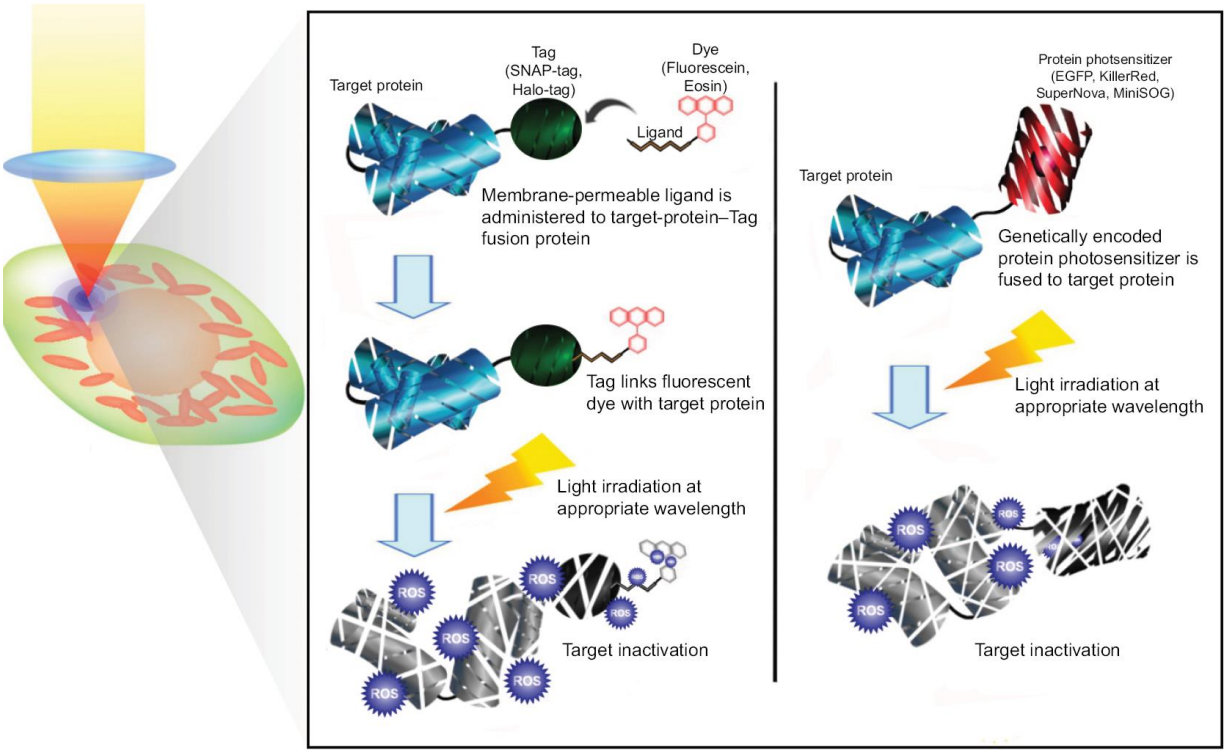


Figure 3.3 Proteins can be genetically targeted with ROS-producing species in two different ways – either with photosensitizer protein or with a tag that a photosensitizer will target and modify. Modified from Figure 1 in Sano et al, 2014[14]

One of the most established ways for specific targeting in biological systems is with genetically encoded proteins. This targeting can be achieved in two general ways – either by

encoding a photosensitizer protein or a encoding targeting protein and subsequently attaching the photosensitizer to it (Figure 3.3).

Encodable photosensitizers, such as miniSOG[15] or KillerRed[8] lack temporal control – they will be activated any time light shines on them. There is a similar issue for the system based on targeting of photosensitizers to a location based on the expressed tags such as SNAP-tag[16]. These systems can have some degree of temporal control based on the addition of the photosensitizer, but it creates a problem of background ROS generation since photosensitizer is active when bound and unbound to the targeting protein.

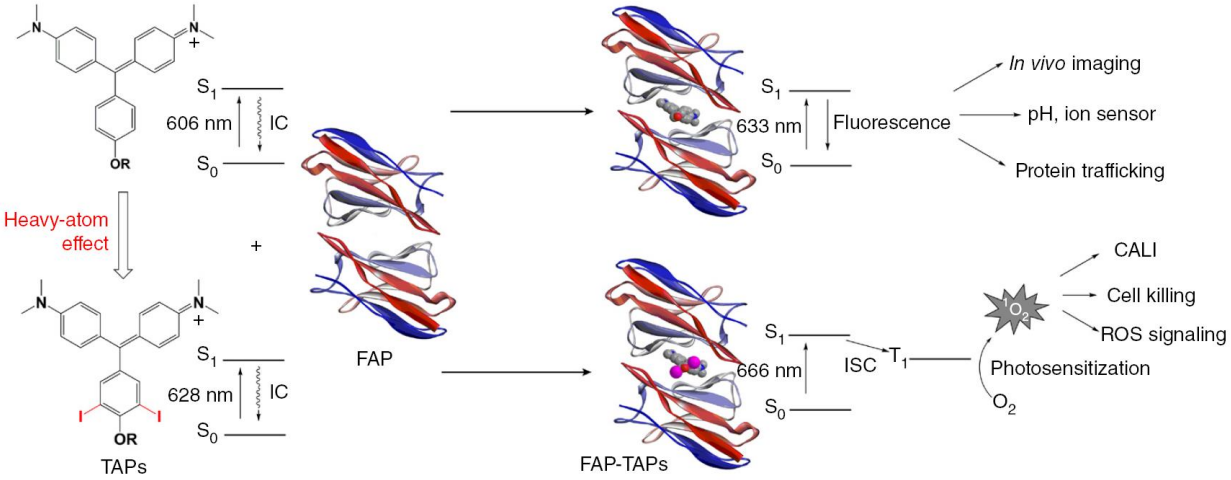


Figure 3.4 Addition of iodine (as a heavy atom) to MG-ester results in a change from activation of fluorescence to singlet oxygen generation. Modified from Figure 1 in He et al, 2016[18]

MG-aptamer (RNA aptamer for Malachite Green) was one of the first examples of a system where ROS generation activates only for a complex but not for the components alone[17]. This approach potentially allows for precise targeting of the ROS generation, low background, and good control over the dose of the ROS being delivered to the system.

Table 3.1 Recent publications using MG-2I for targeted damage

| Title | Target | System | Brief description of work | Reference |
|---|---|---|---|---|
| Antibody-Linked Fluorogen-Activating Proteins for Antigen Detection and Cell Ablation | EGFR | Mammalian cells (HaCaT, A431) | Selective targeting and ablation of EGFR-expressing cells using antibody-FAP conjugate and MG-2I coupled with light | 19 |
| Chemoptogenetic damage to mitochondria causes rapid telomere dysfunction | Mitochondria | HEK293 | Selective ROS-induce damage to mitochondria leads to telomere damage without general DNA damage | 20 |
| Targeted and Persistent 8-Oxoguanine Base Damage at Telomeres Promotes Telomere Loss and Crisis | Telomere | HeLa | 8-oxo guanine formation in telomeres promotes their shortening and, after complete telomere loss, causes dicentric chromosomes and anaphase bridges. | 21 |
| Chemoptogenetic Ablation of Neuronal Mitochondria in Vivo with Spatiotemporal Precision and Controllable Severity | Mitochondria | Zebrafish neurons | New tool allows for neuronal damage of varying intensity in zebrafish with spatiotemporal control | 22 |

Previously, our lab reported[18] an MG-ester analog, MG-2I, that is activated to generate singlet oxygen and fluorescence only when bound to a fluorogen activating protein (FAP) and excited with far-red light (Figure 3.4). The unique properties of this system provide a very reliable and controlled method to localize singlet oxygen generation by chemoptogenetic targeting with activation achieved only by addition of the MG2I dye and excitation with suitable light. The short range of singlet oxygen activity in live cells (~20 nm) opens the possibility of

targeted ablation of specific proteins with very high spatiotemporal control (Table 3.1). Having a fluorogenic system that operates in a different spectral window from MG-2I would allow us to create a framework for acute inaction of two different proteins in a living cell under chemoptogenetic control.

Although spectral tuning of fluorogens for activation by a single FAP has been demonstrated[23–26], the FAP-TAPS system established with MG2I, however, relies on structural modifications that are incompatible with those used to shift spectral properties of the MHN-ester/dL5** complex (to 456 nm excitation and 532 nm emission for the complex). In the MHN fluorogen, the base aromatic ring where heavy atoms were introduced in MG-2I has been removed (Figure 3.5)[24]. Modifications of the smaller fluorogen with bulky heavy atom substituents may have a pronounced negative impact on the binding and activation of the MHN fluorogen since the crystal structure of the dL5** interacting with MG-based fluorogen suggests lack of free space in the region of the where the fluorophore of MHN-ester should bind[27].

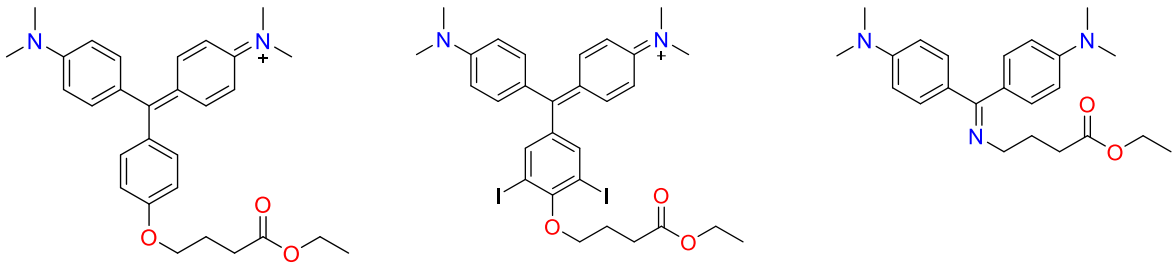

MG-ester
633 nm/668 nm

MG-2I
666 nm/693 nm

MHN-ester
456 nm/532 nm

Figure 3.5 Variations to MG-ester bring new properties – ROS generation (MG-2I) or different spectral region (MHN-ester); excitation/emission wavelength of complexes with dL5** listed below each fluorogen

To create a fluorogen with ROS generation in a different spectral window we sought to modify another fluorogen by introducing heavy atoms to the conjugated system. Another advantage of using another fluorogen-activator protein pair is that in addition to spectral diversity, we also obtain chemoselectivity, with different ligands potentially recognized only by their cognate activator protein.

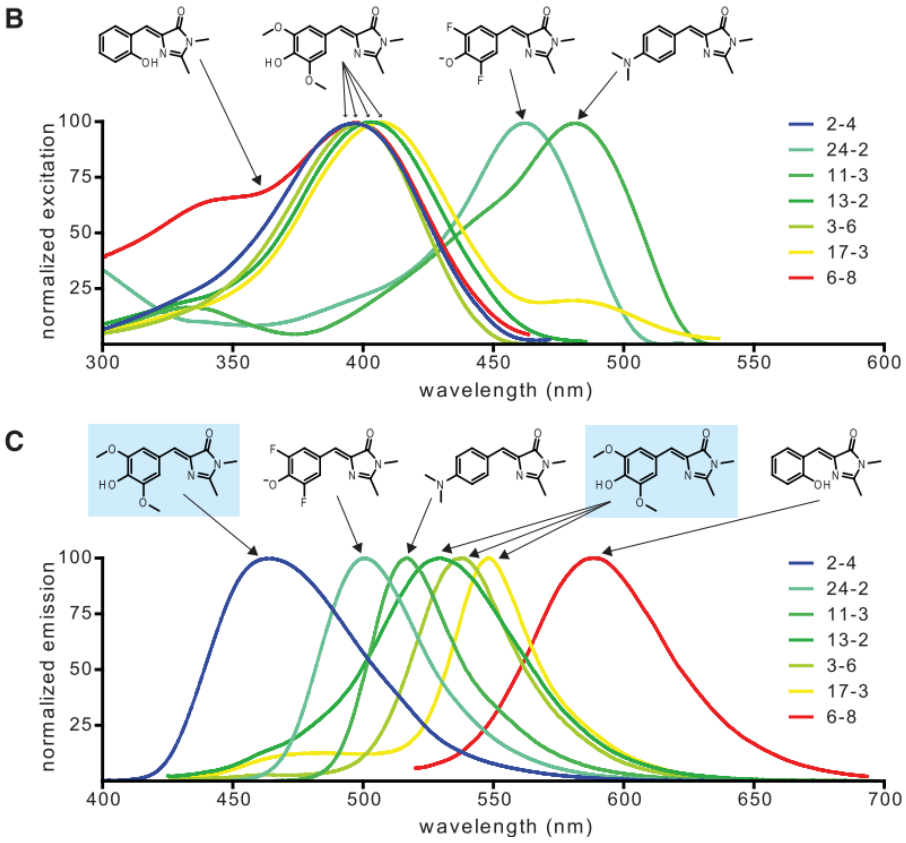


Figure 3.6 Fluorescence spectra of GFP analogs bound to selected RNA aptamers. Modified from Figure 2 in Paige et al, 2011[29]

As the fluorophore of one of the most used fluorescent proteins eGFP, HBI, and its analogs, were a crucial part of the development of fluorescent RNAs and more recently – engineered dye-activating proteins. The potential fluorogenic properties of chemically modified GFP chromophore were first recognized by Laren Tolbert[28] and exploited in the RNA mimics of

green fluorescent protein[29] the Jaffrey lab used SELEX[30] to generate aptamers for analogs of HBI with various spectral properties (Figure 3.6). A critical feature of these HBI-scaffold fluorogens is that they are very low fluorescence background and are not easily activated by binding to biological components due to the unique and efficient relaxation pathways of the free molecule's electronic excited state. Nevertheless, bound to a suitable specific biomolecule, these dye-biomolecule complexes can show high molecular brightness and very strong activation properties when compared to larger fluorogen dyes such as malachite green and its derivatives.

Later work was done to improve properties of the best aptamer-dye pair (DFHBI dye, Figure 3.7, and Spinach aptamer), including structural studies[31,32], additional selections[33–35], and various applications of the aptamer[36–40]. Even though modifications to the aptamer change binding to the dye as well as spectral properties, modification of the dye has the potential to affect these properties to a much larger degree. The Jaffrey lab developed[41] a couple of new fluorophores that bind to the same aptamer as the original DFHBI (Spinach2[42]) with similar $K_d$ but having higher brightness.

Complexes of DFHBI analogs with aptamers have high brightness and were used in several ways to track metabolites[43] and mRNAs[44] in cellular environments. This is definitely an improvement on the original complex but it preserves the inherent limitation of the system in terms of variability of applications – there are almost no points for modification on the DFHBI to introduce new functionality and nucleic acid binding partner means that targeting anything but nucleic acids requires significant effort. To target a specific small molecule or a protein one would have to obtain an aptamer for that target and conjugate these two aptamers together[45]. This has the potential to create systems where fluorogen activation is dependent on target binding[46].

Table 3.2 Properties of the DFHBI and DFHBI-1T with mFAP2a/b. Based on the data from[47]

| | $\lambda_{ex}$ (nm) | $\lambda_{em}$ (nm) | ε ($M^{-1}cm^{-1}$) | Q.Y. | Kd (μM) | Brightness ($M^{-1}cm^{-1}$) |
|---|---|---|---|---|---|---|
| DFHIB | 423 | 489 | 30100 | 0.001 | - | - |
| DFHBI/mFAP2a | 491 | 505 | 64900 | 0.060 | 0.15 | 3890 |
| DFHBI/mFAP2b | 495 | 509 | 60500 | 0.093 | 1.8 | 5630 |
| DFHBI-1T | 426 | 495 | 35400 | - | - | - |
| DFHBI-1T/mFAP2a | 493 | 505 | 75100 | 0.129 | 5.8 | 9690 |
| DFHBI-1T/mFAP2b | 494 | 505 | 37800 | 0.005 | 11 | 189 |

Recently, de novo designed binding proteins for DFHBI[48] fluorogens were reported, providing a genetically targetable DFHBI binding and activating protein system. These proteins (mFAP2a and mFAP2b) bind to DFHBI and DFHBI-1T[49] with micromolar affinities and activate fluorescence by a factor of at least 60. They were expressed in yeast, bacteria, and COS-7 cells with low background after labeling with fluorogen.

Given our own results with halogen substitutions in the MG chromophore system, we prepared a HBI variant modified from DFHBI by substituting the fluorines with iodines (Figure 3.7) to obtain DIHBI which might have potential to be a ROS generator, with favorable spectral properties, high activation upon binding, and the potential for selective genetic targeting and independent activation compatible with the dL5-MG2I FAP-TAPS system. We chose this chromophore over other fluorogens like OTB[50] and TO[51] mostly because of the low background signal and great compatibility with biological systems.

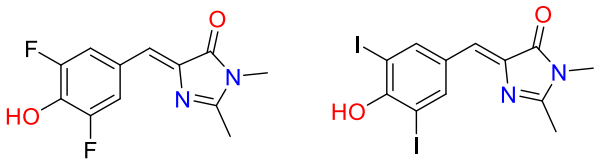


Figure 3.7 Structure of DFHBI and it is proposed analog DIHBI

## 3.1 Results and discussion

Synthesis of the new dye (Figure 3.8) was performed similarly to the original method published by J. Paige[29] with adjusted solvent volumes and different purification method for the final product.

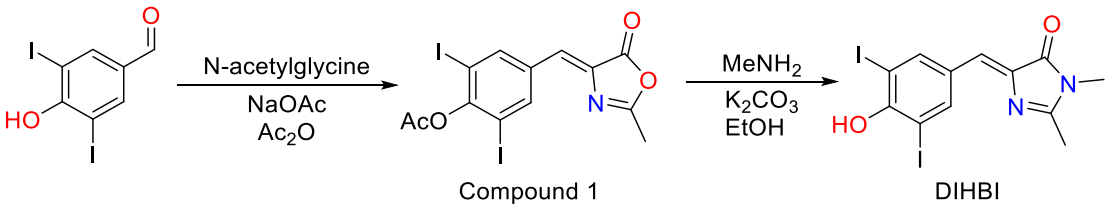


Figure 3.8 Synthetic scheme for DIHBI

In comparison to the best known fluorogen for Spinach (DFHBI-1T), DIHBI shows a lower extinction coefficient (26700 $M^{-1}cm^{-1}$ for DIHBI vs 35400 $M^{-1}cm^{-1}$ for DFHBI-1T[41], Figure 3.9). DIHBI shows a noticeable shift in the absorption spectrum in comparison to DFHBI-1T (430 nm vs 420 nm). To evaluate these dyes in these proteins we initiated a collaboration with the Baker Lab and Institute for Protein Design at University of Washington, who provided the proteins necessary for biochemical and spectroscopic characterization. Upon binding the protein mFAP2b, the absorption maximum for DIHBI shifts from 428 nm to 498 nm (Figure 3.10) which is similar to what was observed upon binding of DFHBI to mFAP2b[48].

The emission spectrum for DIHBI/mFAP2b shows a maximum at 514 nm (Figure 3.11). With absorption maximum at 498 nm this complex demonstrates Stokes shift similar to DFHBI-1T and DFHBI when complexed to mFAP2b. These measurements were carried out in excess dye (10µM dye and 180nM mFAP2b) and were not suitable for the fold activation measurement. To determine extinction coefficient of the dye-mFAP2b complex we have made a sample containing 500 nM dye and 2.5 µM mFAP2b and it was found to be 46700 $M^{-1}cm^{-1}$ (at 495 nm).

DFHBI displays similar behavior, roughly doubling its extinction coefficient from 30100 $M^{-1}cm^{-1}$ to 60500 $M^{-1}cm^{-1}$ upon binding to mFAP2b[47].

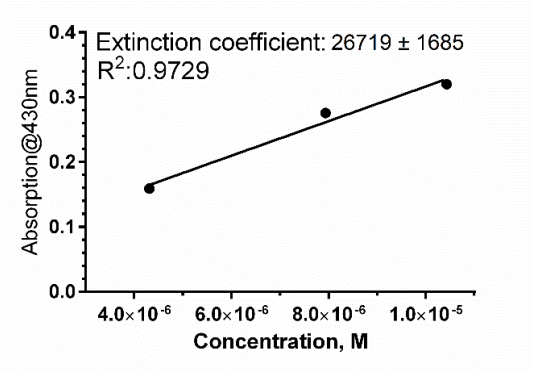


Figure 3.9 Extinction coefficient of DIHBI

The fluorescence quantum yield of the DIHBI/mFAP2b was found to be 0.70 (using fluorescein (0.97) as a standard in 0.1 M NaOH[52]). These spectroscopic properties establish DIHBI/mFAP2b brightness (quantum yield x extinction coefficient) of 32700 which is close to the brightness of eGFP[53] (33600), higher than DFHBI-1T/Spinach2[41] (29140), and much higher than mFAP2b/DFHBI-1T (189) or mFAP2a/DFHBI-1T (9690)[47].

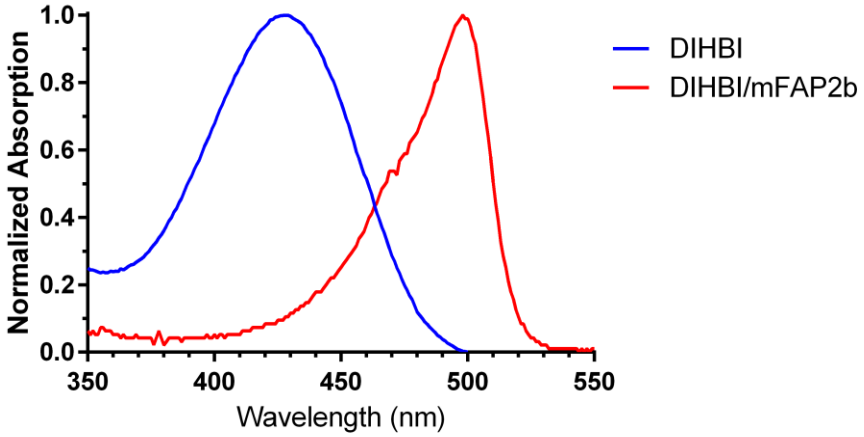


Figure 3.10 Change in the absorption spectrum of DIHBI upon binding to mFAP2b (10 µM dye for dye only sample; 500 nM dye, 2.5 µM mFAP2b)

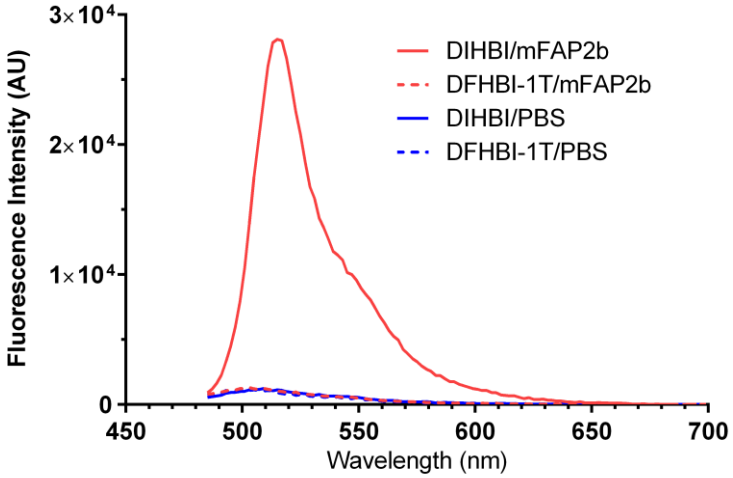


Figure 3.11 Changes in fluorescence spectra of DFHBI-1T and DIHBI upon binding to mFAP2b (10 µM dye with 200 nM mFAP2b, excitation wavelength 460 nm)

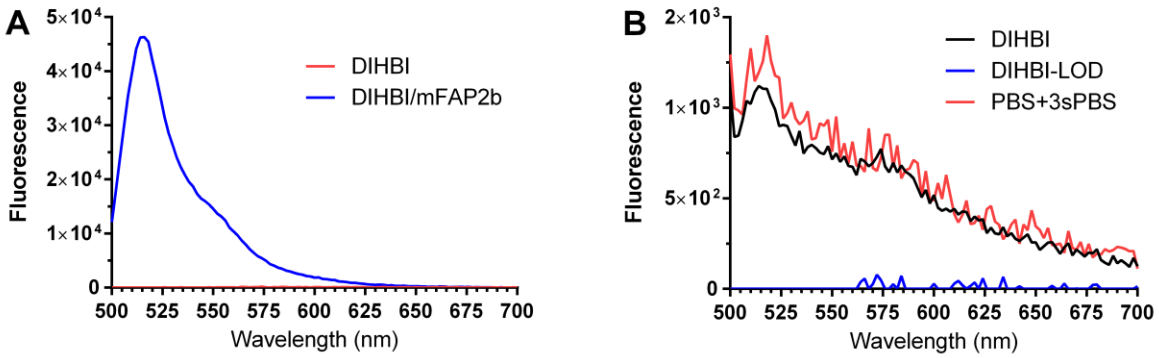


Figure 3.12 Fluorescence activation of DIHBI (200nM) with mFAP2b (3.4µM) in PBS (A) and closer look at the DIHBI signal after accounting for the PBS blank sample signal levels (B) to establish the Limit of Detectability in the plate reader.

Fluorescence fold activation of the DIHBI upon binding to the excess mFAP2b (200 nM dye, 3.4 µM protein, Figure 3.12A) is practically infinite since using the same gain almost no fluorescence signal from DIHBI alone was detected. To make sure that the observed signal from DIHBI is not noise we have checked what portion of the signal is above 3 standard deviations of the signal obtained from PBS alone (Figure 3.12B). There is almost no signal from DIHBI (black

line) that is above signal from PBS+3σ (red line). There are only several data points where DIHBI is higher (blue line). From this data we conclude that fold activation for DIHBI is practically infinite as we are not able to reliably detect signal from the dye and the complex using the same settings of the detector.

DIHBI can exist in two forms – phenol and phenolate which have different spectral properties. Only phenolate form is colored so it is important to have phenolate form present at cellular pH to get absorption of the light. According to the pH titration experiment presented in Figure 3.13, the $pK_a$ for DIHBI in aqueous solution is 5.3. This means that in all the cellular environments except for lysosomes and late endosomes[54] the dye should be mostly in the deprotonated, colorized phenolate form.

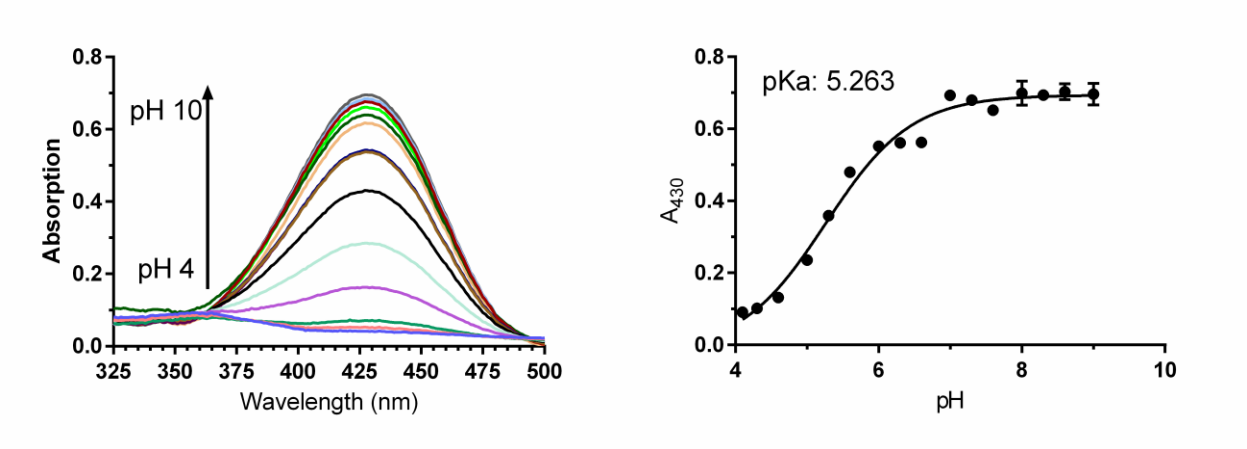


Figure 3.13 $pK_a$ test of DIHBI

DIHBI binds to mFAP2b with apparent $K_d$ of 2.2 nM (Figure 3.14) that is higher than both DFHBI and DFHBI-1T (1.83μM and 10.53μM respectively[47]) which is surprisingly tight for a protein that was designed for a similar but different target. This is not a unique case of a protein selected for one target demonstrating high affinity to other dyes[23]. This promiscuity of binding suggests the flexibility of the binding site in the protein since it can accommodate a

substitution of fluorine atoms with iodine which are much larger and can cause steric clash. (in our experiments with MG-2I substitution of hydrogen to iodine caused a drop in Kd from 7 pM for MG-ester to 122 pM for MG-2I)[18]. DIHBI binds to mFAP2a with $K_d$ of 0.77μM that falls between DFHBI (0.15μM) and DFHBI-1T (5.8μM)[47]. Unfortunately, due to limited quantities of mFAP2a we were not able to conduct any further experiments.

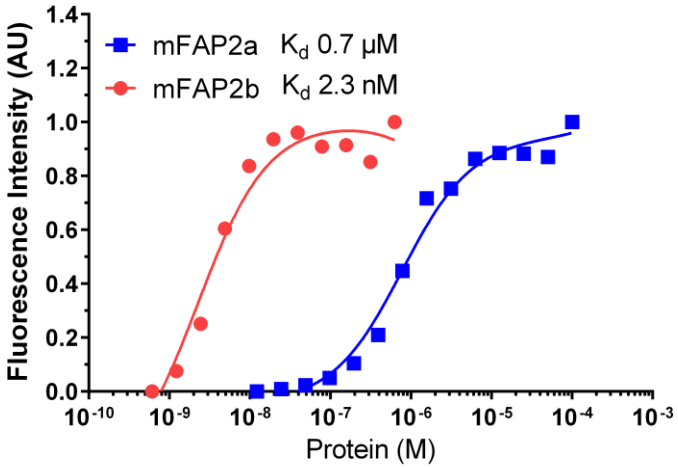


Figure 3.14 $K_d$ of DIHBI for mFAP2a (blue) and mFAP2b (red); for mFAP2a dye was kep at 100 nM, for mFAP2b – at 10 nM

Since DIHBI has good binding to mFAP2b, exists in colorized form at cellular pH and uses different spectral window from MG-2I we moved on to test the ROS generation of the DIHBI/mFAP2b complex. As previously detailed for MG-2I,[18] we used ADPA bleaching as a measure of singlet oxygen production in solutions containing dye, dye+protein, and fluorescein as a photosensitizer standard dye, leveraging a deuterated medium to prolong the lifetime of $^1O_2$[55] and sodium azide to quench it[56] to establish the role of singlet oxygen in the ADPA bleaching process.

Figure 3.15 shows changes in the remaining ADPA fluorescence signal during illumination of samples with and without mFAP2b (5x excess of one or the other binding partner to have consistent 500nM of complex and fluorescein as a control for ROS production[57]). In PBS without sodium azide (panel A) there is noticeable bleaching of ADPA by samples that contain both DIHBI and mFAP2b and almost no bleaching with only the dye present. If we substitute PBS for dPBS (panel B, 80% of the mixture is $D_2O$), there is noticeably more bleaching than in PBS under the same exposure conditions. With addition of sodium azide in both PBS and dPBS (panels C and D respectively) bleaching from dye-protein complex completely suppressed which confirms generation of singlet oxygen, which is quenched by $NaN_3$, is responsible for the ADPA reduction by the dye-protein complex under illumination.

It is worth noting that samples with excess dye and excess protein had slightly different ROS production activity in PBS and dPBS, but we would need to perform more experiments to investigate how reproducible this phenomenon is.

As an unfortunate side effect, DIHBI/mFAP2b photodegrades over time (Figure 3.17) and after ~600 s there is almost no detectable fluorescence. Unfortunately, we could not trace the effect on the absorbance in the same experiment due to the low initial absorption of the samples and we ran out of protein to conduct a separate experiment to trace the effects on the absorbance. It is unlikely that singlet oxygen is the main driving force of the of the dye bleaching since we do not see the increase in bleaching rate in $D_2O$ nor the decrease in the bleaching rate with sodium azide, and the rapid, unimolecular . In order to prove definitively that this bleaching is not singlet oxygen mediated we should conduct bleaching experiment for complexes in the media with no molecular oxygen present.

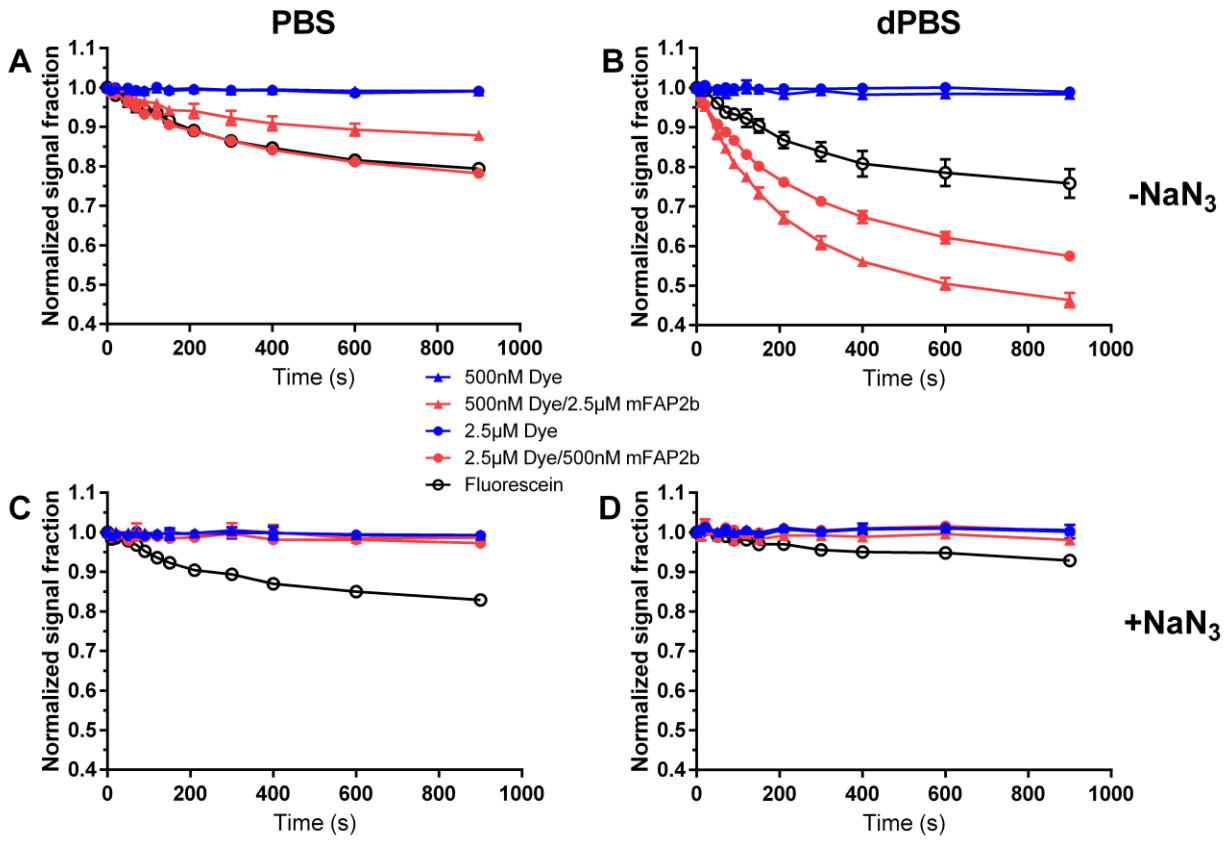


Figure 3.15 Remaining ADPA signal after bleaching by DIHBI with and without mFAP2b (500 nM dye, 2.5μM protein and reverse) in PBS and dPBS (80% $D_2O$) as well as with and without 10 mM $NaN_3$; each sample was run with 5 replicates and outlier wells were removed based on initial ADPA signal levels prior to any exposure using Z factor rejection criteria; illumination by LED with emission maximum 495 nm and light flux of 25.8 mW/cm$^2$

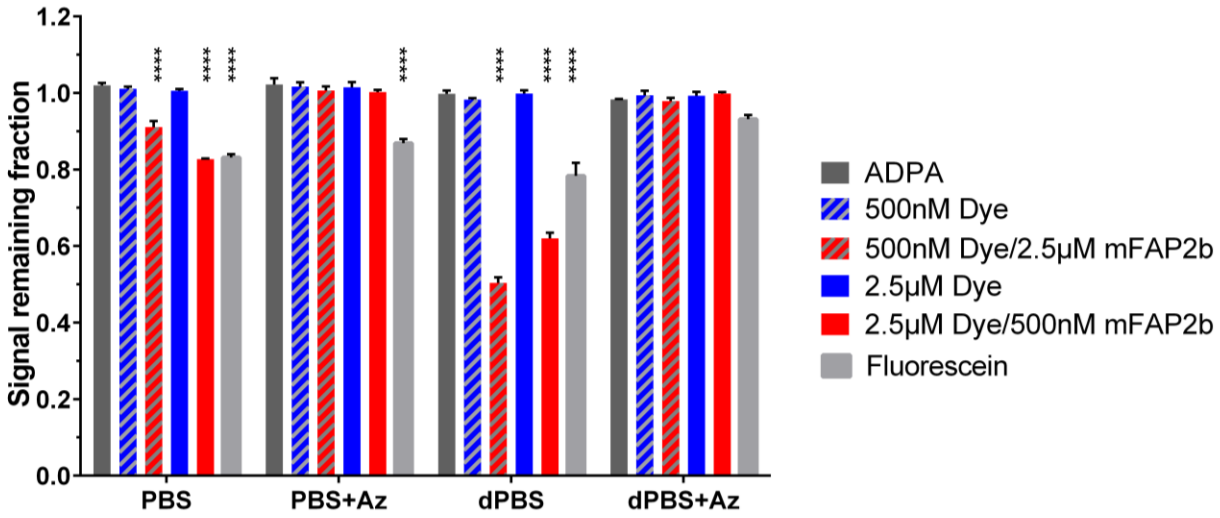


Figure 3.16 Remaining ADPA fluorescence signal after 600 s of illumination normalized to ADPA only sample. Samples that are significantly bleached in comparison to ADPA only samples are marked

We also did not observe any noticeable difference in bleaching rates with excess dye vs excess protein samples which suggests that the dye exchange after bleaching is not happening. In a separate experiment we added new dye to a complex after bleaching all fluorescence with no fluorescence recovery after 12h of incubation (data not shown) which suggests that it is the complex or the protein that is being altered during illumination rather than the free dye molecule since incubation with the fresh dye does not result in the fluorescence recovery.

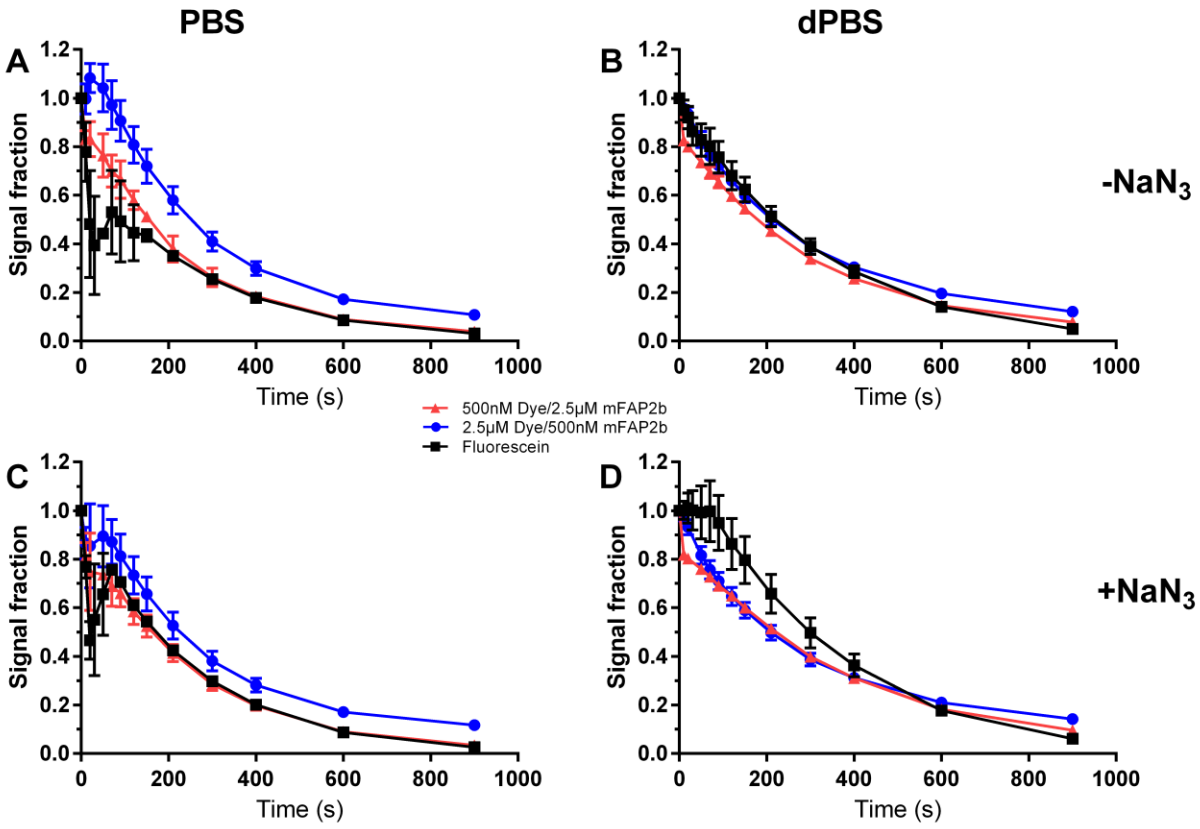


Figure 3.17 Reduction of the dye fluorescence with illumination. All samples were run with 5 replicates and outliers were discarded

Since fluorescence bleaching and singlet oxygen generation happen at the same time it is hard to extract the $^1O_2$ quantum yield from this dataset. Compared to fluorescein, which has a reported $^1O_2$ quantum yield of 0.03, the dPBS results of mFAP-DIHBI suggest that the $^1O_2$ quantum yield may be nearly twice as high (0.05-0.06. It is also possible to detect singlet oxygen generation directly using singlet oxygen emission at 1268 nm[58] which should give us a more quantitative measurement of the singlet oxygen quantum yield under non-bleaching excitation conditions.

## 3.2 Summary and future directions

Overall, we have synthesized a new dye, DIHBI, that binds to a previously published artificial protein and activates fluorescence. In addition to having high brightness, this complex also demonstrates singlet oxygen production. Unfortunately, we were not able to finish all the experiments needed to fully characterize this complex before the university was closed for quarantine.

Since we have not characterized the performance of this dye in cells it is worth performing experiments to establish if singlet oxygen produced by this complex is capable of providing robust singlet oxygen perturbations in cells before self-bleaching. Since MG-2I and DIHBI operate in two different spectral regions it is possible for them to be used simultaneous. This gives researchers the possibility to generate singlet oxygen in two genetically targeted locations independently.

This can be useful in studies of molecular mechanisms in cell, ROS-mediated signaling as well as cell-based studies ranging from selectively ablating one of the cell populations in a mixed sample to killing a single bacterial strain in a biofilm. As an example of a problem that can benefit from a specific localized ROS production is the hypothesis that ROS generation in lysosomes and then in mitochondria results in higher cytotoxicity and more effective immune representation of the cancer cells[59].

Another possible avenue for progress with this system is the synthesis and evaluation of a new dye, DIHBI-1T using similar modification as the ones introduced to DFHBI-1T in comparison to DFHBI (Figure 3.18)[41]. If the trend observed for DFHBI modifications persists we could expect to see 40% increase in extinction coefficient and increase in brightness and/or singlet oxygen production (DFHI-1T demonstrated 30% increase in the quantum yield). Another

possible modification to increase ROS production as well as introduce slight red shift in spectral characteristics is change oxygen in the carbonyl group to sulfur (Figure 3.18)[60]. This approach did not always result in the increase in the extinction coefficient but in all described cases in the paper singlet oxygen quantum yield was increased. As these two modifications do not exclude each other a structure with both modifications can be tested as well (Figure 3.18).

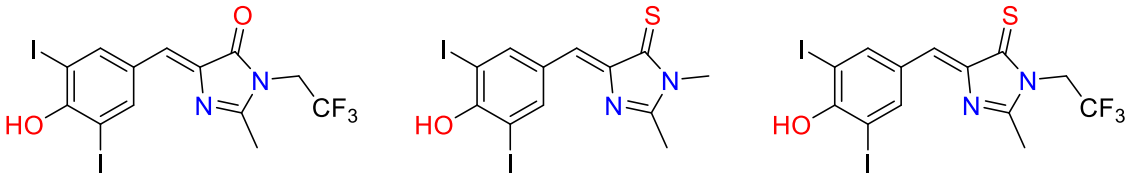


Figure 3.18 Proposed structure for new DIHBI analogs

## 3.3 Materials and methods

### 3.3.1 SYNTHESIS OF THE PROBE

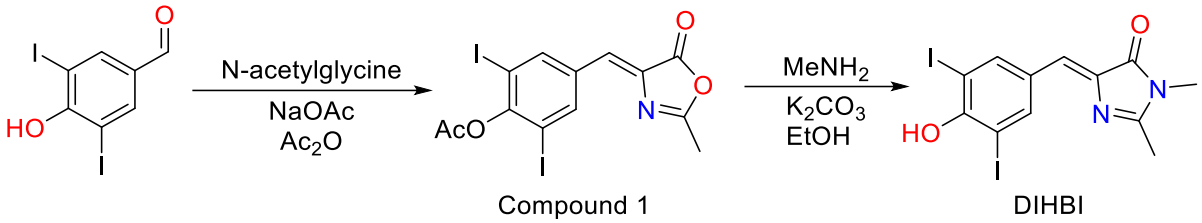


Figure 3.19 Synthetic scheme for DIHBI synthesis

The synthesis of the dye was performed based on the procedure published by J. Paige[29] with some adjustments for the second synthetic step.

**(Z)-2,6-diiodo-4-((2-methyl-5-oxooxazol-4(5H)-ylidene)methyl)phenyl acetate** (Compound 1). A mixture of the aldehyde (2.362g, 6.23 mmol), N-acetylglycine (0.740g, 6.23 mmol), and freshly dried Sodium Acetate (0.5182g, 6.23 mmol) in acetic anhydride (2.33 mL) was stirred at 110°C for 2 hours. After cooling to room temperature, 23 mL of cold (-20°C) ethanol was added and the resulting mixture was stirred overnight at room temperature. Next day mixture was filtered, washed with ~15 mL of cold ethanol, boiling water, and hexanes. $^{1}$H NMR (500 MHz, Methanol-$d_4$) δ 8.04 (s, 2H, 4, 6), 7.28 (s, 1H, 9), 2.39 (s, 3H, 16), 2.11 (s, 3H, 20).

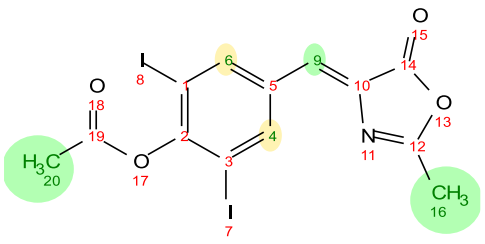

Figure 3.20 Structure of Compound 1 with assignments for NMR

**(Z)-5-(4-hydroxy-3,5-diiodobenzylidene)-2,3-dimethyl-3,5-dihydro-4H-imidazol-4-one** (DIHBI). To a mixture of Compound 1 (1g, 2 mmol) and $K_2CO_3$ (0.4g, 2.9 mmol) in 50 mL Ethanol, 600µL of 40% methylamine in water was added provoking the change of the color of the mixture from yellow to red. After ~1 hour of boiling precipitate started to form. After refluxing the reaction mixture for 12 hours in total, it was cooled down to room temperature, filtered. Solid was partitioned between ethyl acetate and acidic brine. Filtrate as well as the dried ethyl acetate layer were dried on the rotary evaporator. The crude product was taken up in basic water with 10% acetonitrile and purified on MPLC using 0.1%$NH_4OH$ in water – Acetonitrile gradient. $^{1}H$ NMR (500 MHz, Methanol-$d_4$) δ 8.45 (s, 2H, 4, 6), 6.83 (s, 1H, 9), 3.18 (s, 3H, 17), 2.38 (s, 3H, 16). $^{13}C$ NMR (126 MHz, Methanol-$d_4$) δ 171.92, 166.76, 157.49, 140.37, 4, 6, 128.69, 127.31, 10, 84.19, 1, 3, 25.48, 21.36. HRMS: expected 466.8759 ($C_{12}H_9I_2N_2O_2^-$), found 466.8749.

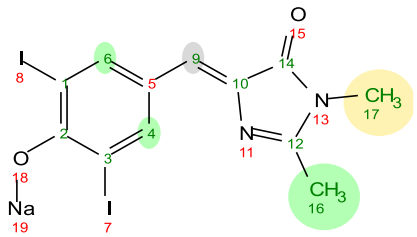


Figure 3.21 Structure of DIHBI with assignments for NMR

**Spectroscopy**

Absorbance and fluorescence spectra were measured using Tecan M1000 using 96- or 384-well clear plates with flat bottom from Greiner®. For reference absorbance and fluorescence spectra absorbance of the samples was kept below 0.1.

$K_d$ was measured in triplicates for all samples with no protein control. For data processing dye only sample signal was subtracted from the dye/protein samples before fitting using GraphPad Prism 6.07.

For extinction coefficient several samples of different weight were taken, dissolved in the same volume of DMSO, diluted in PBS in triplicates by transferring the same volume of the DMSO stock, and measured in a cuvette with 1 cm path length (with accounting for PBS absorption).

**Quantum Yield**

Quantum yield was determined by comparing integrated emission intensity of DIHBI/mFAP2b (in PBS) and fluorescein in 0.1 M NaOH[52] of the same optical density at the excitation wavelength (490 nm). For the sample of 500nM DIHBI with 2.5uM mFAP2b quantum yield was found to be 70%.

**ROS generation test**

For ROS generation test we performed a series of illuminations using 495nm LED with a flat illumination profile across the plate with light intensity of 2.46 $mW/cm^2$ as measured by Coherent FieldMaxII-TOP light meter with UV-VIS light sensor #1098313. After each illumination fluorescence of ADPA, DIHBI/mFAP2b, and fluorescein was read using TECAN M1000. Excitation/emission wavelength were set to 356/404nm for ADPA, 485/525nm for DIHBI/mFAP2b, and 488/515nm for fluorescein. Each sample was run with 5 replicates. Data from the time point 0 was analyzed for outliers using Z score and samples that had higher Z score than a threshold (1.5 for 5 replicates, 1.15 for 4 replicates) were removed from the analysis (up to 2 samples removed).

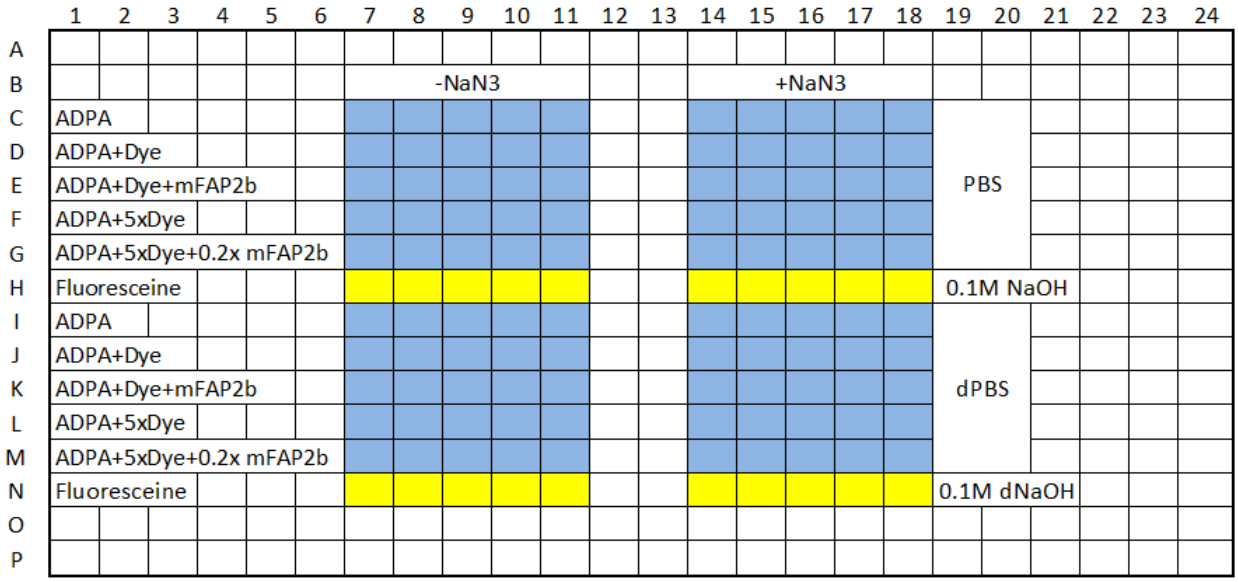


Figure 3.22 Plate map for the ROS generation test

## 3.4 References


(1) Bae, Y. S.; Oh, H.; Rhee, S. G.; Yoo, Y. Do. Regulation of Reactive Oxygen Species Generation in Cell Signaling. *Mol. Cells* **2011**, *32* (6), 491–509. https://doi.org/10.1007/s10059-011-0276-3.

(2) Snezhkina, A. V.; Kudryavtseva, A. V.; Kardymon, O. L.; Savvateeva, M. V.; Melnikova, N. V.; Krasnov, G. S.; Dmitriev, A. A. ROS Generation and Antioxidant Defense Systems in Normal and Malignant Cells. *Oxid. Med. Cell. Longev.* **2020**, *2019*. https://doi.org/10.1155/2019/6175804.

(3) Dayem, A. A.; Hossain, M. K.; Lee, S. Bin; Kim, K.; Saha, S. K.; Yang, G. M.; Choi, H. Y.; Cho, S. G. The Role of Reactive Oxygen Species (ROS) in the Biological Activities of Metallic Nanoparticles. *Int. J. Mol. Sci.* **2017**, *18* (1), 1–21. https://doi.org/10.3390/ijms18010120.

(4) Forrester, S. J.; Kikuchi, D. S.; Hernandes, M. S.; Xu, Q.; Griendling, K. K. Reactive Oxygen Species in Metabolic and Inflammatory Signaling. *Circ. Res.* **2018**, *122* (6), 877–902. https://doi.org/10.1161/CIRCRESAHA.117.311401.

(5) Kimura, S.; Waszczak, C.; Hunter, K.; Wrzaczek, M. Bound by Fate: The Role of Reactive Oxygen Species in Receptor-like Kinase Signaling. *Plant Cell* **2017**, *29* (4), 638–654. https://doi.org/10.1105/tpc.16.00947.

(6) Zandalinas, S. I.; Mittler, R. ROS-Induced ROS Release in Plant and Animal Cells. *Free Radic. Biol. Med.* **2018**, *122* (November 2017), 21–27. https://doi.org/10.1016/j.freeradbiomed.2017.11.028.

(7) Ghosh, N.; Das, A.; Chaffee, S.; Roy, S.; Sen, C. K. *Reactive Oxygen Species, Oxidative Damage and Cell Death*; Elsevier Inc., 2017. https://doi.org/10.1016/B978-0-12-805417-

8.00004-4.

(8) Bulina, M. E.; Chudakov, D. M.; Britanova, O. V.; Yanushevich, Y. G.; Staroverov, D. B.; Chepurnykh, T. V.; Merzlyak, E. M.; Shkrob, M. A.; Lukyanov, S.; Lukyanov, K. A. A Genetically Encoded Photosensitizer. *Nat. Biotechnol.* **2006**, *24* (1), 95–99. https://doi.org/10.1038/nbt1175.

(9) Kennedy, J. C.; Pottier, R. H. New Trends in Photobiology. Endogenous Protoporphyrin IX, a Clinically Useful Photosensitizer for Photodynamic Therapy. *J. Photochem. Photobiol. B Biol.* **1992**, *14* (4), 275–292. https://doi.org/10.1016/1011-1344(92)85108-7.

(10) Chatterjee, D. K.; Fong, L. S.; Zhang, Y. Nanoparticles in Photodynamic Therapy: An Emerging Paradigm. *Adv. Drug Deliv. Rev.* **2008**, *60* (15), 1627–1637. https://doi.org/10.1016/j.addr.2008.08.003.

(11) Liu, Y.; Qin, R.; Zaat, S. A. J.; Breukink, E.; Heger, M. Antibacterial Photodynamic Therapy: Overview of a Promising Approach to Fight Antibiotic-Resistant Bacterial Infections. *J. Clin. Transl. Res.* **2015**, *1* (3), 140–167. https://doi.org/10.18053/jctres.201503.002.

(12) Atchison, J.; Kamila, S.; Nesbitt, H.; Logan, K. A.; Nicholas, D. M.; Fowley, C.; Davis, J.; Callan, B.; McHale, A. P.; Callan, J. F. Iodinated Cyanine Dyes: A New Class of Sensitisers for Use in NIR Activated Photodynamic Therapy (PDT). *Chem. Commun.* **2017**, *53* (12), 2009–2012. https://doi.org/10.1039/C6CC09624G.

(13) Zou, J.; Yin, Z.; Ding, K.; Tang, Q.; Li, J.; Si, W.; Shao, J.; Zhang, Q.; Huang, W.; Dong, X. BODIPY Derivatives for Photodynamic Therapy: Influence of Configuration versus Heavy Atom Effect. *ACS Appl. Mater. Interfaces* **2017**, *9* (38), 32475–32481. https://doi.org/10.1021/acsami.7b07569.

(14) Sano, Y.; Watanabe, W.; Matsunaga, S. Chromophore-Assisted Laser Inactivation - towards a Spatiotemporal-Functional Analysis of Proteins, and the Ablation of Chromatin, Organelle and Cell Function. *J. Cell Sci.* **2014**, *127* (8), 1621–1629. https://doi.org/10.1242/jcs.144527.

(15) Shu, X.; Lev-Ram, V.; Deerinck, T. J.; Qi, Y.; Ramko, E. B.; Davidson, M. W.; Jin, Y.; Ellisman, M. H.; Tsien, R. Y. A Genetically Encoded Tag for Correlated Light and Electron Microscopy of Intact Cells, Tissues, and Organisms. *PLoS Biol.* **2011**, *9* (4). https://doi.org/10.1371/journal.pbio.1001041.

(16) Keppler, A.; Ellenberg, J. Chromophore-Assisted Laser Inactivation of α- And γ-Tubulin SNAP-Tag Fusion Proteins inside Living Cells. *ACS Chem. Biol.* **2009**, *4* (2), 127–138. https://doi.org/10.1021/cb800298u.

(17) Babendure, J. R.; Adams, S. R.; Tsien, R. Y. Aptamers Switch on Fluorescence of Triphenylmethane Dyes. *J. Am. Chem. Soc.* **2003**, *125* (48), 14716–14717. https://doi.org/10.1021/ja037994o.

(18) He, J.; Wang, Y.; Missinato, M. A.; Onuoha, E.; Perkins, L. A.; Watkins, S. C.; St Croix, C. M.; Tsang, M.; Bruchez, M. P. A Genetically Targetable Near-Infrared Photosensitizer. *Nat. Methods* **2016**, *13* (3), 263–268. https://doi.org/10.1038/nmeth.3735.

(19) Ackerman, D. S.; Altun, B.; Kolodieznyi, D.; Bruchez, M. P.; Tsourkas, A.; Jarvik, J. W. Antibody-Linked Fluorogen-Activating Proteins for Antigen Detection and Cell Ablation. *Bioconjug. Chem.* **2019**, *30* (1), 63–69. https://doi.org/10.1021/acs.bioconjchem.8b00720.

(20) Qian, W.; Kumar, N.; Roginskaya, V.; Fouquerel, E.; Opresko, P. L.; Shiva, S.; Watkins, S. C.; Kolodieznyi, D.; Bruchez, M. P.; Van Houten, B.; Qian; Kumar; Roginskaya; Fouquerel; Opresko, P. L.; Shiva, S.; Watkins, S. C.; Kolodieznyi, D.; Bruchez, M. P.;

Van Houten, B. Chemoptogenetic Damage to Mitochondria Causes Rapid Telomere Dysfunction. *Proc. Natl. Acad. Sci.* **2019**, *116* (37), 18435–18444. https://doi.org/10.1073/pnas.1910574116.

(21) Fouquerel, E.; Barnes, R. P.; Uttam, S.; Watkins, S. C.; Bruchez, M. P.; Opresko, P. L. Targeted and Persistent 8-Oxoguanine Base Damage at Telomeres Promotes Telomere Loss and Crisis. *Mol. Cell* **2019**, *75* (1), 117-130.e6. https://doi.org/10.1016/j.molcel.2019.04.024.

(22) Xie, W.; Jiao, B.; Bai, Q.; Ilin, V. A.; Sun, M.; Burton, C. E.; Kolodieznyi, D.; Calderon, M. J.; Stolz, D. B.; Opresko, P. L.; St Croix, C. M.; Watkins, S.; Van Houten, B.; Bruchez, M. P.; Burton, E. A. Chemoptogenetic Ablation of Neuronal Mitochondria in Vivo with Spatiotemporal Precision and Controllable Severity. *Elife* **2020**, *9*, 1–24. https://doi.org/10.7554/eLife.51845.

(23) Özhalici-Ünal, H.; Pow, C. L.; Marks, S. A.; Jesper, L. D.; Silva, G. L.; Shank, N. I.; Jones, E. W.; Burnette, J. M.; Berget, P. B.; Armitage, B. A. A Rainbow of Fluoromodules: A Promiscuous ScFv Protein Binds to and Activates a Diverse Set of Fluorogenic Cyanine Dyes. *J. Am. Chem. Soc.* **2008**, *130* (38), 12620–12621. https://doi.org/10.1021/ja805042p.

(24) Pratt, C. P.; He, J.; Wang, Y.; Barth, A. L.; Bruchez, M. P. Fluorogenic Green-Inside Red-Outside (GIRO) Labeling Approach Reveals Adenylyl Cyclase-Dependent Control of BKα Surface Expression. *Bioconjug. Chem.* **2015**, *26* (9), 1963–1971. https://doi.org/10.1021/acs.bioconjchem.5b00409.

(25) Zhang, M.; Chakraborty, S. K.; Sampath, P.; Rojas, J. J.; Hou, W.; Saurabh, S.; Thorne, S. H.; Bruchez, M. P.; Waggoner, A. S. Fluoromodule-Based Reporter / Probes Designed for

in Vivo Fluorescence Imaging. *J. Clin. Invest.* **2015**, *125* (10), 3915–3927. https://doi.org/10.1172/JCI81086.cues.

(26) He, J. Utilizing Malachite Green Derivatives to Diversify Fluorogen- Activating Proteins ( FAPs )' Applications, Carnegie Mellon University, 2016. https://doi.org/10.1184/R1/10059941.v1.

(27) Szent-Gyorgyi, C.; Stanfield, R. L.; Andreko, S.; Dempsey, A.; Ahmed, M.; Capek, S.; Waggoner, A. S.; Wilson, I. A.; Bruchez, M. P. Malachite Green Mediates Homodimerization of Antibody VL Domains to Form a Fluorescent Ternary Complex with Singular Symmetric Interfaces. *J. Mol. Biol.* **2013**, *425* (22), 4595–4613. https://doi.org/10.1016/j.jmb.2013.08.014.

(28) Conyard, J.; Kondo, M.; Heisler, I. A.; Jones, G.; Baldridge, A.; Tolbert, L. M.; Solntsev, K. M.; Meech, S. R. Chemically Modulating the Photophysics of the GFP Chromophore. *J. Phys. Chem. B* **2011**, *115* (6), 1571–1577. https://doi.org/10.1021/jp111593x.

(29) Paige, J. S.; Wu, K. Y.; Jaffrey, S. R. RNA Mimics of Green Fluorescent Protein. *Science (80-. ).* **2011**, *333* (6042), 642–646. https://doi.org/10.1126/science.1207339.

(30) Tuerk, C.; Gold, L. Systematic Evolution of Ligands by Exponential Enrichment: RNA Ligands to Bacteriophage T4 DNA Polymerase. *Science* **1990**, *249* (4968), 505–510. https://doi.org/10.1126/science.2200121.

(31) You, M.; Jaffrey, S. R. Structure and Mechanism of RNA Mimics of Green Fluorescent Protein. *Annu. Rev. Biophys.* **2015**, *44* (1), 187–206. https://doi.org/10.1146/annurev-biophys-060414-033954.

(32) Warner, K. D.; Chen, M. C.; Song, W.; Strack, R. L.; Thorn, A.; Jaffrey, S. R.; Ferré-D'Amaré, A. R. Structural Basis for Activity of Highly Efficient RNA Mimics of Green

Fluorescent Protein. *Nat. Struct. Mol. Biol.* **2014**, *21* (8), 658–663. https://doi.org/10.1038/nsmb.2865.

(33) Yuan, S.; Alper, H. S. Improving Spinach2- and Broccoli-Based Biosensors for Single and Double Analytes. *Biotechnol. Notes* **2020**. https://doi.org/10.1016/j.biotno.2020.01.001.

(34) Filonov, G. S.; Moon, J. D.; Svensen, N.; Jaffrey, S. R. Broccoli: Rapid Selection of an RNA Mimic of Green Fluorescent Protein by Fluorescence-Based Selection and Directed Evolution. *J. Am. Chem. Soc.* **2014**, *136* (46), 16299–16308. https://doi.org/10.1021/ja508478x.

(35) Autour, A.; Westhof, E.; Ryckelynck, M. ISpinach: A Fluorogenic RNA Aptamer Optimized for in Vitro Applications. *Nucleic Acids Res.* **2016**, *44* (6), 2491–2500. https://doi.org/10.1093/nar/gkw083.

(36) Song, W.; Filonov, G. S.; Kim, H.; Hirsch, M.; Li, X.; Moon, J. D.; Jaffrey, S. R. Imaging RNA Polymerase III Transcription Using a Photostable RNA-Fluorophore Complex. *Nat. Chem. Biol.* **2017**, *13* (11), 1187–1194. https://doi.org/10.1038/nchembio.2477.

(37) Panchapakesan, S. S. S.; Jeng, S. C. Y.; Unrau, P. J. RNA Complex Purification Using High-Affinity Fluorescent RNA Aptamer Tags. *Ann. N. Y. Acad. Sci.* **2015**, *1341* (1), 149–155. https://doi.org/10.1111/nyas.12663.

(38) Guo, P.; Haque, F. RNA Nanotechnology and Therapeutics: Methods and Protocols. *RNA Nanotechnol. Ther. Methods Protoc.* **2015**, *1297*, 1–239. https://doi.org/10.1007/978-1-4939-2562-9.

(39) Zaitseva, S. O.; Baleeva, N. S.; Zatsepin, T. S.; Myasnyanko, I. N.; Turaev, A. V.; Pozmogova, G. E.; Khrulev, A. A.; Varizhuk, A. M.; Baranov, M. S.; Aralov, A. V. Short Duplex Module Coupled to G-Quadruplexes Increases Fluorescence of Synthetic GFP

Chromophore Analogues. *Sensors* **2020**, *20* (3), 915. https://doi.org/10.3390/s20030915.

(40) Arora, A.; Sunbul, M.; Jäschke, A. Dual-Colour Imaging of RNAs Using Quencher- and Fluorophore-Binding Aptamers. *Nucleic Acids Res.* **2015**, *43* (21), gkv718. https://doi.org/10.1093/nar/gkv718.

(41) Song, W.; Strack, R. L.; Svensen, N.; Ja, S. R.; Jaffrey, S. R. Plug-and-Play Fluorophores Extend the Spectral Properties of Spinach. *J. Am. Chem. Soc.* **2014**, *136* (4), 1198–1201. https://doi.org/10.1021/ja410819x.

(42) Strack, R. L.; Disney, M. D.; Jaffrey, S. R. A Superfolding Spinach2 Reveals the Dynamic Nature of Trinucleotide Repeat–Containing RNA. *Nat. Methods* **2013**, *10* (12), 1219–1224. https://doi.org/10.1038/nmeth.2701.

(43) Wang, X. C.; Wilson, S. C.; Hammond, M. C. Next-Generation RNA-Based Fluorescent Biosensors Enable Anaerobic Detection of Cyclic Di-GMP. *Nucleic Acids Res.* **2016**, *44* (17), gkw580. https://doi.org/10.1093/nar/gkw580.

(44) Ying, Z.-M.; Tu, B.; Liu, L.; Tang, H.; Tang, L.-J.; Jiang, J.-H. Spinach-Based Fluorescent Light-up Biosensors for Multiplexed and Label-Free Detection of MicroRNAs. *Chem. Commun.* **2018**. https://doi.org/10.1039/C8CC00123E.

(45) Bouhedda, F.; Autour, A.; Ryckelynck, M. Light-Up RNA Aptamers and Their Cognate Fluorogens: From Their Development to Their Applications. *Int. J. Mol. Sci.* **2017**, *19* (1), 44. https://doi.org/10.3390/ijms19010044.

(46) Kellenberger, C. A.; Wilson, S. C.; Sales-Lee, J.; Hammond, M. C. RNA-Based Fluorescent Biosensors for Live Cell Imaging of Second Messengers Cyclic Di-GMP and Cyclic AMP-GMP. *J. Am. Chem. Soc.* **2013**, *135* (13), 4906–4909. https://doi.org/10.1021/ja311960g.

(47) Klima, J. C. Design of De Novo Mini Fluorescence Activating Proteins as PH and Calcium Biosensors, University of Washington, 2019.

(48) Dou, J.; Vorobieva, A. A.; Sheffler, W.; Doyle, L. A.; Park, H.; Bick, M. J.; Mao, B.; Foight, G. W.; Lee, M. Y.; Gagnon, L. A.; Carter, L.; Sankaran, B.; Ovchinnikov, S.; Marcos, E.; Huang, P. S.; Vaughan, J. C.; Stoddard, B. L.; Baker, D. De Novo Design of a Fluorescence-Activating β-Barrel. *Nature* **2018**, *561* (7724), 485–491. https://doi.org/10.1038/s41586-018-0509-0.

(49) Skúpa, K.; Urban, J. Modifications of the Chromophore of Spinach Aptamer Based on QM:MM Calculations. *J. Mol. Model.* **2017**, *23* (2), 46. https://doi.org/10.1007/s00894-017-3232-0.

(50) Zanotti, K. J.; Silva, G. L.; Creeger, Y.; Robertson, K. L.; Waggoner, A. S.; Berget, P. B.; Armitage, B. A. Blue Fluorescent Dye-Protein Complexes Based on Fluorogenic Cyanine Dyes and Single Chain Antibody Fragments. *Org. Biomol. Chem.* **2011**, *9* (4), 1012–1020. https://doi.org/10.1039/c0ob00444h.

(51) Rastede, E. E.; Tanha, M.; Yaron, D.; Watkins, S. C.; Waggoner, A. S.; Armitage, B. a. Spectral Fine Tuning of Cyanine Dyes: Electron Donor-Acceptor Substituted Analogues of Thiazole Orange. *Photochem. Photobiol. Sci.* **2015**, *14* (9), 1703–1712. https://doi.org/10.1039/c5pp00117j.

(52) Lakowicz, J. R. *Principles of Fluorescence Spectroscopy*; Lakowicz, J. R., Ed.; Springer US: Boston, MA, 2006. https://doi.org/10.1007/978-0-387-46312-4.

(53) Shaner, N. C.; Steinbach, P. A.; Tsien, R. Y. A Guide to Choosing Fluorescent Proteins. *Nat. Methods* **2005**, *2* (12), 905–909. https://doi.org/10.1038/nmeth819.

(54) Saftig, P.; Klumperman, J. Lysosome Biogenesis and Lysosomal Membrane Proteins:

Trafficking Meets Function. *Nat. Rev. Mol. Cell Biol.* **2009**, *10* (9), 623–635. https://doi.org/10.1038/nrm2745.

(55) Merkel, P. B.; Nilsson, R.; Kearns, D. R. Deuterium Effects on Singlet Oxygen Lifetimes in Solutions. a New Test of Singlet Oxygen Reactions. *J. Am. Chem. Soc.* **1972**, *94* (3), 1030–1031. https://doi.org/10.1021/ja00758a072.

(56) Hoebeke, M.; Piette, J.; van de Vorst, A. Photosensitized Production of Singlet Oxygen by Merocyanine 540 Bound to Liposomes. *J. Photochem. Photobiol. B Biol.* **1991**, *9* (3–4), 281–294. https://doi.org/10.1016/1011-1344(91)80166-F.

(57) Gandin, E.; Lion, Y.; Van de Vorst, A. Quantum Yield of Singlet Oxygen Production By Xanthene Derivatives. *Photochem. Photobiol.* **1983**, *37* (3), 271–278. https://doi.org/10.1111/j.1751-1097.1983.tb04472.x.

(58) Khan, A. U.; Kasha, M. Direct Spectroscopic Observation of Singlet Oxygen Emission at 1268 Nm Excited by Sensitizing Dyes of Biological Interest in Liquid Solution. *Proc. Natl. Acad. Sci. U. S. A.* **1979**, *76* (12), 6047–6049. https://doi.org/10.1073/pnas.76.12.6047.

(59) Kessel, D. Photodynamic Therapy: Promotion of Efficacy by a Sequential Protocol. *J. Porphyr. Phthalocyanines* **2016**, *20* (1–4), 302–306. https://doi.org/10.1142/S1088424616500073.

(60) Tang, J.; Wang, L.; Loredo, A.; Cole, C.; Xiao, H. Single-Atom Replacement as a General Approach towards Visible-Light/near-Infrared Heavy-Atom-Free Photosensitizers for Photodynamic Therapy. *Chem. Sci.* **2020**. https://doi.org/10.1039/d0sc02286a.

# 4 INSTRUMENTATION AND PROTOCOLS FOR QUANTITATIVE OPTICAL STIMULUS OF CHEMOPTOGENETIC SYSTEMS

Successful photodynamic perturbation of biological systems requires precise and reliable control over the localization of the photosensitizer as well as light application to the target site. The perturbation to a specific photosensitive system can be proportional to either or both the light intensity and exposure duration (dosing rate and/or total dose) of the applied light. To conduct precise experiments with photoperturbations, it is essential to develop systems that apply measured optical doses at precise intensities. Quantitative calibration of the power and uniformity of the light delivery and the size of the affected area play a crucial role in developing and conducting reproducible experiments based on precise optically activated perturbations.

One of the tools that can be used for the cell ablation in a lab setting is a microscope. We have shown previously that by using spinning disk confocal microscopy it is possible to perform photoablation of cells labeled with a FAP-TAPS photosensitizer complex[1]. Because of the limited illumination area under the microscope objective (~ <mm length scale), this approach is not suitable for large-scale population-based experiments like metabolomic, genomic or proteomic assays requiring hundreds or thousands of cells.

Another problem with confocal microscope-based photosensitization is how hard it is to quantify the exact amount of light that the sample receives because of different illumination patterns utilized in different microscopes and the focal plane receiving different light intensity than the rest of the height of the cell.

Components of mammalian cells have different tolerance and buffering towards ROS generation[3,4] which means that the same dose of light delivered over different period of time

would have different effect on cells. Furthermore, since the cells are not flat, focusing of the microscopes becomes an additional variability to the experiment.

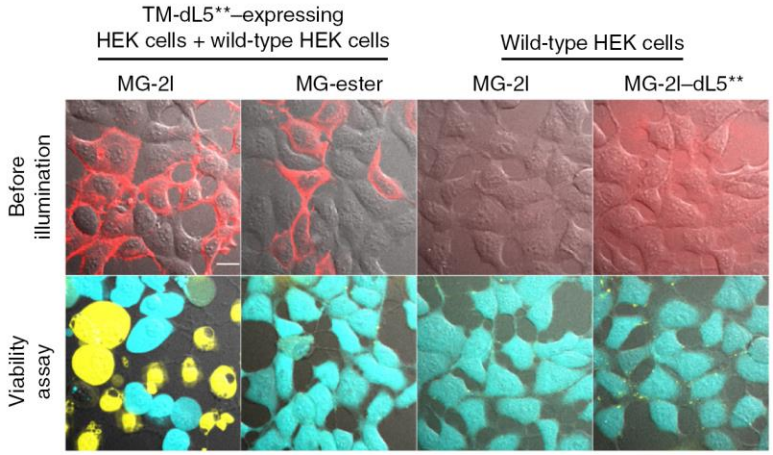


Figure 4.1 Illumination with a spinning disk confocal microscope can be used for cellular ablation[1]. Yellow stain in the viability assay marks dead cells, restricted to the cells that expressed dL5, bound MG2I and were exposed to 660 nm light in the microscope. Scale bar (10 μm). Modified from Figure 3 of He et al, 2016[1]

Instrumentation with reproducible and even illumination is required to address these challenges for large-scale cellular experiments. It is possible to solve these issues using a laser beam that can have flat illumination profile over an area that is larger than several cells. Another possible approach is to use another light source, like LED, to achieve flat illumination across the whole samples. For our previous experiments with FAP-TAP system[1] we have used a simple system based on a 100W “deep red” LED light source (Lightbox 1.0, Figure 4.2).

The main chamber of the Lightbox was constructed from wood and painted white to minimize light absorption from the light source. As the light source we have used 100 W LED from Chanzon. This LED array of 10x10 light emitting elements produces stable light and has an emission spectrum close to the absorption maximum of the MG-2I/dL5** complex (666 nm).

It is known that efficiency and longevity of the LED depends on the operating temperature so it is important to keep the LED unit cool[5,6]. To keep the temperature stable, we have used a CPU cooler that is designed for more than 100 W of cooling capacity. As a power source we have used a power supply rated at 300 W and 24 V output (which matches the required voltage for the LED). This was a deliberate choice to keep the power supply below the rated load of the LED and prolong its life span. We have seen over time that the power from one or several rows of LEDs on the array can decrease, which would cause reductions in both overall power intensity and illumination uniformity in this simple design.

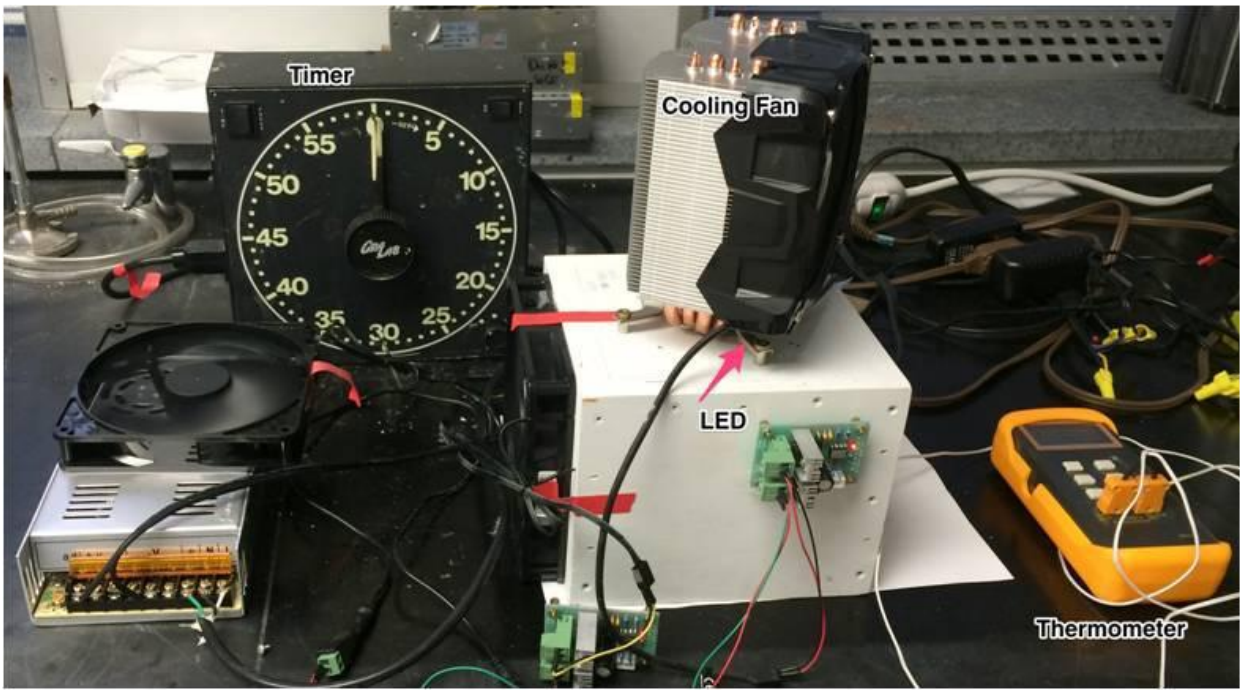


Figure 4.2 Old design of the Lightbox 1.0[1]

Since the sample will receive the heat from the LED it has to be kept cool during the irradiation. For that we have made two holes in the wooded box opposite from each other and attached 120 mm fan to one of them to keep a steady airflow over the sample. Temperature of the sample was monitored using external thermometer with a thermocouple. Illumination time

can be set using the external timer or the system can be unplugged from the power with no harm to the equipment.

This Lightbox achieved the set goal of creating reproducible conditions for illumination of samples and was relatively cheap (total cost of under $100 for the required elements of the lightbox). The system however was not easily transportable for sharing with other researchers because of the number of loose elements in the design, it is not compact (which is important for saving space in the laboratory) and it does not allow for control of the light intensity during illumination.

## 4.1 New generations of Lightbox

### 4.1.1 LIGHTBOX 1.1

While the previous light box satisfied all requirements for experimental control, it left much to be desired in usability and inter-lab portability. First, the bulky design consumed precious bench space. Second, the number of loose elements in combination with lightbox size limited ease of transport and collaboration. Lastly, the design did not allow for control of the light intensity. These limitations prompted the creation of a new lightbox.

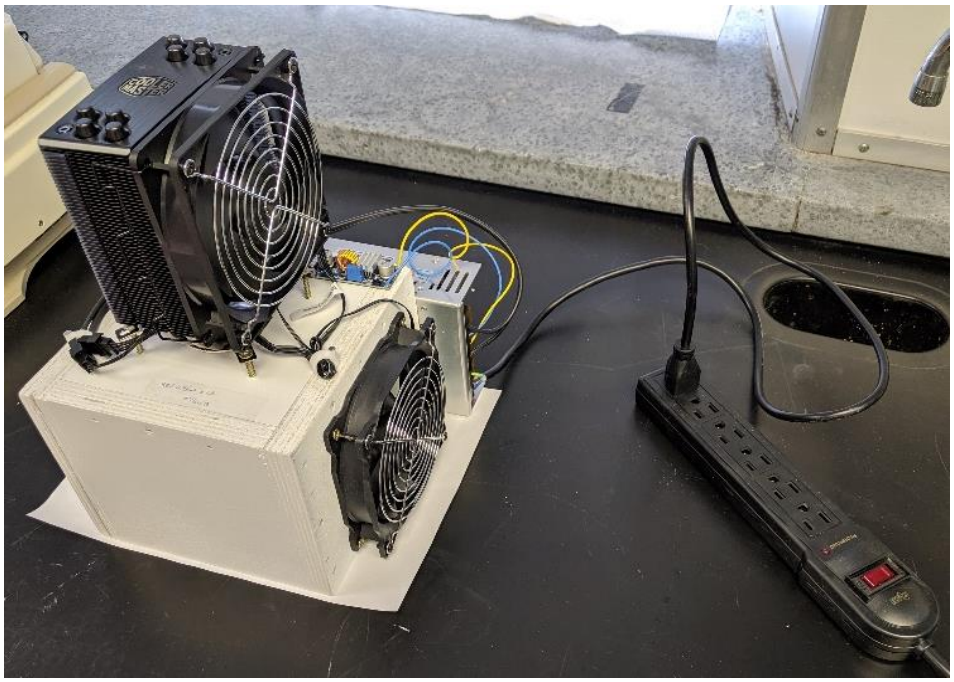

Figure 4.3 Lightbox 1.1 for being sent to collarotators so they can start doing experiments while they are bulding their own version

First, we set out to build several lightboxes that were easier to transport to our collaborators (Figure 4.3) that addressed the shortcomings of the first generation of the light box. A key difference implemented in the new lightbox has to do with the number of separate units that one has to transport. This system has only two separate elements – central wooden chamber

with cooling fans attached to it and power supply in comparison to over 5 elements for the old light box. Fans are powered through DC-DC step down converter adjusted to 12 V output. This eliminates the need for separate power supplies and control units for the fans. In addition, the fans are protected by fan grills to decrease the possibility of accidental damage to samples or researchers.

### 4.1.2 LIGHTBOX 2.0

Even though this new iteration of the lightbox addresses one of the concerns that we had with the system, it left the rest of them on the table (mostly regarding the control of the light intensity). We also received good results from Edward Burton (Univ. of Pitt.) who built a similar system with the goal of illuminating zebrafish for behavioral studies[7] (system was called Fish Fryer). We set to improve the design of our Lightbox based on the Fish Fryer, which was implemented in an open LED design, illuminated from the bottom, and controlled through an Arduino Duo USB electronics controller.

First, the next generation light box, Lightbox 2.0 (Figure 4.4), introduces change in the LED orientation from top to bottom. This allows us to keep it fixed and users do not have a need to move it constantly. Additionally, by making this switch we also allowed for easy modulation of the distance between the LED and the sample. This allows for regulation of the light intensity that sample receives as well as the spread of the light. The inverted system also allows for potential modularity by changing the LED to one of the several different colors of high-intensity LED arrays available online (620-625 nm, 460-470 nm, 490 nm, 520-530 nm, 590-595 nm, 440-450 nm, 850 nm, 940 nm, 730 nm).

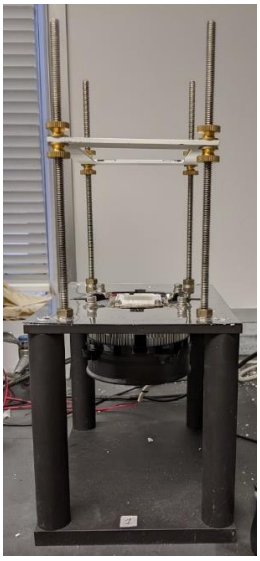

Figure 4.4 Lightbox 2.0 assembly with all elements visible (computerm illumination chamber, control box and light shield; left) and only illumination chamber without light shield (right).

This inversion of the system and change in the stage design for the lightbox resulted in a need to use smaller heatsink and as a result, higher air flow fan on it to keep the LED temperature stable. However, the smaller size of the cooler allows for easy storage and change of the LED assemblies (Figure 4.5) according to the needs of the experiment.

Figure 4.5 LED assemblies allow for easy modification of the Lightbox 2.0 to experimental needs. On left, a bare LED unit, on right, an LED unit directed through a frosted dispersing lens to improve illumination uniformity across larger samples.

To add better control of the light dose delivered to samples we have used an Arduino to control Lightbox 2.0 (following Prof. Burton's design and using his control code as a base for our modifications). The electrical scheme for the Lightbox 2.0 is presented in Figure 4.6. Unitization of the DC-DC step-up and step-down converters allowed us to use only a single power supply (24 V) for the 660 nm LED (required 24 V), 490nm LED (requires 32 V), and fans (require 12 V). To switch between required voltages for different LEDs we use toggle switches that allow to select only one of two possible voltages. This design was made to minimize the potential of human error and setting the wrong voltage for the LED since overvoltage can damage the LED. Another advantage of this solution is the flexibility of the DC-DC step-up converter that allows us to get different voltages if we would like to use LEDs that have different power requirements.

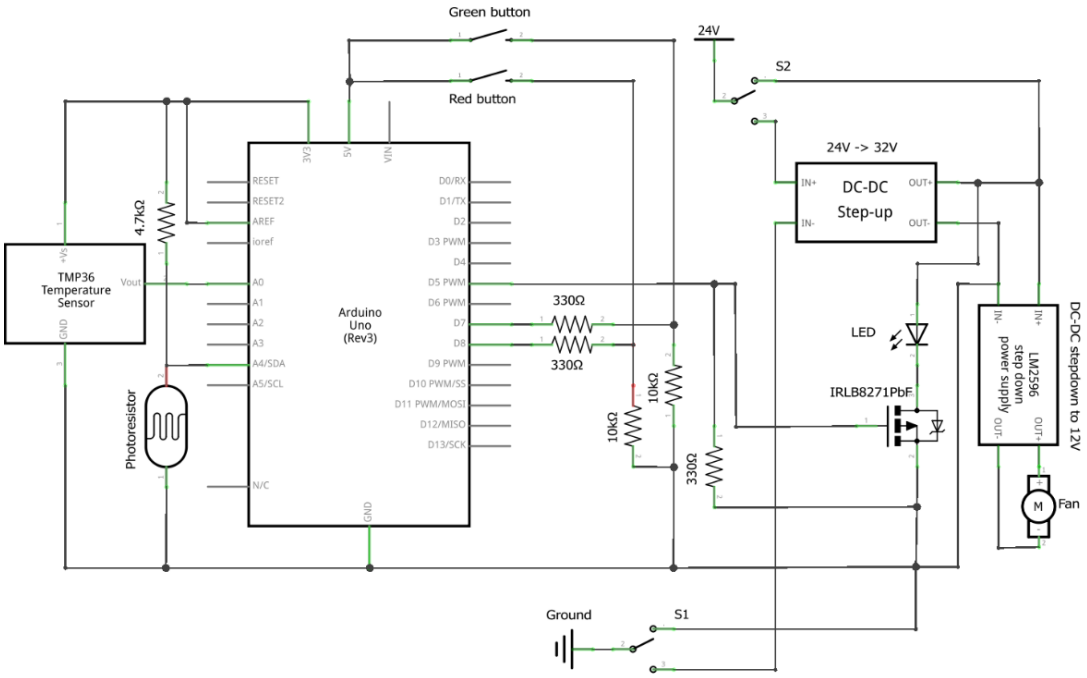


Figure 4.6 Electrical scheme of the new Lightbox 2.0 control; our modifications include sensors and a possibility to select the voltage for LED; original design by Ed Burton.

Control of the LED intensity is performed using Pulse Width Modulation (PWM) control where voltage is switched on and off and results in a linear response of the light intensity vs duty cycle (measure of how much time the current is allowed to go through vs being blocked) as demonstrated on Figure 4.7. This allows us to address one of the concerns that we had for the Lightbox – the control of the light intensity illuminated from the LED can be adjusted without the need to change anything physically in the system.

Another important advantage of using Arduino for controlling the LED illumination is that the user has the convenience of selecting the target illumination time for the experiments in seconds (that is the precision we settled on, although it can be adjusted) and relative power of the LED from a connected computer. During the illumination, the system will output how long the illumination is happening for and the light dose the sample has received. Light dose output depends on having the user set the same height for the sample holder or measuring the light intensity at the new position and putting it in the code of the program (full code for the program used is available in Appendix and includes code for usage of temperature and light sensors available on the electrical scheme but not in use due to the problems discussed later with more details). Using Arduino control also allows us to output the total light dose received by the sample in the end of each exposure period based on the external calibration.

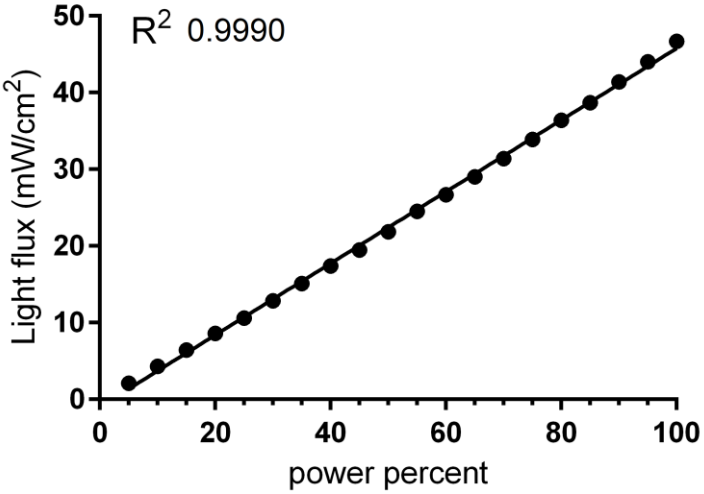


Figure 4.7 Light flux from the LED scaled almost perfectly with power percent setting using PWM. Light flux was measured using Coherent FieldMaxII-TOP light meter with OP-2 VIS light sensor

Next thing that we have investigated for the Lightbox 2.0 is the light shield that is responsible for protection of the user from LED illumination since this powerful light could be harmful. Initially we have tried to remove the reflections to make it possible to run an experiment with negative illumination control on the same plate as samples that were illuminated. To do this we have constructed a prototype from a cardboard box covered in a black vinyl on the inside that should absorb any light coming to it. Unfortunately, this resulted in a drastic drop in the amount of light being delivered to the sample in comparison to the old lightbox based on the lack of reflected light (Figure 4.8).

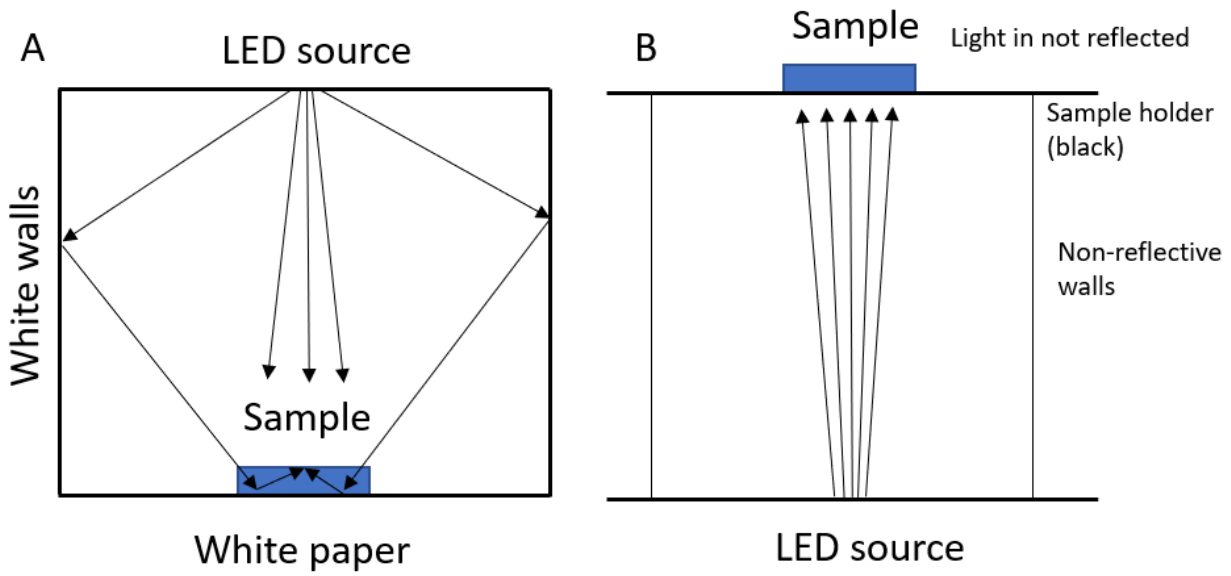


Figure 4.8 Difference in the light path for the old light box with reflections (A) and the new light box without reflections (B)

To get some of the reflected light we have made several prototypes by covering walls of light shield with aluminum foil. Even though this did increase the light being delivered to the sample, the light spread across the sample was not great. The only configuration that we have tried that worked well was the Styrofoam container which did have some bleed though of the light (Figure 4.9, left) but still dispersed and reflected enough light to increase the light delivered to the sample. We also re-painted the sample holder from black to white in order to reduce the light absorption as well as heating of the sample and applied the layer of flexible mirror on the base of the light box (Figure 4.9, right). These modifications combined with the Styrofoam light shield resulted in the increase of the light dose samples received by a factor of 2.1.

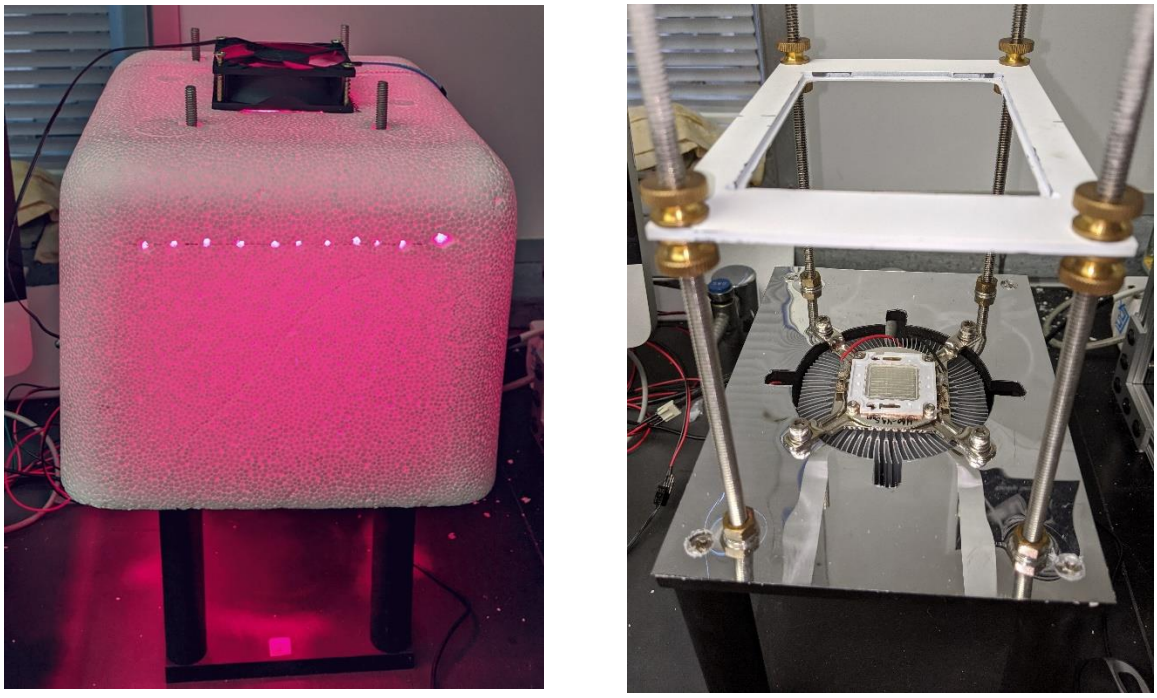

Figure 4.9 Light bleed through the Styrofoam light shield (left) and lightbox modifications to inrease light reflections (right)

Since we are using a Styrofoam box as a light shield, the samples become overheated since there is no airflow over the sample and a lot of heat is being generated by the LED. To increase cooling, we decided to add a small (80mm) fan on top of the Styrofoam box and added a piece of the flexible mirror with some spacers to cover the hole. This setup (Figure 4.10) allows for airflow to be present without light escaping the system. In addition to the fan hole, there are additional small holes at the top of the light shield (can be seen on Figure 4.9 as bright spots) that in theory might add some airflow to the system, but are unlikely to significantly reduce temperatures. These holes were not included in versions of the lightbox given to our collaborators.

We started this upgrade process with the goal of having a system capable of illumination of the plate where all the wells receive the same amount of light. To check that each well

receives the same light dose we decided to use Cy5 bleaching as an indicator of relative light dose/well. Cy5 was suitable because it is known to photodegrade[8] and has absorption maximum (650 nm) close to the emission maximum of the LED (660 nm).

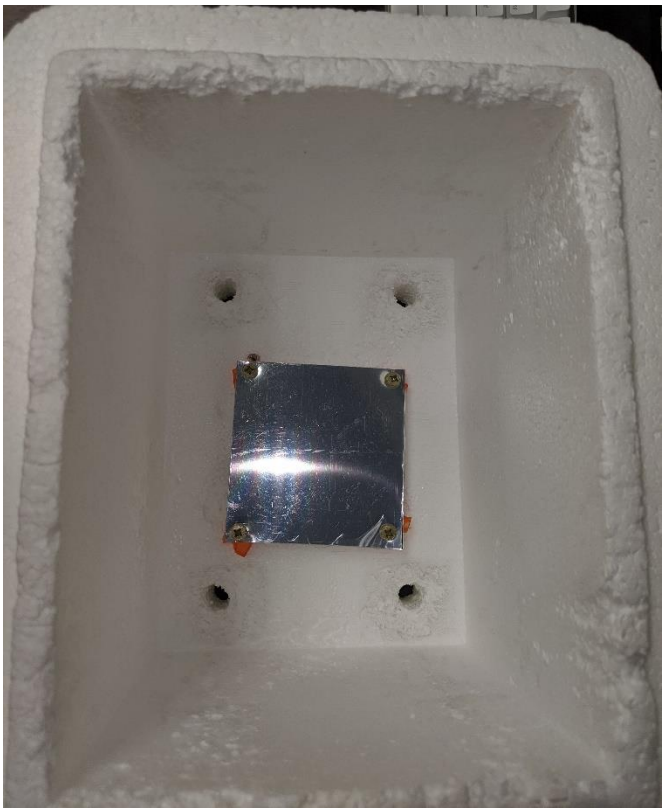

Figure 4.10 The hole for the 80mm cooling fan is covered by flexible mirror with spacers

After some experimentation we settled on using fluorescence bleaching rather than absorbance bleaching. This choice was motivated by the stability of the reading on our plate reader. Since both absorption and fluorescence readings require the samples to be illuminated, it also causes bleaching. We have tested a number of different parameters for the TECAN that can affect the stability of the signal (Figure 4.11, A-C) using a ratio of standard deviation to the average value (STDEV/AVG) as a score representing uniformity of readings. We discovered that most of the tested parameters had negligible effect on the stability of the reading. Results for the

number of flashes increase of the variation past 50 flashes is weird but the nature of it remains unknown. Unfortunately, we also confirmed that each reading of the fluorescence of the plate results in 0.4% bleaching of the Cy5 ( Figure 4.11, D).

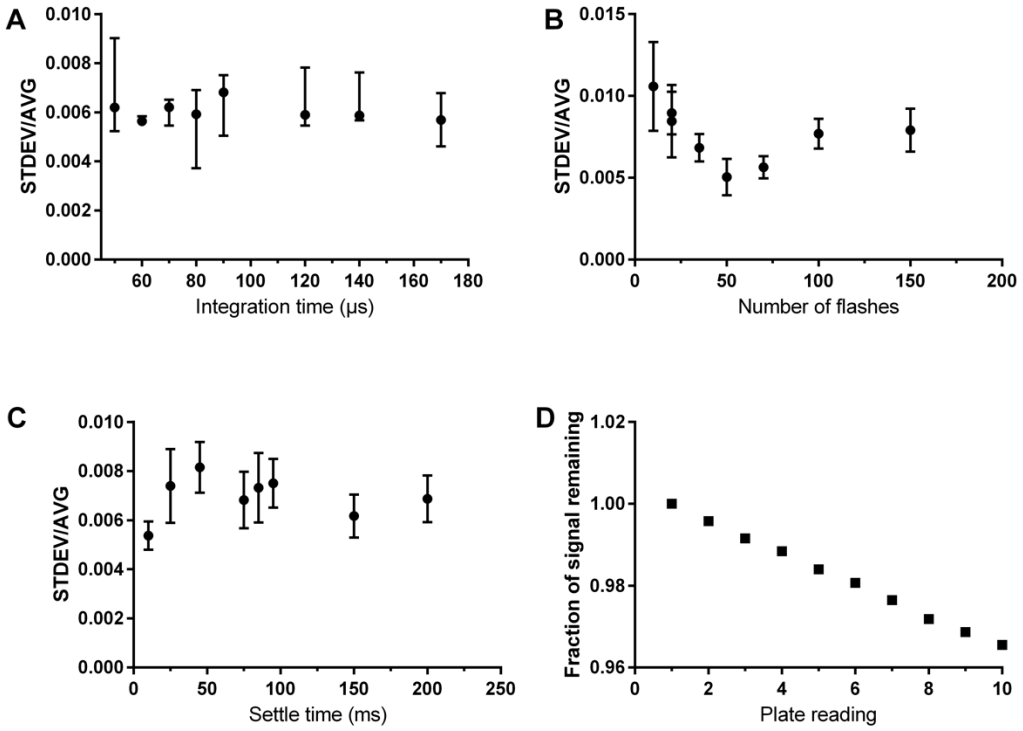


Figure 4.11 Testing of different parameters for reading of Cy5 fluorescence:Integration time (A), number of flashes (B), settle time (C) and number of times each plate is read (D)

After these tests, we settled on the following parameters for our calibration experiments: 50 flashes, 10 ms settle time, 60 µs integration time. To decrease the influence of variations of the reading on our calibration results we decided to do bleaching of multiple plates rather than multiple readings of the sample plate.

To test the uniformity of the bleaching we dispensed 100µL of Cy5 solution into each well (10 µM, controlled using 250000 $M^{-1}cm^{-1}$ extinction coefficient; total absorption in wells

~0.1). Since the height of the plate holder can affect the spread of the light from the LED, we need to find the height at which all wells receive the same dose of light. To quantify the light dose, we use relative bleaching of Cy5 after plates were exposed to the irradiation.

| | | | | | | | | | | | |
|---|---|---|---|---|---|---|---|---|---|---|---|
| 18 | 18 | 18 | 21 | 21 | 20 | 19 | 20 | 20 | 19 | 19 | 19 |
| 17 | 14 | 16 | 17 | 19 | 18 | 18 | 18 | 16 | 15 | 15 | 19 |
| 18 | 16 | 15 | 15 | 18 | 18 | 17 | 18 | 17 | 16 | 16 | 17 |
| 18 | 16 | 15 | 17 | 18 | 18 | 17 | 18 | 18 | 16 | 16 | 18 |
| 17 | 16 | 15 | 15 | 17 | 17 | 16 | 17 | 18 | 17 | 16 | 16 |
| 18 | 17 | 16 | 16 | 19 | 17 | 17 | 17 | 18 | 18 | 17 | 17 |
| 17 | 15 | 15 | 17 | 16 | 15 | 15 | 15 | 16 | 16 | 17 | 15 |
| 19 | 15 | 17 | 17 | 18 | 18 | 19 | 18 | 19 | 18 | 18 | 19 |

| | | | | | | | | | | | |
|---|---|---|---|---|---|---|---|---|---|---|---|
| 19 | 19 | 19 | 21 | 22 | 21 | 19 | 21 | 20 | 19 | 18 | 20 |
| 16 | 23 | 25 | 25 | 25 | 23 | 22 | 21 | 20 | 20 | 20 | 17 |
| 17 | 20 | 21 | 24 | 23 | 23 | 22 | 21 | 19 | 19 | 19 | 16 |
| 18 | 21 | 20 | 21 | 22 | 23 | 22 | 21 | 18 | 19 | 20 | 17 |
| 18 | 20 | 20 | 20 | 21 | 21 | 22 | 23 | 23 | 20 | 20 | 16 |
| 18 | 21 | 21 | 21 | 20 | 21 | 21 | 22 | 23 | 22 | 22 | 16 |
| 18 | 21 | 21 | 19 | 19 | 19 | 20 | 19 | 21 | 22 | 23 | 15 |
| 19 | 16 | 18 | 19 | 20 | 20 | 18 | 19 | 18 | 17 | 17 | 17 |

Figure 4.12 Cy5 bleaching test for light uniformity. Each number represents the percent of the Cy5 bleached, samples were illuminated for 4 minutes with 100% LED power; sample was positioned 12 cm from LED without a lens (left) or 11 cm with a sandblasted lens (right)

After irradiation for 4 minutes at 100% LED power we do have some edge effects, but overall bleaching is uniform (STDEV/AVG score was 0.08, Figure 4.12, left). We have also tested addition of the wide-angle light reflector collimator (specified angles for light spread 90-120°) but only after modifying the lens by sandblasting it on both sides we have achieved a more even distribution of intensities (Figure 4.12, right) with better light uniformity (STDEV/AVG score of 0.05). This lens also allowed us to drop the stage by one centimeter which resulted in slightly deeper bleaching. There is still some edge effect present, however, the difference between edge wells and center cells is smaller than for the case of the 12 cm height of the sample with no lens.

## 4.2 LightCoffin as a way to conduct dose-response experiments in one go

We have received a different version of Lightbox from Simon Watkins and Travis Wheeler from University of Pittsburgh. While Lightbox 2.0 was constructed with the goal of having all wells receiving the same dose of light, LightCoffin (based on the visual similarities and the goal of illuminating of samples to generate reliable optical stimulus across multiple experimental specimens, Figure 4.13) was constructed to have a spread of the light dosages over an illuminated sample of sizes compatible with multiwell plate formats. This allows researchers to use a single plate to test for the effect of light dose on their samples, where the same or different samples are contained in specific wells, each of which receives a calibrated and precise light dose.

The system uses same LED arrays as source of light as the Lightbox 2.0 but of a wider selection (365 nm, 395 nm, 440 nm, 525 nm, 660 nm). The LED sources are mounted on a motorized track, which is cooled with a liquid circulating cooler, and reduces sample heating to nondetectable levels over minutes of exposure. Light sources can be changed by pushing the button that corresponds to the LED user is interested in. Time can be changed in the increments of 5 seconds using the “Time” knob and the intensity can be adjusted using the “Intensity” knob. This control does not have any stops so to perform reproducible experiments users should stick to performing illuminations at 100% intensity, or the controller should be changed to a stopped and indexed proportional dial.


Figure 4.13 LightCoffin

When evaluating this instrument, it was observed that the proximity of the LED to the specimen resulted in a roughly gaussian illumination pattern over the scale of a 96-well plate. While we considered designs that would spread the light more uniformly, we also realized that the spatial heterogeneity of the illumination could be used to generate wide-range dose-response curves for light exposures across multiple specimens simultaneously, a process previously conducted one-exposure-level-at-a-time in the uniform illumination light boxes 1.0, 1.1 and 2.0.

We calibrated the illumination intensity incident on each well of a 96-well plate based on Cy5 bleaching again, by illuminating 5 plates independently for 2 minutes each in the instrument. The wells in the center of the plate receive much higher dose of light than the ones on the sides (Figure 4.14) with the difference between the center of the plate and edges reaching 15-fold between highest bleaching (95% Cy5 bleached) and lowest bleaching (6% being bleached).

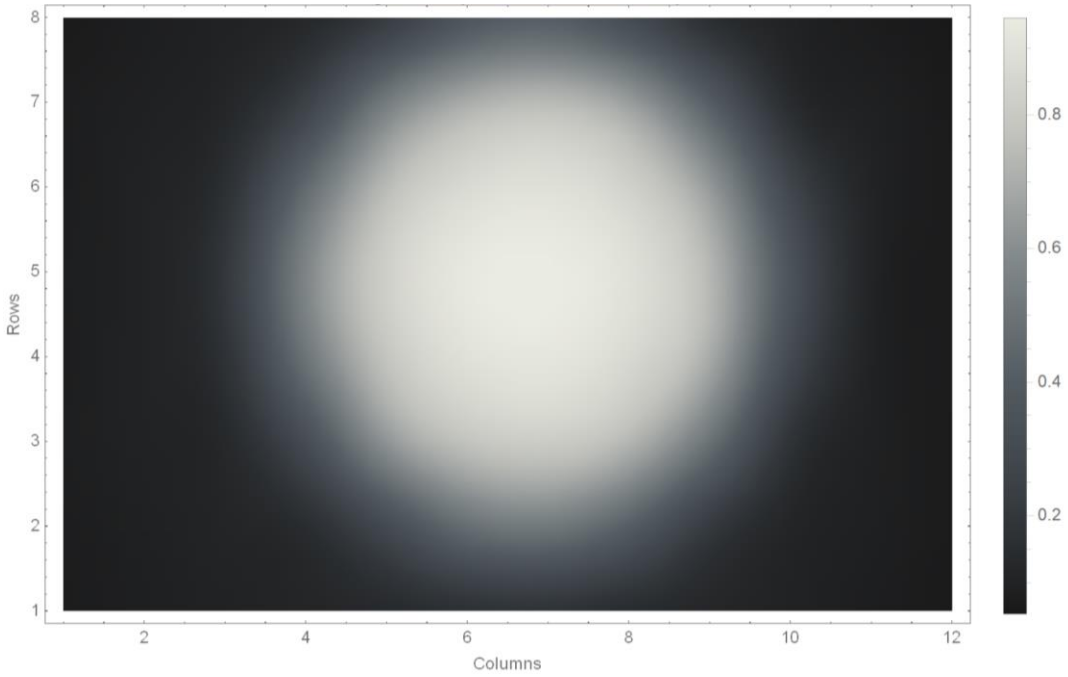


Figure 4.14 Illumination intensity map for the 96-well plate with 2nd order smoothing for an easier visual control of the light spread. White color represents the higher fraction of Cy5 bleached.

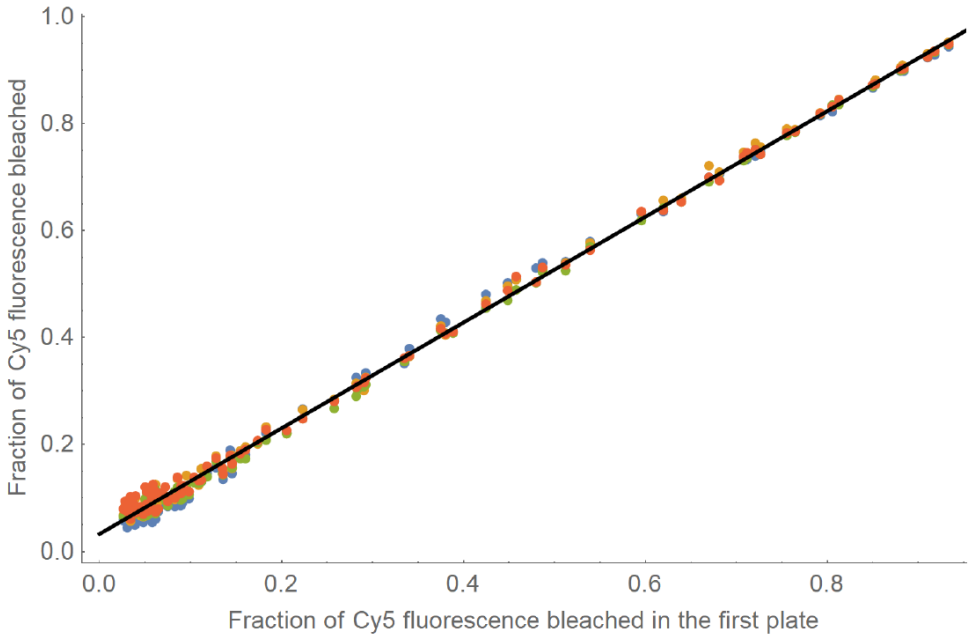


Figure 4.15 Validation of reproducibility of the bleaching between replicates

This bleaching is consistent between several replicates with each position on the plate receiving the same light dose across all replicates. To demonstrate it, we plotted bleaching fraction of Cy5 in each well of 4 plates against the bleaching of the same well in the last plate. In a perfect case we would expect to see a line y=x+b where b is a background bleaching from handling. The slope of our fitted line is 0.989 (with $R^2$ value of 0.998) which is close to 1. To exclude human errors as much as possible from this process we created a Mathematica notebook that makes all the calculations and plotting for user and generates the PDF report for the calibration performed (for the full code see Appendix). Periodic checks on the LEDs are required as some or all elements of it can burn out which can result in the change of the spread of light dose received by the sample.

Figure 4.16 Sample holder with a dish adaptor used for the light intensity measurement

Having the data of bleaching of Cy5 in each well we can create an assignment of the light dosages received by wells. To do that we need to assign the light flux that we read in the center

of the plate using the light meter (described earlier) with 1:1000 attenuator to the highest bleached well. Reproducibility of the position of the light sensor is critical and achieved by using an aluminum adaptor plate in which light sensor with attenuator fits (Figure 4.16).

Illumination from the LED is stable with minor drop in light flux (0.67%) over 11 minutes (Figure 4.17) while expected illumination duration for experiments was within 5 minutes. Bleaching of samples after 5 minutes of LED active (1 minute bleaching at 100% power, control bleaching using LED that was allowed to equilibrate for 10 minutes without illumination) saw a minor difference (5% but the one of the plates had anomalous several wells, data not shown). Dropping light power from 580 mW/cm$^2$ to 290 mW/cm$^2$ results in dropping of the maximum fraction bleached signal only from 0.50 to 0.32. This is expected as bleaching typically is observed as an exponential curve rather than a straight line.

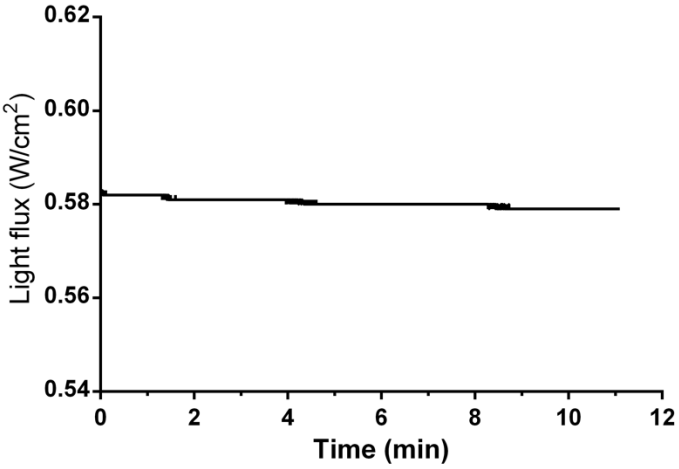


Figure 4.17 Light flux is stable during the reasonable illumination time

Based on the light flux received by each well we observe different bleaching rates (Figure 4.18). After fitting of those curves to an exponential decay we can obtain a map of decay coefficients that correlate with the light flux for each well. We assigned the measured light flux

in the center of the plate measured with a light power meter and scaled it to other wells to obtain the light flux through those wells (the Mathematica code for these operations is included in the appendix). Resulting light flux for each well is shown on Figure 4.19.

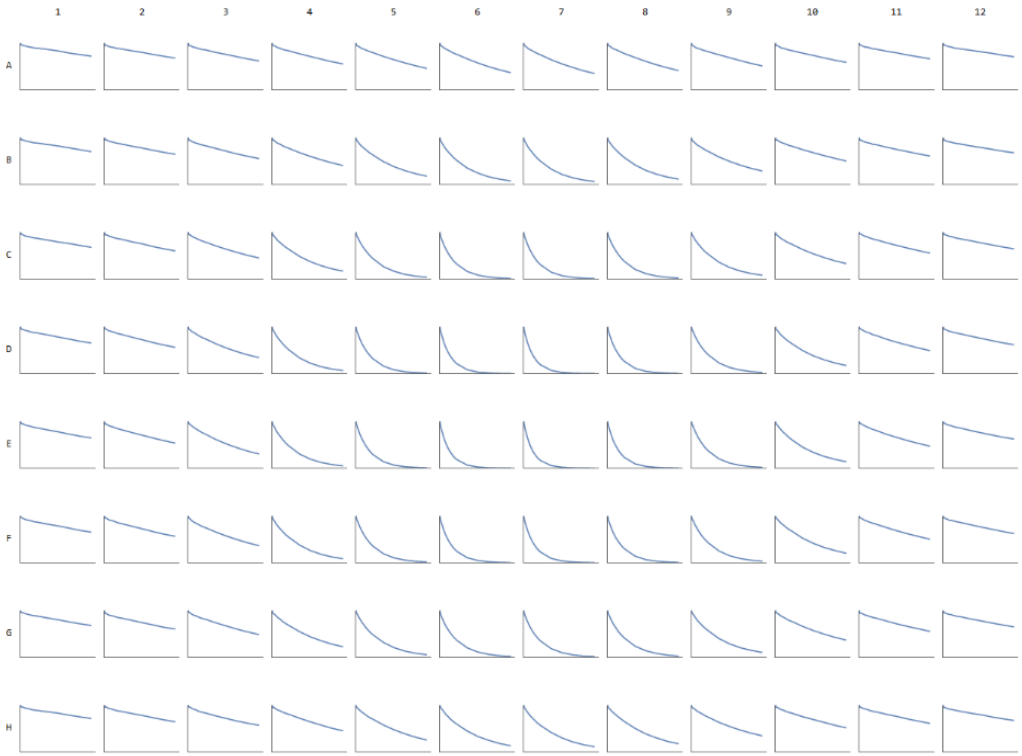


Figure 4.18 Bleaching graphs for each well of a 96-well plate, illumination with 100% LED power with various time steps

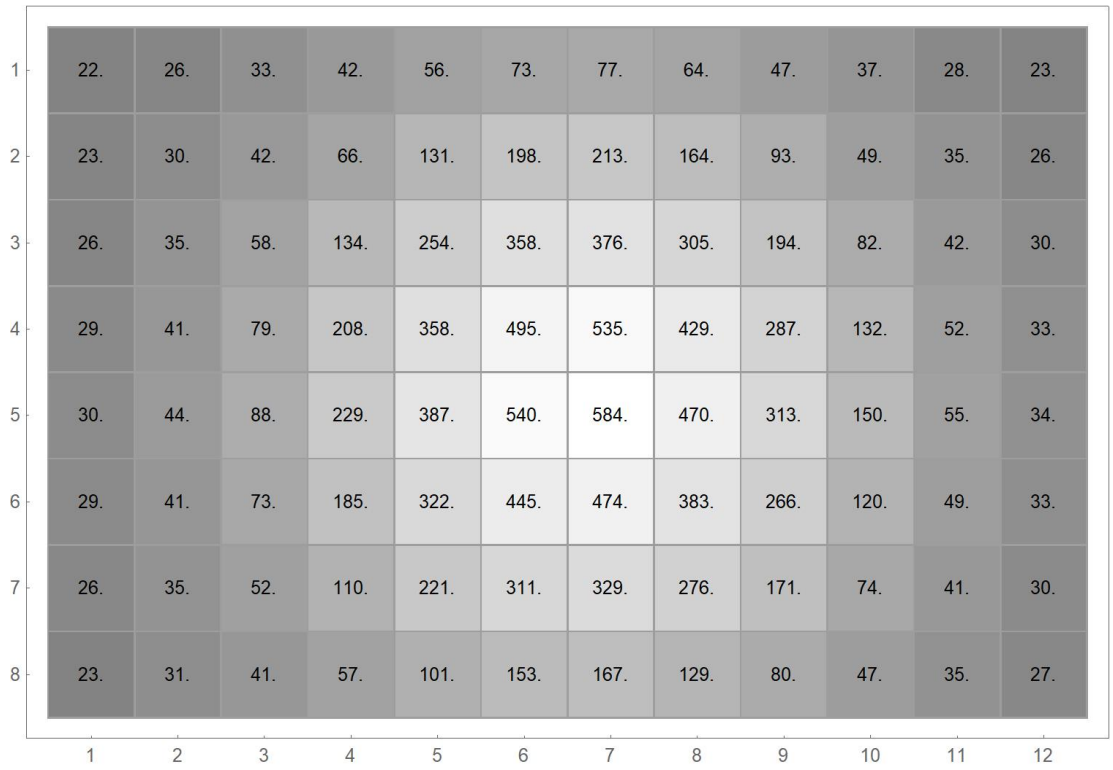


Figure 4.19 Power map of the plate. Each number represents the light flux in mW/cm$^2$

In summary, LightCoffin allows for a different type of experiment from Lightbox 2.0 where samples in a plate receive different light dose instead of every well receiving the same light dose. We have made a calibration routine for the user that is easy to use and allows for control of the LightCoffin stability and light spread between different samples, days and even researchers. The same calibration and validation routine can be established for other LEDs as well once the proper dye for photobleaching is selected.

## 4.3 Future directions

We have made a second generation of the Lightbox that is modular, has adjustable light power output as well as developed a method to quantify the uniformity and position-dependent power of the illumination of the sample plate. We have tested several prototypes of the light shield and found the one that reflects and spreads the light inside the sample holder part of the Lightbox 2.0 without overheating the sample.

Unfortunately, we were not able to build in concurrent temperature and light intensity monitoring as we discovered that reading from both of those are not stable enough to be used. This can be due to a couple of different issues – since light sensor is based on the resistance changing when the light falls on the sensor it also can change the resistance when heated resulting in the drift in the value we obtain using this sensor. Another possible reason is that PWM control of the LED also affects the values that we obtain from sensors. Potential way how to mitigate the latter issue is to use a separate Arduino board with an isolated power source to do the reading from the sensors. As an alternative, we can try placing the photodiode in a way that it is not directly exposed to the heat which should help with the stability.

Another thing that can be improved is adding the second LED array. Size of two of them stacked next to each other is slightly smaller than the plate (Figure 4.20) and should help to achieve uniform illumination at lower height of the sample holder. Having two LED emitters instead of one and sample holder in a lower position should improve the maximum light flux that we can use to illuminate samples at least two-fold. This will also allow to use a fixed, rather than movable sample holder and use only Arduino-based light flux regulation for experiments reducing the number of things that user must check before the start of the experiment. It also

might make it possible to remove the need for a reflective light shield which would make the control and quantification of the light dose delivered to the sample much easier.

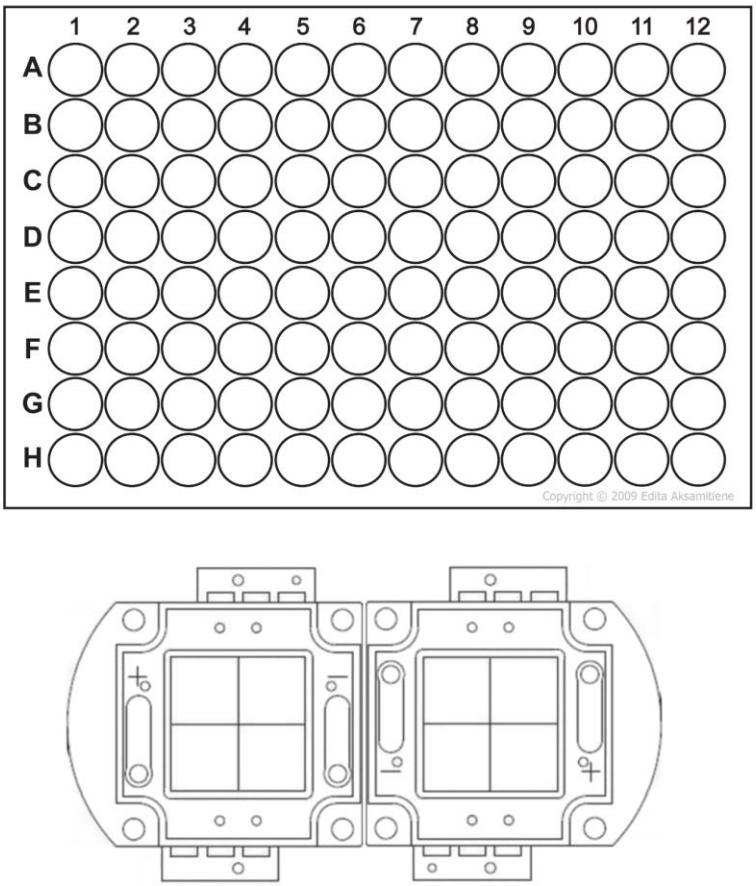


Figure 4.20 Relative size of the 96-well plate and 2 LED emitting arrays stacked side-by-side

The construction of the Lightbox can be improved as well – adding a transparent barrier between the LED and the sample compartments would reduce the amount of heat being delivered to the sample. Lightshield can be made from white opaque plastic. Coupled with the increase in the light power that should make the lightbox smaller overall and make it easier to use.

## 4.4 References


(1) He, J.; Wang, Y.; Missinato, M. A.; Onuoha, E.; Perkins, L. A.; Watkins, S. C.; St Croix, C. M.; Tsang, M.; Bruchez, M. P. A Genetically Targetable Near-Infrared Photosensitizer. *Nat. Methods* **2016**, *13* (3), 263–268. https://doi.org/10.1038/nmeth.3735.

(2) Zipfel, W. R.; Williams, R. M.; Webb, W. W. Nonlinear Magic: Multiphoton Microscopy in the Biosciences. *Nat. Biotechnol.* **2003**, *21* (11), 1369–1377. https://doi.org/10.1038/nbt899.

(3) Kuimova, M. K.; Yahioglu, G.; Ogilby, P. R. Singlet Oxygen in a Cell: Spatially Dependent Lifetimes and Quenching Rate Constants. *J. Am. Chem. Soc.* **2009**, *131* (1), 332–340. https://doi.org/10.1021/ja807484b.

(4) Da Silva, E. F. F.; Pedersen, B. W.; Breitenbach, T.; Toftegaard, R.; Kuimova, M. K.; Arnaut, L. G.; Ogilby, P. R. Irradiation- and Sensitizer-Dependent Changes in the Lifetime of Intracellular Singlet Oxygen Produced in a Photosensitized Process. *J. Phys. Chem. B* **2012**, *116* (1), 445–461. https://doi.org/10.1021/jp206739y.

(5) Ralston, J. M.; Mann, J. W. Temperature and Current Dependence of Degradation in Red-Emitting GaP LED's. *J. Appl. Phys.* **1979**, *50* (5), 3630–3637. https://doi.org/10.1063/1.326313.

(6) Plotog, I.; Vladescu, M. Power LED Efficiency in Relation to Operating Temperature. *Adv. Top. Optoelectron. Microelectron. Nanotechnologies VII* **2015**, *9258* (February 2015), 92582O. https://doi.org/10.1117/12.2072276.

(7) Xie, W.; Jiao, B.; Bai, Q.; Ilin, V. A.; Sun, M.; Burton, C. E.; Kolodieznyi, D.; Calderon, M. J.; Stolz, D. B.; Opresko, P. L.; St Croix, C. M.; Watkins, S.; Van Houten, B.; Bruchez, M. P.; Burton, E. A. Chemoptogenetic Ablation of Neuronal Mitochondria in

Vivo with Spatiotemporal Precision and Controllable Severity. *Elife* **2020**, *9*, 1–24. https://doi.org/10.7554/eLife.51845.

(8) Altman, R. B.; Terry, D. S.; Zhou, Z.; Zheng, Q.; Geggier, P.; Kolster, R. A.; Zhao, Y.; Javitch, J. A.; Warren, J. D.; Blanchard, S. C. Cyanine Fluorophore Derivatives with Enhanced Photostability. *Nat. Methods* **2012**, *9* (1), 68–71. https://doi.org/10.1038/nmeth.1774.

# 5 SUMMARY AND OUTLOOK

In this work, we set out to demonstrate the application of rational design of fluorogens to influence the properties of the resulting FAP-fluorogen complex. Based on the previously published modifications, we have developed an AMG-ester – new fluorogen that is brighter than its analog MG-ester. In addition to higher brightness, AMG-ester is also pH-sensitive in the biologically relevant range which allows us to use it to specifically label proteins in acidic conditions (late endosomes and lysosome). This capability is potentially valuable for studying protein trafficking particularly when it is related to the lysosomal storage disorder. The biggest problem of this project remains synthesis that does not have high yield or good reproducibility.

We have also altered the structure of DFHBI to include iodine atoms with the goal of utilizing DIHI with de-novo designed protein (mFAP2b) as a photosensitizer orthogonal to MG-2I. DIHBI binds to mFAP2b with 2.4 nM affinity and has fluorescence activation higher than the dynamic range of our instrument. It also demonstrates singlet oxygen generation comparable to fluorescein. Unfortunately, because of the lockdown we were not able to test DIHBI/mFAP2b in cells. Having biologically and spectrally orthogonal MG-2I/dK5** and DIHBI/mFAP2b systems allow for genetically targeted singlet oxygen generation in two different locations with high spatiotemporal control. This could be used for studies of the cell signaling, metabolism and repair mechanisms as well as studies that include ablation of a subpopulation in a mixed sample (biofilms, cancer cells, etc.).

We have developed a new instrument for reliable and repeatable illumination of cells in order to perform population-based experiments. Lightbox 1.1 is a version of Lightbox 1.0 with improved construction for ease of shipment to collaborators. Lightbox 2.0 added Adruino-based

control of the illumination duration as well as light intensity. Distance between LED and the sample holder can be adjusted and at 11 cm sample height each well of the 96-well plate gets almost equal dose of light. There are improvements that we could add to the system – we did not manage to make temperature and light sensor working reliably and we can potentially increase the amount of light the system is capable of delivering to the sample by more than twice by substituting a single LED array for two.

We have developed the calibration of the LightCoffin – a different type of the lightbox that we have obtained from Dr. Simon Watkins and Trevor Wheeler. We designed a way to measure the light flux received by each well of the 96-well plate, confirmed the stability of the illumination and created Mathematica scripts that allow users to generate calibration reports with only 2 measurements each time the instrument needs to be calibrated.

# 6 APPENDIX

## 6.1 Full code of the Arduino program ran on the Lightbox 2.0

```
// Original coding by Bennet Van Houten vanhoutenb@upmc.edu
// Modifications by Dmytro Kolodieznyi kolodieznyi@gmail.com from Marcel
Bruchez group
//
++++++++++++++++++++++++++++++++++++++++++++++++++++++++++++++++++++++++++++++
++++++++++++++++++++++++++++++++++
// <DECLARE GLOBAL VARIABLES>
//
++++++++++++++++++++++++++++++++++++++++++++++++++++++++++++++++++++++++++++++
++++++++++++++++++++++++++++++++++

// Set global variables, including initial values for buttons (not being
pressed)
// and defaults for power (100%) and time (5 minutes)

#define aref_voltage 3.3

double ExposureTime = 600;         // default exposure time
byte PowerPercent = 100;           // default LED power %

const float calibration = 176e-3; // radiant flux density of the light in
w/cm22

//pins used for I/O
const byte RedLightPin = 5;
const byte RedButtonPin = 8;
const byte GreenButtonPin = 7;
const byte temperaturePin = 0;
const byte LightSensorPin = 4;

char inputBuffer[16];
const int SensorAveraging = 200;
byte RedButtonState = 1;
byte GreenButtonState = 0;
long InputNumber = 0;
double Power;
float PowerPInput_float;
byte PowerPInput;
int readingsT;                    // the readings from the temperature input
long totalT = 0;                  // the running total
int averageT = 0;                 // the average
int readingsL;                    // the readings from the light input
long totalL = 0;                  // the running total
int averageL = 0;                 // the average


//
++++++++++++++++++++++++++++++++++++++++++++++++++++++++++++++++++++++++++++++
++++++++++++++++++++++++++++++++++
```

```
// <SETUP SCRIPT>
//
++++++++++++++++++++++++++++++++++++++++++++++++++++++++++++++++++++++++++++++++
++++++++++++++++++++++++++++++++++

void setup() {

  // set up the pin numbers and modes for red light, red and green buttons on
control unit, and temperature sensor
  Serial.begin(9600);
  pinMode(RedLightPin, OUTPUT);
  pinMode(RedButtonPin, INPUT);
  pinMode(GreenButtonPin, INPUT);
  analogReference(EXTERNAL);
  // Make sure the red light is off
  digitalWrite(RedLightPin, LOW);

  // Calculate initial (default) power setting
  PowerPInput_float = PowerPercent * 2.55;
  PowerPInput = (int) PowerPInput_float;
  Power = PowerPInput * calibration * ExposureTime / 255;

  // Open the serial port so the status indicator works and show 'ready'
message
  Serial.println();
  Serial.println("READY");
  Serial.println();
  Serial.println("Press GREEN button to change light exposure");
  Serial.println();
  Serial.print("Press RED button to start light exposure for ");
  Serial.print(ExposureTime);
  Serial.print(" s with LED power percent ");
  Serial.println(PowerPercent);
  Serial.print("Radiant flux density was calibrated to be ");
  Serial.print(calibration);
  Serial.println(" W/cm2");
  Serial.print("Total exposure would be ");
  Serial.print(Power);
  Serial.println(" J/cm2");
  }


//
++++++++++++++++++++++++++++++++++++++++++++++++++++++++++++++++++++++++++++++++
++++++++++++++++++++++++++++++++++
// <MAIN LOOP>
//
++++++++++++++++++++++++++++++++++++++++++++++++++++++++++++++++++++++++++++++++
++++++++++++++++++++++++++++++++++

// The loop function looks for presses of the red or green buttons to direct
the program to either
// the <settings> or <light> functions

void loop() {
```

```
  RedButtonState = digitalRead(RedButtonPin);
  GreenButtonState = digitalRead(GreenButtonPin);

  if (RedButtonState == 1)
  {
    light(ExposureTime, PowerPercent);
  }

  else if (GreenButtonState == 1)
  {
    ExposureTime = SetExposure(ExposureTime);
    PowerPercent = SetPercentage(PowerPercent);
  }

}

//
++++++++++++++++++++++++++++++++++++++++++++++++++++++++++++++++++++++++++++++++
++++++++++++++++++++++++++++++++++
// <SETTING>
//
++++++++++++++++++++++++++++++++++++++++++++++++++++++++++++++++++++++++++++++++
++++++++++++++++++++++++++++++++++

// Exposure time settings
int SetExposure(int ExposureTime) {

  Serial.println();
  Serial.println();
  Serial.print("Current exposure time is ");
  Serial.print(ExposureTime);
  Serial.println(" s");
  Serial.println();
  Serial.println("Enter new exposure time in seconds and press <SEND>");

  while (Serial.available() == 0)
  {
  }

  while (Serial.available() > 0)
  {
    Serial.readBytes(inputBuffer, sizeof(inputBuffer));
    InputNumber = atoi(inputBuffer);
//    memset(inputBuffer, 0, sizeof(inputBuffer));
  }

  Serial.println(InputNumber);

  if (InputNumber < 1 || InputNumber > 18000)
  {
    Serial.println("Exposure time must be an integer between 1 s and 5 hours
(18000 seconds)");
    InputNumber = ExposureTime;
  }
```

```
  return InputNumber;
}

// Power percentage settings
int SetPercentage(int PowerPercent) {

  Serial.println();
  Serial.println();
  Serial.print("Current LED percentage is ");
  Serial.print(PowerPercent);
  Serial.println();
  Serial.println("Enter LED power percentage and press <SEND>");

  while (Serial.available() == 0)
  {
  }

  while (Serial.available() > 0)
  {
    Serial.readBytes(inputBuffer, sizeof(inputBuffer));
    InputNumber = atoi(inputBuffer);
    memset(inputBuffer, 0, sizeof(inputBuffer));
  }

  Serial.println(InputNumber);

  if (InputNumber < 1 || InputNumber > 100)
  {
    Serial.println("LED power must be an integer between 1 and 100
percents");
    InputNumber = PowerPercent;
  }

  Power = PowerPInput * calibration * ExposureTime / 2.55;

  Serial.println();
  Serial.println();
  Serial.println();
  Serial.println("READY");
  Serial.println();
  Serial.println("Press GREEN button to change light exposure");
  Serial.println();
  Serial.print("Press RED button to start light exposure for ");
  Serial.print(ExposureTime);
  Serial.print(" s with LED power percent ");
  Serial.println(PowerPercent);
  Serial.print("Radiant flux density was calibrated to be ");
  Serial.print(calibration);
  Serial.println(" W/cm2");
  Serial.print("Total exposure would be ");
  Serial.print(Power);
  Serial.println(" J/cm2");

  while (GreenButtonState == 1) {
```

```
    GreenButtonState = digitalRead(GreenButtonPin);
  }

  GreenButtonState = 0;
  return InputNumber;
}

//
++++++++++++++++++++++++++++++++++++++++++++++++++++++++++++++++++++++++++++++++
++++++++++++++++++++++++++++++++++
// <LIGHT>
//
++++++++++++++++++++++++++++++++++++++++++++++++++++++++++++++++++++++++++++++++
++++++++++++++++++++++++++++++++++

void light(long ExposureTime, int PowerPercent) {

  long delayloop = 0;
  long reportloop = 0;
  long reportloop2 = 0;

  // Convert s to ms for timer
  long LightTime = ExposureTime * 1000;

  // send "light on" report to monitor
  Serial.println();
  Serial.println("LED source ON");

  // make note of the time, calculate input PWM and turn the light on
  long timestamp = millis();
  long timestamp2 = millis();
  long timestamp4 = millis();

  PowerPInput_float = PowerPercent * 2.55;
  PowerPInput = (int) PowerPInput_float;
  Power = PowerPInput * calibration * ExposureTime / 2.55;
  analogWrite(RedLightPin, PowerPInput);
  //Serial.print("Power input");
  //Serial.println(PowerPInput);

  // Time the exposure relative to the timestamp and give progress updates
every few seconds
  Serial.println();
  Serial.println();
  Serial.println("Exposure progress:");
  Serial.print("s");
  Serial.print("\t");
  Serial.println("J/m2");

  //Exposure loop
  while (delayloop < LightTime) {

    delayloop = millis() - timestamp;
    reportloop = millis() - timestamp2;
    reportloop2 = millis() - timestamp4;
```

```
    int VoltageLightReading = analogRead(LightSensorPin);
    float voltageLight = VoltageLightReading * aref_voltage / 1024;

    //Reporting cycle (time, current exposure)
    int report_timer = 1000 - SensorAveraging;
    if (reportloop >= report_timer)
    {
    float CurrentEnergy = delayloop * calibration * PowerPercent / 1000;

    timestamp2 = millis();
    Serial.print(((delayloop + SensorAveraging) / 1000));
    Serial.print("\t");
    Serial.println(CurrentEnergy);
    }

  }

  // Once delayloop > light time, turn off red light and document time at
which light went off
  // Send light exposure completion details to interface; set button state to
0

  digitalWrite(RedLightPin, LOW);
  long timestamp3 = millis();
  float Time6 = timestamp3 - timestamp;
  float Energy = (Time6) * calibration * PowerPInput / 2.55;
  float energy = Energy / 1000;

  Serial.println();
  Serial.println();
  Serial.println("LED source OFF");
  Serial.println();
  Serial.println("Exposure completed");
  Serial.print("Start time (ms) : ");
  Serial.println(timestamp);
  Serial.print("End time (ms) : ");
  Serial.println(timestamp3);
  Serial.print("Exposure time (s): ");
  Serial.println((Time6 / 1000));
  Serial.print("Exposure energy (J/cm2): ");
  Serial.println(energy);
  //Serial.print("Exposure energy pract (J/cm2): ");
  //Serial.println(CurrentEnergyPract);
  Serial.println();
  Serial.println();

  PowerPInput_float = PowerPercent * 2.55;
  PowerPInput = (int) PowerPInput_float;
  Power = PowerPInput * calibration * ExposureTime / 2.55;

  Serial.println();
  Serial.println("READY");
  Serial.println();
  Serial.println("Press GREEN button to change light exposure");
```

```
  Serial.println();
  Serial.print("Press RED button to start light exposure for ");
  Serial.print(ExposureTime);
  Serial.print(" s with LED power percent ");
  Serial.println(PowerPercent);
  Serial.print("Radiant flux density was calibrated to be ");
  Serial.print(calibration);
  Serial.println(" W/cm2");
  Serial.print("Total exposure would be ");
  Serial.print(Power);
  Serial.println(" J/cm2");

  RedButtonState = 0;

}
```

## 6.2 Mathematica code for conversion of the bleaching data read by TECAN to maps and key characteristics for LightCoffin validation

```
(*Set the directory with files as well as the input file name*)
SetDirectory["path-to-files"];
inputFileName = "file-with-data";

(*Import data from files for all 5 runs and average readings from each
well,b=before illumination,a=after illumination*)
import5a=Mean[#]&/@(DeleteCases[#,""]&/@Import[inputFileName,{"Data",2}][[40;
;135,2;;]]);
import5b=Mean[#]&/@(DeleteCases[#,""]&/@Import[inputFileName,{"Data",3}][[40;
;135,2;;]]);
import4a=Mean[#]&/@(DeleteCases[#,""]&/@Import[inputFileName,{"Data",4}][[40;
;135,2;;]]);
import4b=Mean[#]&/@(DeleteCases[#,""]&/@Import[inputFileName,{"Data",5}][[40;
;135,2;;]]);
import3a=Mean[#]&/@(DeleteCases[#,""]&/@Import[inputFileName,{"Data",6}][[40;
;135,2;;]]);
import3b=Mean[#]&/@(DeleteCases[#,""]&/@Import[inputFileName,{"Data",7}][[40;
;135,2;;]]);
import2a=Mean[#]&/@(DeleteCases[#,""]&/@Import[inputFileName,{"Data",8}][[40;
;135,2;;]]);
import2b=Mean[#]&/@(DeleteCases[#,""]&/@Import[inputFileName,{"Data",9}][[40;
;135,2;;]]);
import1a=Mean[#]&/@(DeleteCases[#,""]&/@Import[inputFileName,{"Data",10}][[40
;;135,2;;]]);
import1b=Mean[#]&/@(DeleteCases[#,""]&/@Import[inputFileName,{"Data",11}][[40
;;135,2;;]]);

(*Calculate bleaching*)
plateBleaching1=MapThread[((#1-#2)/#1)&,{import1b,import1a}];
plateBleaching2=MapThread[((#1-#2)/#1)&,{import2b,import2a}];
plateBleaching3=MapThread[((#1-#2)/#1)&,{import3b,import3a}];
plateBleaching4=MapThread[((#1-#2)/#1)&,{import4b,import4a}];
plateBleaching5=MapThread[((#1-#2)/#1)&,{import5b,import5a}];

(*Split into rows for a heatmap*)
plate1=Partition[plateBleaching1,12];
plate2=Partition[plateBleaching2,12];
plate3=Partition[plateBleaching3,12];
plate4=Partition[plateBleaching4,12];
plate5=Partition[plateBleaching5,12];

(*Display heatmap of bleaching*)
averages=MapThread[Mean[{#1,#2,#3,#4,#5}]&,{plate1,plate2,plate3,plate4,plate
5}];
densityPlot=ListDensityPlot[
      averages,
      PlotLegends->Placed[Automatic,Right],
      ColorFunction->ColorData["GrayTones"],
      InterpolationOrder->2,
      ClippingStyle->Automatic,
```

```
      AspectRatio->8/12,
      ImageSize->Large,
      PlotLabel->"Bleaching of the Cy5 in well of the 96-well plate",
      FrameLabel->{"Columns","Rows"}];

(*Make data lines*)
line2=MapThread[{#1,#2}&,{plateBleaching1,plateBleaching2}];
line3=MapThread[{#1,#2}&,{plateBleaching1,plateBleaching3}];
line4=MapThread[{#1,#2}&,{plateBleaching1,plateBleaching4}];
line5=MapThread[{#1,#2}&,{plateBleaching1,plateBleaching5}];

(*Fit for well-to-well variations between plates*)
fit = LinearModelFit[Flatten[{line2,line3,line4,line5},1],x,x];

(*Check reproducibility of the bleaching between different plates*)
linePlot=Show[ListLinePlot[{line2,line3,line4,line5},Joined->False],
      Plot[fit[x],{x,0,1},PlotStyle->Black],
      ImageSize->Large,
      Frame->{True,True,False,False},
      FrameLabel->{"Bleaching of wells in the first plate","Bleaching of
wells in other plates"}];

(*Get average bleaching of the column 12 that is supposed to be our no light
control*)
average12Column=Mean[averages[[;;,12]]];

(*Get maximum bleaching for the plate*)
maxBleaching=Max[averages];

(*Get bleaching ratio between max bleaching and masked column*)
bleachingRange=maxBleaching/average12Column;

(*Get the date of the report*)
dateFull = Import[inputFileName,{"Data",2}][[34,2]];
date = StringReplace[StringSplit[dateFull," "][[1]],"/"->"-"];

(*Export PDF with the results*)
exportData=Grid[{
{"Date of the check: "<>date},
{"Based 5 plates of Cy5.18 plates bleached by 2 minute illumination of the
660 nm light at 100% power"},
{},
{Rasterize[densityPlot,RasterSize->1500,ImageResolution->600,ImageSize-
>400]},
{},
{"Check for variability of the bleching between replicates:"},
{Rasterize[linePlot,RasterSize->1500,ImageResolution->600,ImageSize->400]},
{"\!\(\*SuperscriptBox[\(R\), \(2\)]\)
"<>ToString[SetAccuracy[fit["RSquared"],4]]<>"\t"<>"Slope
"<>ToString@SetAccuracy[fit["BestFitParameters"][[2]],4]},
{"Maximum bleaching: "<>ToString[SetAccuracy[maxBleaching,3]]},
{"AVG bleaching of column 12: "<>ToString[SetAccuracy[average12Column,3]]},
{"Ratio of the highest bleaching to the column 12 bleaching:
"<>ToString[SetAccuracy[bleachingRange,3]]}
}];
```

```
Export[
      "LightCoffin-check-"<>date<>".pdf",
      exportData];
```

## 6.3 Mathematica code for making plots and maps for light flux based on the bleaching kinetics

```
(*Set the directory with files as well as the input file name*)
SetDirectory["d:\\Documents\\Box Sync\\Bruchez_lab\\lightbox\\bleaching-
calibration\\"];
inputFileName = "2020-07-16 light coffin bleaching test";
dataPoints = {0,5,15,35,55,75,95,125,155,255,355,455,555,655};
measuredPower = 584;
plateRows = {"","A","B","C","D","E","F","G","H"};

importDataRaw=Import[inputFileName<>".xlsx",{"Data",;;-
2}][[;;,40;;135,2;;4]];
importDataAverage = Map[(Mean[#]&)/@#&,importDataRaw];
morphedData =
Reverse[#]&/@(importDataAverage[[;;,#]]&/@Table[n,{n,1,Length[importDataAvera
ge[[1]]]}]);
dataSeries =
Map[MapThread[{#1,#2}&,{dataPoints,Normalize[#,First]}]&,morphedData];

bleachingGraphsGrid = Table[
ListLinePlot[dataSeries[[y*12+x+1]],PlotRange->{{0,700},{0,1}},Ticks->None],
      {y,0,7},
      {x,0,11}
      ];
addedColumnsB = Prepend[bleachingGraphsGrid,Range[1,12]];
addedRowsB = MapThread[Prepend, {addedColumnsB, plateRows}];
Export["bleachingGrid.png",Grid@addedRowsB];

fit = FindFit[#,a*Exp[-k*x],{a,k},x]&/@dataSeries;
fittedConstants = k/.fit;
tableConstants = Table[
      SetAccuracy[fittedConstants[[y*12+x+1]]*100,3],
      {y,0,7},
      {x,0,11}
      ];
addedColumns = Prepend[tableConstants,Range[1,12]];
addedRows = MapThread[Prepend, {addedColumns, plateRows}];
Export[inputFileName<>"-constants"<>".csv",addedRows];

dataIllumination = Normalize[fittedConstants,Max]*measuredPower;
tablePowers = Table[
      SetAccuracy[dataIllumination[[y*12+x+1]],3],
      {y,0,7},
      {x,0,11}
      ];
addedColumnsP = Prepend[tablePowers,Range[1,12]];
addedRowsP = MapThread[Prepend, {addedColumnsP, plateRows}];
Export[inputFileName<>"-powers"<>".csv",addedRowsP];
tablePowersA = Table[
      SetAccuracy[dataIllumination[[y*12+x+1]],1],
      {y,0,7},
      {x,0,11}
```

```
      ];
platePowers = MatrixPlot[
      tablePowersA,
      ColorFunction->GrayLevel,
      FrameTicks->{Range[8],Range[12]},
      Mesh->All,
      ImageSize->Large,
      Epilog->{Black,MapIndexed[Text[#1,Reverse[#2-
1/2]]&,Reverse[tablePowersA],{2}]}
      ];
Export[inputFileName<>"-Power.png",Rasterize[platePowers,RasterSize-
>1500,ImageResolution->600]];

dataNormalized = Normalize[fittedConstants,Max];
tableNormalized = Table[
      SetAccuracy[dataNormalized[[y*12+x+1]],3],
      {y,0,7},
      {x,0,11}
      ];
addedColumnsN = Prepend[tableNormalized,Range[1,12]];
addedRowsN = MapThread[Prepend, {addedColumnsN, plateRows}];
Export[inputFileName<>"-normalized.csv",addedRowsN];

densityPlot = ListDensityPlot[
      tablePowers,
      PlotLegends->Placed[Automatic,Right],
      ColorFunction->ColorData["GrayTones"],
      InterpolationOrder->2,
      ClippingStyle->Automatic,
      AspectRatio->8/12,
      ImageSize->Large,
      PlotLabel->"Light power based on Cy5 bleaching",
      FrameLabel->{"Columns","Rows"}];
Export[inputFileName<>"-graph.png",Rasterize[densityPlot,RasterSize-
>1500,ImageResolution->600,ImageSize->400]];
```

## 6.4 MG-2I cannot be used for cellular ablation with 2-photon excitation

2-photon excitation provides great advantages over 1-photon excitation – because of the longer excitation wavelength less light is lost due to dispersion and absorption by tissue and spatial control is much greater due to the need of two beams of excitation light to intersect to excite the probe. To capitalize on this phenomenon, we decided to test if it is possible to use MG-2I to ablate cells with 2-photon excitation. Based on our instrumental capabilities we decided to use excitation in the Y-band of MG-2I (450 nm, Figure 6.1).

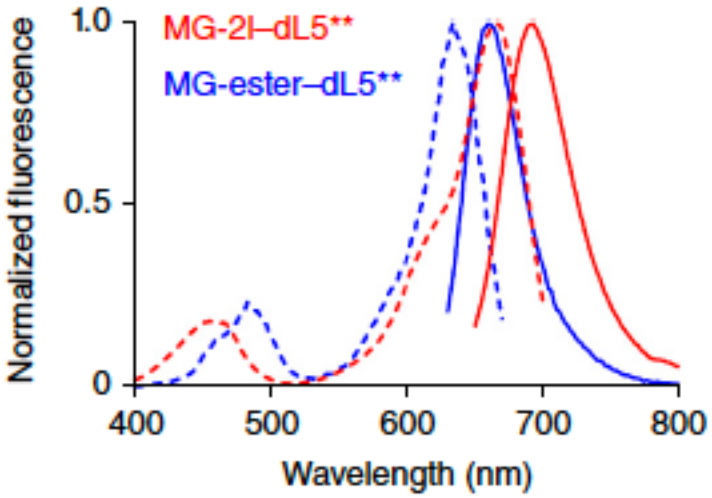


Figure 6.1 Excitation and emission spectra of MG-2I and MG-ester complexed to dL5**. Modified from Figure 1 from He et al, 2016[1]

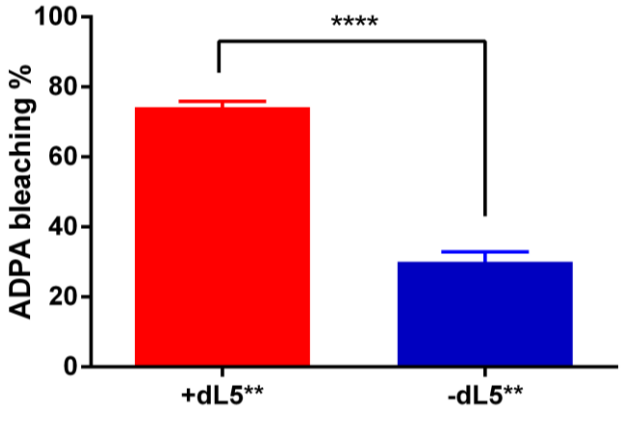

Figure 6.2 Addition of dL5** to MG-2I sample results in significant increase of ADPA bleaching after 20 minutes of 450nm LED illumination

We first tested if MG-2I/dL5** produces singlet oxygen when illuminated with 450 nm (Figure 6.2). It is clear from ADPA bleaching data that MG-2I complex with dL5** does indeed activate ROS production when excited with 450 nm in a similar way as with 660 nm excitation.

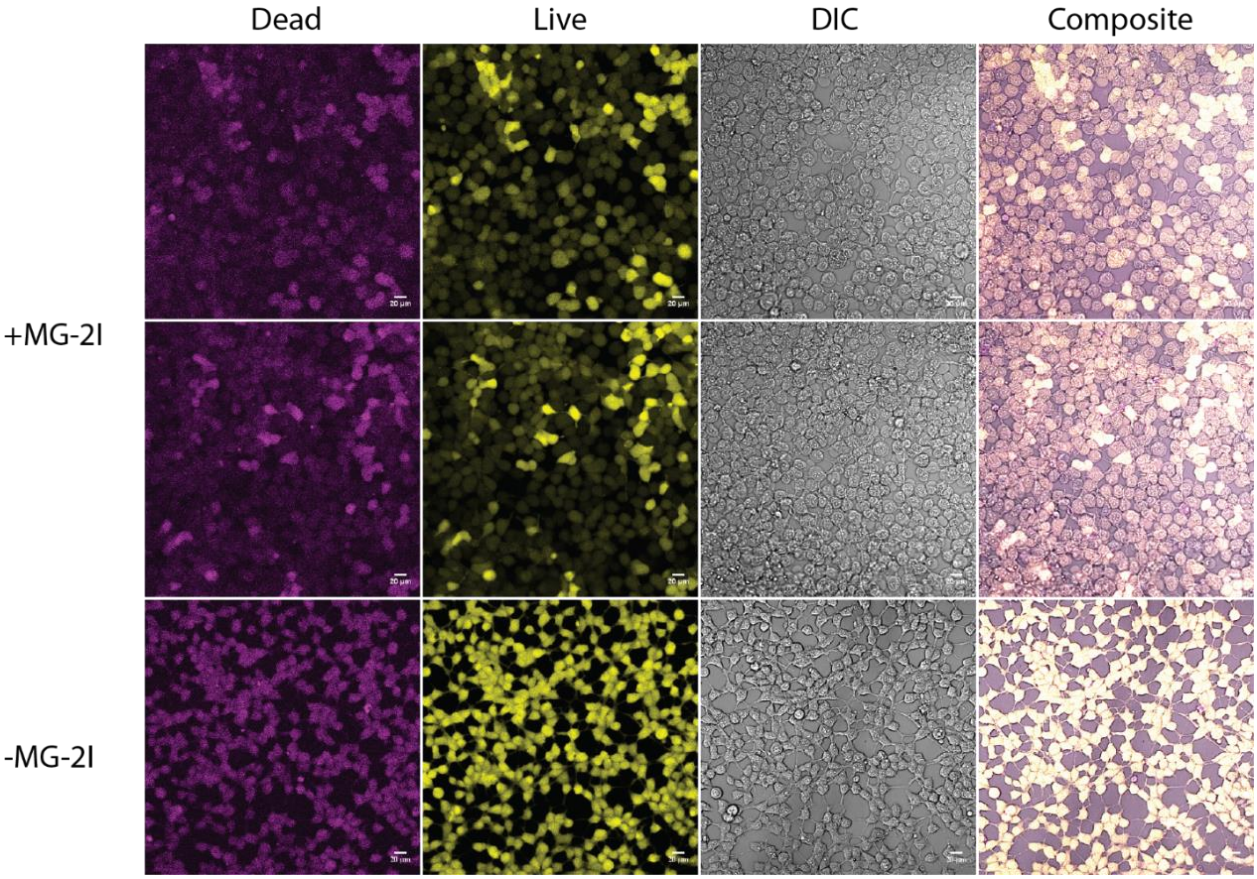


Figure 6.3 Live/Dead assay of MG-2I labeled FAT-TM cells after illumination with 450nm lightbox for 30 minutes; live cells are marked yellow, dead cells are marked magenta

We have also tested the possibility of killing cells using 450 nm excitation (Figure 6.3). Samples containing MG-2I have clearly shown diminished number of cells that survived illumination. Unfortunately, with the setup that we used for imaging there was crosstalk between

our live (Calcein-AM) and dead (Ethidium Homodimer) stains, but from the image it is clear that majority of cells have significantly lower metabolic activity after illumination with 450 nm light.

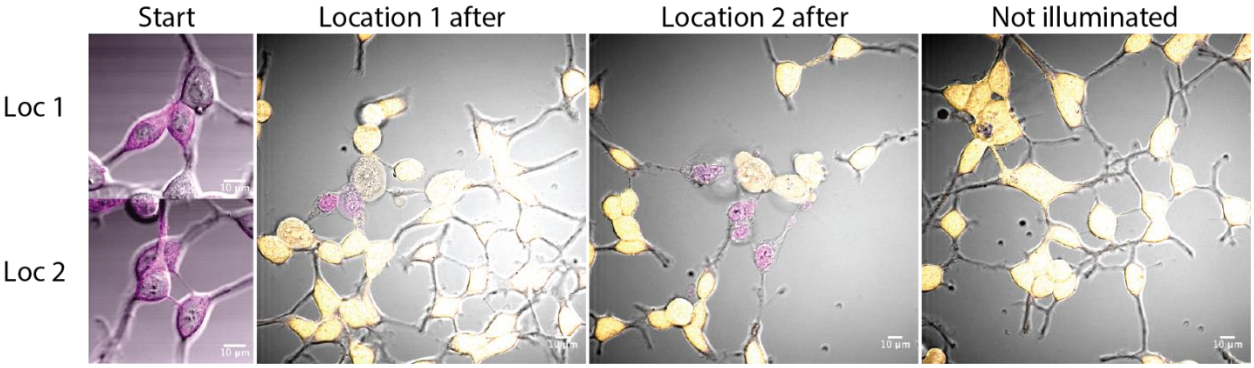


Figure 6.4 Live/death staining after illumination of several locations for cells using laser scanning confocal microscope; FAP-TM cells illuminated for 100 frames (~3 seconds) with 100% laser power in locations 1 and 2

Our previous work used spinning disk confocal microscope for microscope-based cell ablation[1] while 2-photon excitation setup that we have uses laser scanning microscope. We have tested the possibility of performing cell ablation using one-photon excitation on a laser-scanning microscope (Figure 6.4). After some trial and error, we have confirmed that if we zoom in on a small location (zoom factor 3) we can induce cell death using one-photon excitation using 40x objective with 633 nm laser.

Our initial experiments with MG-2I two-photon excitation at 900 nm resulted in a weird result (Figure 6.5). At the end of the illumination cells demonstrate some bubbles being formed both in positive and in negative cells. At the same time, positive cells were all killed while wild type cells have partially recovered (Figure 6.6).

We have used 20% laser power in all these experiments and decided to look at a range of wavelengths in order to find a lower laser power that will possibly allow us to perform cell ablation without killing negative cells (Figure 6.9). We also changed how we were conducting

experiments by focusing on cells labeled with Hoescht 33342 (top part of the image), measuring the time lapse for each of the saved locations for 122 seconds with different laser power, exchanging the media to a media with Calcein-AM/Ethidium Homodimer stain containing media and incubating for 30 minutes. We have also extracted the last frame of the time lapses to see the effect of the laser power on bubbles formation.

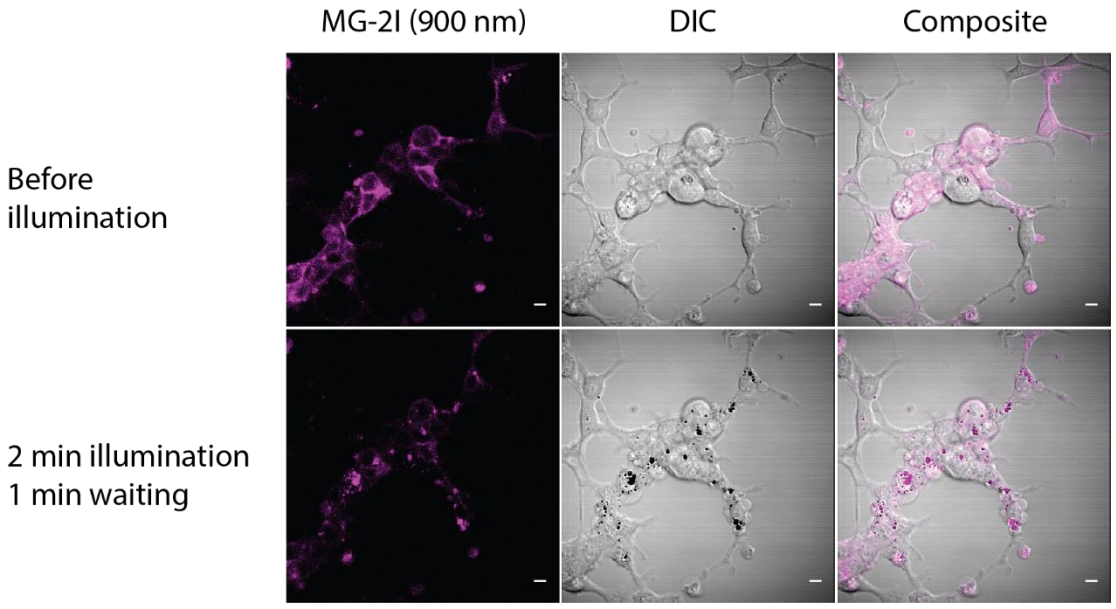


Figure 6.5 Bubbles are forming after 2 minutes of continuous scanning with 900 nm excitation and 20% laser power, mixture of WT and FAP-TM HEK293 cells

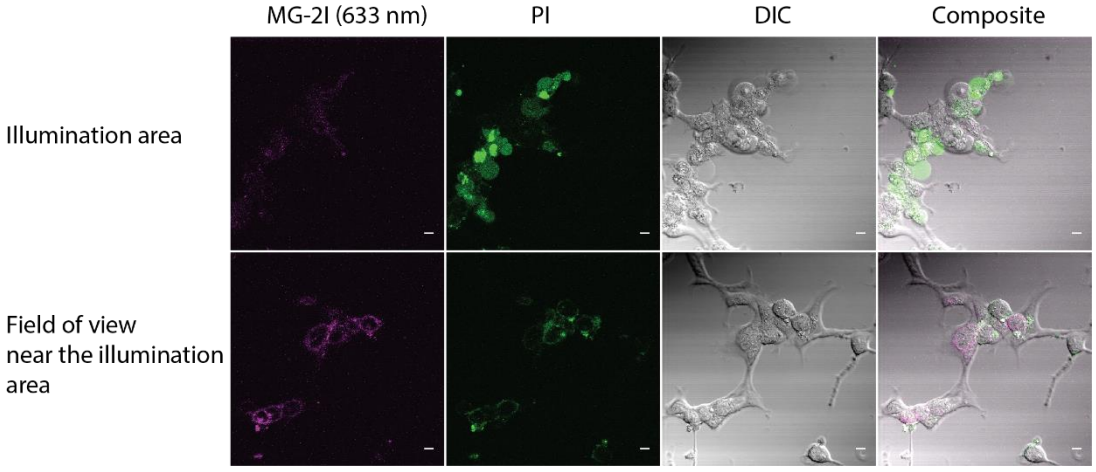

Figure 6.6 Death staining with Propidium Iodide of the field that was illuminated with 900 nm light as well as the adjacent cells

We have also tested the scalability of the light flux at 900 nm for our light source vs power percent set in the software to make sure that there are no sudden jumps that would explain the sharp difference we see in cell viability with the increase of laser power for cell ablation tests (Figure 6.7).

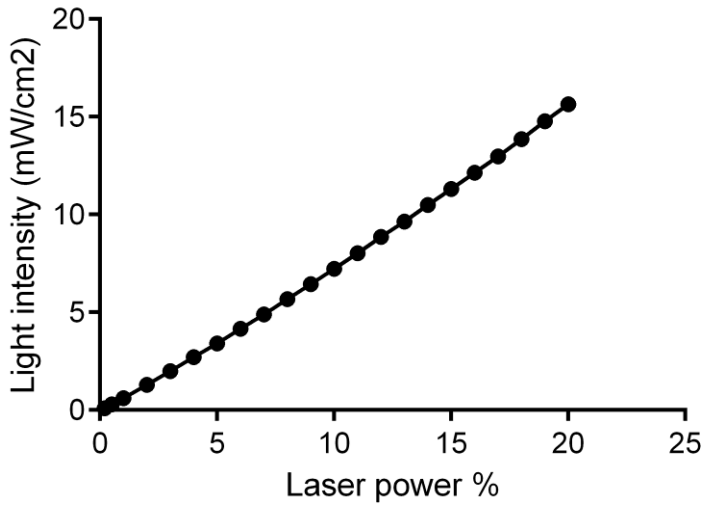


Figure 6.7 Scaling of laser power vs power % setting in the software

One of the possibilities of what can cause certain cell components to absorb 900 nm excitation would be a presence of Phenol Red as in the acidic media it has absorption at 450 nm and thus, can potentially absorb 900 nm two photon excitation (Figure 6.8). To test this hypothesis, we grew cells for 3 generations in a media with no phenol red and did side-by-side comparison in how many frames it takes for bubbles to form in identical conditions. Unfortunately, we observed no noticeable difference (data not shown). We have also tested depletion of hydrogen peroxide using sodium pyruvate as another possible reason for bubbles

formation but unfortunately saw no difference in experiments with and without sodium pyruvate (data not shown).

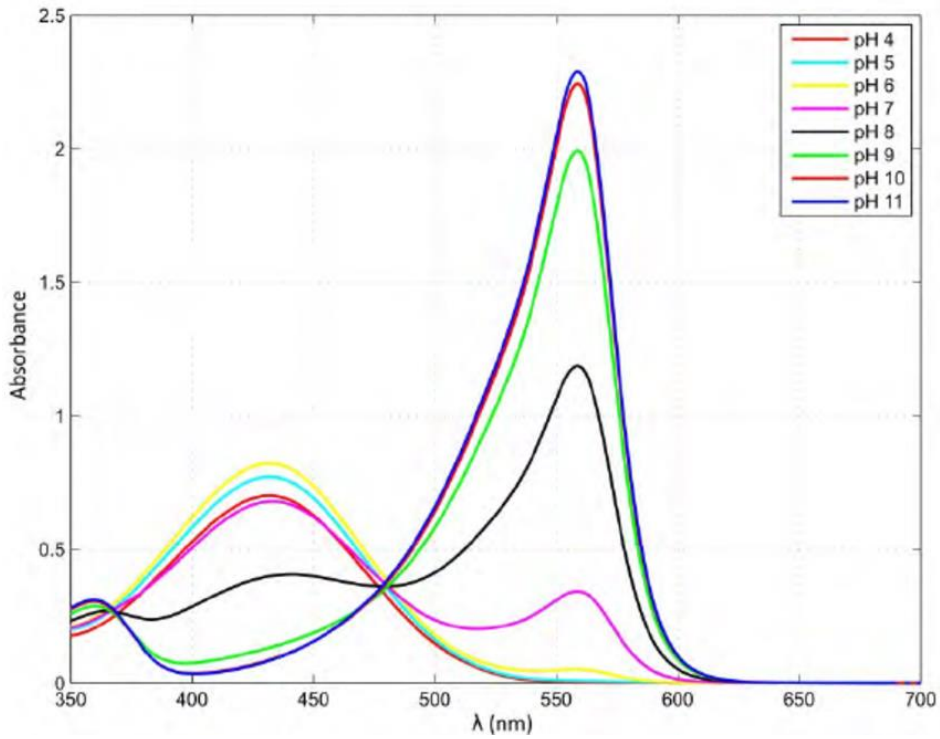


Figure 6.8 Absorption spectra of Phenol Red at different pH. Adopted from Rovati et al, 2012[3]

In summary, we set out to test if we can use two-photon excitation for MG-2I induced cell photoablation. After establishing that we can induce death using MG-2I using 450 nm excitation as well as 633 nm using laser scanning microscope we were not able to find conditions where we can cause cell death of cells with MG-2I but not in cells without dye. We have tested the possibility of acidic form of Phenol Red interfering as well as hypothesis of hydrogen peroxide causing cell death upon illumination. Unfortunately, we did not find the reason for wild type cells (or cells without dye) during illumination with 900 nm laser.

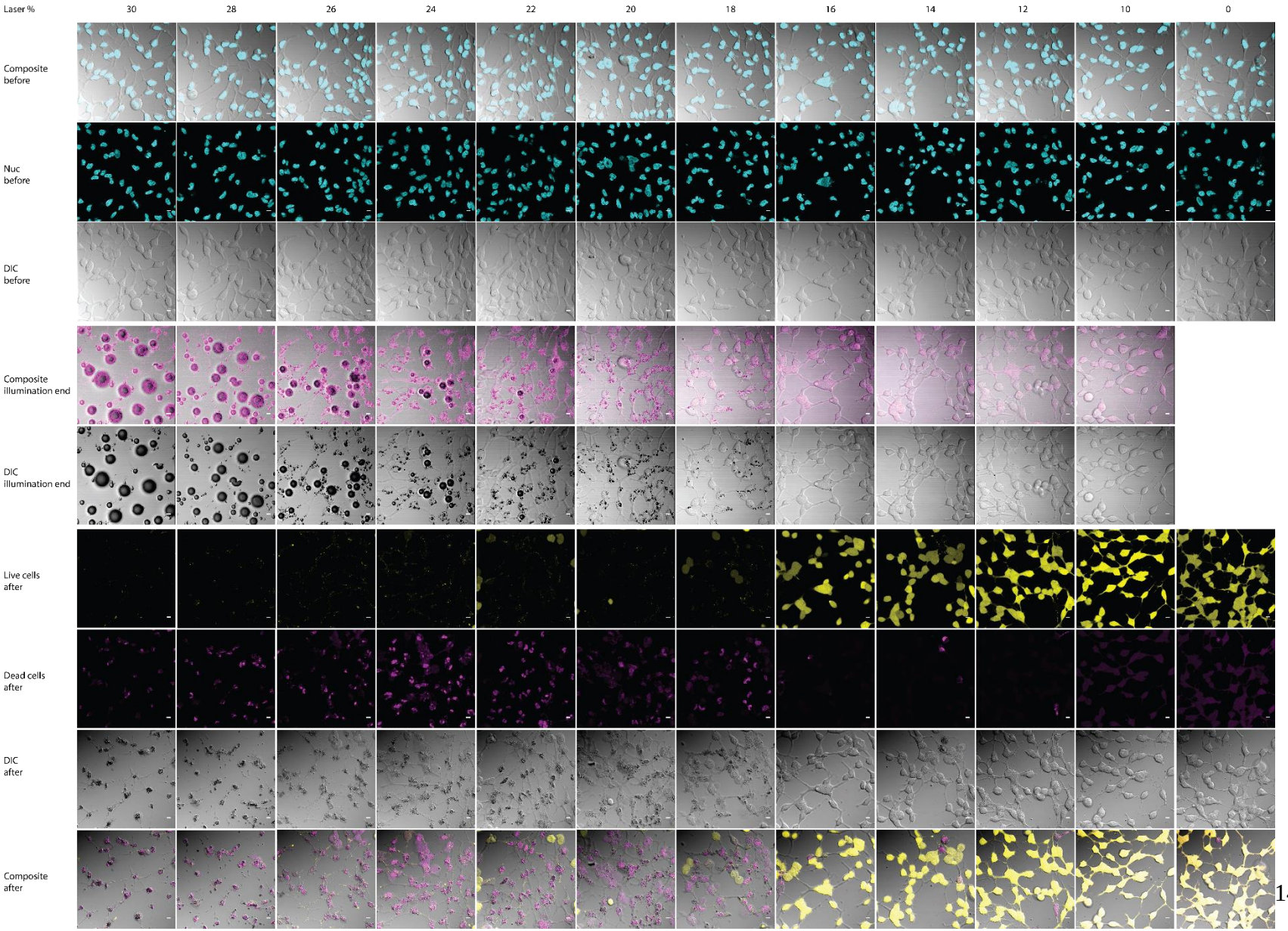
Laser %
30
28
26
24
22
20
18
16
14
12
10
0
Composite before
Nuc before
DIC before
Composite illumination end
DIC illumination end
Live cells after
Dead cells after
DIC after
Composite after

Figure 6.9 Testing of effect of different laser power for MG-2I 2-photon excitation on cell viability, FAP-TM HEK293 cells were labeled with 400 nM of MG-2I and illuminated for 122 seconds using Zeiss 510 microscope, 40x oil objective used

## 6.5 References


(1) He, J.; Wang, Y.; Missinato, M. A.; Onuoha, E.; Perkins, L. A.; Watkins, S. C.; St Croix, C. M.; Tsang, M.; Bruchez, M. P. A Genetically Targetable Near-Infrared Photosensitizer. *Nat. Methods* **2016**, *13* (3), 263–268. https://doi.org/10.1038/nmeth.3735.

(2) Franco, R.; Panayiotidis, M. I.; Cidlowski, J. A. Glutathione Depletion Is Necessary for Apoptosis in Lymphoid Cells Independent of Reactive Oxygen Species Formation. *J. Biol. Chem.* **2007**, *282* (42), 30452–30465. https://doi.org/10.1074/jbc.M703091200.

(3) Rovati, L.; Fabbri, P.; Ferrari, L.; Pilati, F. Plastic Optical Fiber PH Sensor Using a Sol-Gel Sensing Matrix. In *Fiber Optic Sensors*; InTech, 2012. https://doi.org/10.5772/26517.